TECHNICAL REPORT STANDARD PAGE

1. Report No.	2. Government Accession No.	3. Recipient's Catalog No.
FHWA/LA.10/452		

4. Title and Subtitle	5. Report Date
Finite Element Simulation of Structural Performance on Flexible Pavements with Stabilized Base/Treated Subbase Materials under Accelerated Loading	December 2011
	6. Performing Organization Code
7. Author(s)	8. Performing Organization Report No.
Zhong Wu, Ph.D., P.E., Xingwei Chen, Ph.D., and Xiaoming Yang	
9. Performing Organization Name and Address	10. Work Unit No.
Louisiana Transportation Research Center 4101 Gourrier Avenue Baton Rouge, LA 70808	
	11. Contract or Grant No. LTRC Project Number: 07-1P State Project Number: 736-99-1405
12. Sponsoring Agency Name and Address	13. Type of Report and Period Covered
Louisiana Transportation Research Center 4101 Gourrier Avenue Baton Rouge, LA 70808	Final Report (November 2006-April 2010)
	14. Sponsoring Agency Code

15. Supplementary Notes

Conducted in Cooperation with the U.S. Department of Transportation, Federal Highway Administration

16. Abstract

Accelerated pavement testing (APT) has been increasingly used by state highway agencies in recent years for evaluating pavement structures and/or materials. However, running an APT experiment is expensive. It requires costly accelerated loading devices and constructing full-scale pavement structures. Since pavement structures can have numerous combinations of pavement layer thicknesses, material types, and mixture designs, it is obviously impractical to test all potential pavement structures under APT. In order to maximize the benefits from an accelerated pavement testing (APT) study and utilize the APT results in the evaluation of other similar pavements with different structural configurations, a computer simulation of APT tests is essential. The objective of the research is to develop a finite element (FE) model(s) to simulate pavement structural performance of stabilized base and treated subbase materials under accelerated loading so that the performance of pavement structures with other stabilized base and subbase materials can be predicted without running APT tests.

A permanent deformation (P-D) material model was proposed in this study to simulate the permanent deformation behavior of pavement base and subgrade materials under repeated loading. This model was modified from a conventional elastoplastic model with a linear strain hardening. All model parameters can be obtained from a laboratory P-D test. A P-D test data analysis spreadsheet by Excel Macro was developed to obtain parameters for the proposed P-D model. The P-D material model was implemented into a commercial FE program, ABAQUS through a user-defined UMAT subroutine. The P-D model was verified by simulating laboratory P-D tests for eight pavement base and subbase/subgrade materials. In addition, a sensitivity analysis was conducted to evaluate the effect of the material model parameters, pavement structures, and load configurations on the permanent deformation of pavement structures. The sensitivity analysis indicated that the proposed P-D model could effectively be used to predict the permanent deformation for different pavement structures.

Three FE models for APT were preliminarily developed to investigate the dimensionality effect: a 3-D model with a moving load, a 3-D model with a repeated load, and an axisymmetric model. Considering the computational efficiency, the axisymmetric model was finally selected in this study. Six APT tests were simulated to calibrate the FE model. In the FE analysis, the load wander effect and the temperature change in pavement was considered. The calculated permanent deformations were in a reasonably good agreement with the field measurements with an average shift factor of 1.13. The FE model and the calibrated shift factor were also used to simulate pavement structures with other base/subbase materials. The predicted results showed that the performance of 2.6 percent lime/6 percent fly ash treated subbase was similar to that of 3.5 percent cement treated subbase. The analysis also showed that the lime/fly ash treated soil could be a viable alternative to the cement treated soil. In addition, the developed FE model was used to predict the permanent deformation of two low-volume roads in Louisiana. Overall, a good agreement was found between the predicted permanent deformations and the field measurements.

Finally, the APT test calibrated FE model was used to develop P-D prediction models (transfer function) for pavement base and subbase/subgrade materials. These materials were classified into four categories: stabilized base materials (e.g., stabilized blended calcium sulfate materials); unbound base materials (e.g., crushed limestone); treated subbase/subgrade materials (e.g., lime, lime/fly ash, and cement treated soils); and untreated subgrade soils. The developed P-D transfer functions were verified by predicting the six APT sections and two typical low volume pavement structures. The predicted permanent deformations generally matched well with the field measurements.

17. Key Words	18. Distribution Statement
Flexible Pavement; Permanent Deformation (Rutting); Stabilized Base; Treated Subbase; Accelerated Pavement Test; Permanent Deformation Test; Finite Element Simulation; Numerical Modeling.	**Unrestricted. This document is available through the National Technical Information Service, Springfield, VA 21161.**

19. Security Classif. (of this report)	20. Security Classif. (of this page)	21. No. of Pages	22. Price
Unclassified	Unclassified	132	

Project Review Committee

Each research project will have an advisory committee appointed by the LTRC Director. The Project Review Committee is responsible for assisting the LTRC Administrator or Manager in the development of acceptable research problem statements, requests for proposals, review of research proposals, oversight of approved research projects, and implementation of findings.

LTRC appreciates the dedication of the following Project Review Committee Members in guiding this research study to fruition.

LTRC Administrator

Zhongjie "Doc" Zhang, Ph.D., P.E.
Pavement and Geotechnical Research Administrator

Members

Phil Arena, FHWA
Jeff Lambert, DOTD
Steve Cai, LSU
Murad Abufarsakh, LTRC
Sam Cooper, LTRC

Directorate Implementation Sponsor

Richard Savoie
DOTD Chief Engineer

Finite Element Simulation of Structural Performance on Flexible Pavements with Stabilized Base/Treated Subbase Materials under Accelerated Loading

by

Zhong Wu, Ph.D., P.E.
Xingwei Chen, Ph.D.
Xiaoming Yang, Ph.D.

Louisiana Transportation Research Center
4101 Gourrier Avenue
Baton Rouge, LA 70808

LTRC Project No. 07-1P
State Project No. 736-99-1405

conducted for

Louisiana Department of Transportation and Development
Louisiana Transportation Research Center

December 2011

ABSTRACT

Accelerated pavement testing (APT) has been increasingly used by state highway agencies in recent years for evaluating pavement structures and/or materials. However, running an APT experiment is expensive. It requires costly accelerated loading devices and constructing full-scale pavement structures. Since pavement structures can have numerous combinations of pavement layer thicknesses, material types, and mixture designs, it is obviously impractical to test all potential pavement structures under APT. In order to maximize the benefits from an accelerated pavement testing (APT) study and utilize the APT results in the evaluation of other similar pavements with different structural configurations, a computer simulation of APT tests is essential. Due to the fact that currently there is no APT-based pavement analysis software immediately available (especially for the permanent deformation analysis of stabilized materials), the objective of this research study is to develop a finite element (FE) prediction program used to simulate pavement structural performance of stabilized base and treated subbase materials under accelerated loading so that the performance of pavement structures with other stabilized base and subbase materials can be predicted without running APT tests.

A permanent deformation (P-D) material model was proposed in this study to simulate the permanent deformation behavior of pavement base and subgrade materials under repeated loading. This model was modified from a conventional elastoplastic model with a linear strain hardening. All model parameters can be obtained from a laboratory P-D test. A P-D test data analysis spreadsheet by Excel Macro was developed to obtain parameters for the proposed P-D model. The P-D material model was implemented into a commercial FE program, ABAQUS, through a user-defined UMAT subroutine. The P-D model was verified by simulating laboratory P-D tests for eight pavement base and subbase/subgrade materials. In addition, a sensitivity analysis was conducted to evaluate the effect of the material model parameters, pavement structures, and load configurations on the permanent deformation of pavement structures. The sensitivity analysis indicated that the proposed P-D model could effectively be used to predict the permanent deformation for different pavement structures.

Three FE models for APT were preliminarily developed to investigate the dimensionality effect: a 3-D model with a moving load, a 3-D model with a repeated load, and an axisymmetric model. Considering the computational efficiency, the axisymmetric model was finally selected in this study. Six APT tests were simulated to calibrate the FE model. In the FE analysis, the load wander effect and the temperature change in pavement was considered. The calculated permanent deformations were in a reasonably good agreement with the field measurements with an average shift factor of 1.13. The FE model and the calibrated shift

factor were also used to simulate pavement structures with other base/subbase materials. The predicted results showed that the performance of 2.6 percent lime/6 percent fly ash (by weight) treated subbase was similar to that of 3.5 percent cement (by weight) treated subbase. The analysis also showed that the lime/fly ash treated soil could be a viable alternative to the cement treated soil. In addition, the developed FE model was used to predict the permanent deformation of two low-volume roads in Louisiana. Overall, a good agreement was found between the predicted permanent deformations and the field measurements.

Finally, the APT test calibrated FE model was used to develop P-D prediction models (transfer function) for pavement base and subbase/subgrade materials. These materials were classified into four categories: stabilized base materials (e.g., stabilized blended calcium sulfate [BCS] material); unbound base materials (e.g., crushed limestone); treated subbase/subgrade materials (e.g., lime, lime/fly ash, and cement treated soils); and untreated subgrade soils. The developed P-D transfer functions were verified by predicting the six APT sections and two typical low volume pavement structures. The predicted permanent deformations generally matched well with the field measurements.

ACKNOWLEDGMENTS

The authors would like to acknowledge the financial support of this research provided by the Louisiana Department of Transportation and Development (LADOTD) and the Louisiana Transportation Research Center (LTRC) under State Project No. 736-99-1405 and LTRC Research Project No. 07-1P.

The authors would like to extend their appreciation for the help from following colleagues: Gavin Gautreau, Alvin Mix, Paden Schilling, Benjamin Comeaux, and Douglas Hinton during the material sampling and testing. The authors also want to thank Dr. Louay Mohammad, Dr. Ananda Herath, and Dr. Murad Abu-Farsakh in some permanent deformation tests and Dr. Qiming Chen in some data analysis. Finally, the help from the pavement section personnel is also greatly appreciated.

IMPLEMENTATION STATEMENT

A unified permanent deformation (P-D) constitutive model for general pavement base and subbase materials was proposed in this study. A finite element (FE) pavement simulation model developed with the application of the proposed P-D model indicated that the FE model is well suited to be used in the simulation of permanent deformation under accelerated loading for various pavement base, subbase, and subgrade materials, including those stabilized or treated soils. In addition, a suite of permanent deformation prediction models (or transfer functions) for various pavement materials were also developed based on the calibrated FE analysis model. In general, both the developed FE model and the transfer functions are recommended for use in the prediction of permanent deformation of pavement structures under accelerated loading. Detailed implementation procedures are provided in Appendix A.

According to the FE simulation results using the developed FE model on other stabilized materials not being tested under the APT experiment of this study, a 12-inch thick, 2.6 percent lime/6 percent fly ash (by weight) treated sandy clay layer would have a similar in situ structural performance to a 12-inch thick, 3.5 percent cement (by weight) treated sandy clay layer under the accelerated loading. This finding is recommended to be constructed and validated by a field project in the state.

Overall, implementation of these two permanent deformation predication approaches will (1) reduce the need of actual running APT tests; (2) help evaluate the potential use of new materials, pavement configurations, design procedures, and other aspects in pavement design and construction; and (3) accumulate experiences to connect APT results with the performance of highway pavements.

TABLE OF CONTENTS

LIST OF TABLES

LIST OF FIGURES

INTRODUCTION

Background

Accelerated pavement testing (APT) has been increasingly used by state highway agencies in recent years for evaluating pavement structures and/or materials. In an APT experiment, an accelerated loading device applies vehicular loads to the pavement section in a compressed time period with controlled field conditions. Field performance of tested pavement materials and structures are monitored, which can then be used in assisting pavement design and analysis. However, running an APT experiment is expensive. It requires costly accelerated loading devices and constructing full-scale pavement structures. Since pavement structures can have numerous combinations of pavement layer thicknesses, material types, and mixture designs, it is obviously impractical to test all potential pavement structures under APT. In an APT program, a minimum number of pavement structures have to be carefully selected, thus the test results will be limited only to those tested pavement structures and materials.

In order to maximize the benefit from an APT study and utilize APT results to evaluate other pavements with similar structural configurations, a predictive model that can simulate the APT tests is needed. Unfortunately, there is no APT-based pavement analysis software currently available. The newly developed *Mechanistic-Empirical Pavement Design Guide* (MEPDG) provides a software package that can be used to predict pavement performance. However, the design method still has some limitations, and the software does not allow users to change or modify the material models and transfer functions embedded in the computer program. For example, in the damage model of the current MEPDG, cementitiously-stabilized layers are assumed to have no contribution to the total permanent deformation of the pavement. This assumption conflicts with the results from the recent APT experiments performed at the Louisiana Pavement Research Facility (PRF), where considerable permanent deformation developed in the stabilized base and treated subbase layers. Without changing or modifying those material models and transfer functions as well as other design criterion issues (e.g., traffic growth functions), the MEPDG design software cannot simulate an APT test efficiently.

This study was proposed to develop an APT-based FE model that serves the need of the computer simulation of APT experiments in the PRF of LTRC. The FE model can be calibrated from pavement performances measured from APT experiments. The calibrated FE model(s) can then be used to simulate performance of other pavement structures on computers without running APT tests. The developed FE models in combination with an

APT field study will: (1) reduce the need of running APT tests; (2) help evaluate the potential use of new materials, pavement configurations, design procedures, and other aspects in pavement design and construction; and (3) accumulate the experience to connect APT results with the performance of highway pavements. As a result, such an effort will greatly enhance and expand the benefits of an APT study.

Literature Review

Numerical Methods for Pavement Analyses

According to continuum mechanics theories, the responses of an object to disturbances (e.g., load, movement, temperature change, etc.) are governed by a series of partial differential equations (PDEs). Analytical solutions to these PDEs are only available under some of the special scenarios with homogeneous materials, regular geometry, and simple boundary conditions. For most of the engineering problems where analytical solutions are unavailable, approximate solutions of PDEs can be obtained through numerical methods. Among the various types of numerical methods currently available, the most popular methods include finite element method (FEM), finite difference method (FDM), discrete element method (DEM), etc. FEM and DEM are similar in the sense that they both require discretization of the problem into a number of cells/grid points. For structural and pavement analysis, FEM is generally believed more sophisticated and versatile than FDM especially when dealing with problems with complex geometries. DEM is a special numerical method that has drawn increasing attentions in recent years. In DEM, the complex constitutive behaviors of granular materials in macro scale are represented by the interaction between individual micro particles, rather than the constitutive equations. However, with the limited computer speed today, it is extremely time-consuming to simulate a pavement section under a large number of cycles of wheel load using DEM.

In pavement analysis, analytical solutions (e.g., Burmister's three-layer system solutions) can be obtained often by assuming that the pavement is constructed with homogeneous, isotropic, linear elastic materials with infinite thickness and is subjected to a monotonic load. These assumptions oversimplify the complex nature of pavement structures and materials. With the fast development of high-speed computers today, numerical methods, especially FEM, have been extensively used in pavement analysis. Compared to analytical solutions, FEM pavement analysis provides better simulation of material behaviors, wheel configurations, and environmental conditions.

Finite Element Simulation of Flexible Pavements

Duncan et al. first applied the FEM to the linear-elastic analysis of flexible pavements *[1]*. The method was later incorporated in the ILLI-PAVE computer program *[2]*. Due to the large amount of computing time and storage required, ILLI-PAVE has not been used for routine design purposes. Another FEM-based pavement analysis program, named MICHI-PAVE, was developed by researchers at Michigan State University *[3]*. MICH-PAVE runs faster than ILLI-PAVE. It also incorporates the non-linear properties of base and subgrade materials. Both ILLI-PAVE and MICHI-PAVE considered only the elastic responses of pavement structures. Lytton and Tseng developed a more sophisticated finite element program, Flexible Pavement Analysis Structural System (FLEXPASS), which has been used by many researchers *[4]*. FLEXPASS was developed based on ILLI-PAVE with a number of modifications including multiple axle loads, slip elements between layers, seasonal materials characterization, and prediction models for rutting, fatigue cracking, and serviceability index. However, the major disadvantage the FLEXPASS program is the lack of flexibility. Users are not allowed to modify or update the material and load models, which are embedded in the program.

General-purpose commercial FE softwares (e.g, ABAQUS, ANSYS, and ADINA) were also used by many researchers to model flexible pavements *[5]*, *[6]*, *[7]*. These commercial FE softwares provide users the maximum flexibility to implement various geometry, constitutive models, and boundary conditions. Generally, creating a FEM model for flexible pavement analysis involves the considerations of (1) dimensionality, (2) simulation of traffic loading, (3) environmental effects, and (4) constitutive material models.

Dimensionality. Three types of numerical models can be used for FE simulation of pavement: three-dimensional (3-D), plane-strain (2-D), and axisymmetric models.

Ideally, a pavement structure and wheel loading requires a 3-D analysis, particularly in predicting the microcracking and fracture responses *[8]*. The 3-D modeling can simulate complex tire imprints, anisotropic material behavior, and the lateral wander of axle loads, but it often requires numerous inputs and considerable computational time *[9]*. Huang et al. developed a 3-D numerical simulation procedure with moving wheel loads to model the APT sections at Louisiana ALF *[6]*. White, Erkens et al., and Desai also created 3-D FE models to simulate of flexible pavements *[5]*, *[10]*, *[11]*.

Two-dimensional plane-strain models can provide satisfactory approximate solutions for certain applications and require relatively little computational time and memory *[8]*. The plane-strain modeling is often valid for a long body where geometry and loading do not vary

significantly in the longitudinal direction. Kim et al. developed a plane-strain model to investigate the effects of supersingle tires on subgrades for typical road cross sections *[12]*. Plane-strain models were used by Wu and White et al. to simulate the flexible pavements as well *[13]*, *[14]*. However, plane-strain models cannot accurately reproduce actual traffic loading, which is limited to the use of line loads *[15]*.

An axisymmetric model simulates pavement structures with a 2-D mesh revolving around a central axis by assuming identical stress states in radial direction. The wheel load in an axisymmetric model is applied in a circular area. The advantage of an axisymmetric model is that a 3-D structure can be analyzed with a 2-D formulation using cylindrical coordinates. Hornych and El Abd used axisymmetric models to simulate the permanent deformation of unbounded granular materials in road pavements *[16]*. Axisymmetric models were also adopted by Helwany et al. and Howard and Warren in their simulation of pavements *[17]*, *[9]*.

Kim compared the numerical results from a plane-strain model and a 3-D model *[18]*. The result indicated that the plane-strain model produced higher calculated stresses, strains, and displacements than the 3-D model. Desai compared the 2-D and 3-D analyses of pavement and found that the calculated stresses from the two models did not show significant difference, whereas the difference in the calculated displacements from the two models was in the order of 20 percent *[8]*. Cho et al. compared 3-D, plane-strain, and axisymmetric models in pavement structural analyses and indicated that the 3-D and axisymmetric models yielded results suitable for the traffic loading analysis *[15]*. A preliminary study was also carried out in the NCHRP project 1-37A in order to select an appropriate dimensionality for the FE response model in the MEPDG design software. It was concluded that the inaccuracy in the response model is much lower compared to the inaccuracy in other components of the design method (e.g., material input, traffic input, transfer functions, etc.). An axisymmetric FE model was finally incorporated into the MEPDG because it runs much faster than the 3-D FE model.

Traffic Loads and Environmental Effects. Pavement structures are subjected to two types of external loads: traffic loads and environmental effects (e.g., frost action, temperature and moisture changes, etc.).

As traffic moves on the highway, a stress pulse is generated in the pavement structure. The magnitude, shape, and duration of the pulse varies with the wheel load, its speed, and the depth in the pavement at which the stress is considered *[19]*. Zaghloul et al. modeled traffic loads by translating the contact areas between the tires and the pavement surface on the FE

mesh and solved the resulting transient problem *[20]*. Simulations of a translating moving load need a 3-D FE model, which consumes considerable computational time. Since the loads are moving on the mesh, the distances between the loads and the mesh boundaries must be far enough to minimize the errors introduced in truncating the infinite domain. To overcome this issue, Kirkner et al. proposed an FE algorithm that was capable of predicting the residual stress state with the passes of moving loads on a layered elastic-plastic halfspace *[21]*, *[22]*. A similar algorithm was independently developed by Dang Van *[23]*. These algorithms are based on the fact that the problem can be simplified as a steady state if loads move at a constant speed. Thus, a moving coordinate system can be used. The displacements in the moving coordinate system can be viewed either in the time domain or in the space domain.

Although in reality a pavement undergoes a moving traffic load, a static analysis has been generally used instead of a dynamic analysis due to the theoretical and practical difficulties involved in dynamic analysis *[18]*. When the load is directly above the given point, the stress at this point is at its maximum, and when the wheel load is at a considerable distance from that point in the pavement, the stress at such point is zero. It is therefore reasonable to assume that the stress wave is either sinusoidal or triangular in shape with the load duration being dependent on the vehicle speed and the depth of the studied point *[19]*. Nazzal utilized a sinusoidal shape stress wave to simulate traffic loads in investigating the benefits of placing geogrids within the base course layer in a flexible pavement structure *[24]*. While Desai and Saad et al. utilized a triangular shape stress wave to simulate pavement traffic loads in their study *[8]*, *[19]*. Terrel et al. concluded that there is no significant difference in the magnitude of the total or resilient strains between the triangular and sinusoidal stress waves after intensive testing *[25]*.

The FE analysis of a pavement structure is a time-consuming process especially when a large number of load cycles are considered. Therefore, an accelerated analysis procedure is desired for an FE analysis involving a large number of load cycles. Desai and Whitenack *[26]* developed a procedure to accelerate the FE analysis based on the assumption that during the repeated load application, there was no inertia due to “dynamic” loading. In their procedure, the FE analysis was performed for only selected initial cycles (e.g., 10 or 20), then the growth of plastic strains after the initial cycles was evaluated by the “extension” based on an empirical relationship between plastic strains and the number of cycles obtained from laboratory test data. Desai later utilized this approach to predict the contours of disturbance around existing cracks in pavement structure after a million load cycles *[8]*.

Environmental factors (e.g., frost action, temperature, and moisture) also influence pavement behavior. Marek and Dempsey analyzed stresses and deflections in flexible pavement systems *[27]*. It was found that the location of the frost line in the pavement system greatly affected the vertical stress at the subgrade-subbase interface and the surface deflection. Chen et al. developed a regression equation for adjusting asphalt modulus at different temperatures based on falling weight deflectometer (FWD) test results *[28]*. Verhasselt and Choquet *[29]* developed a one-dimensional kinetic diffusion model to account for long-term aging effects on the properties of asphalt. Another aging model was developed by Mirza and Witczak for predicting the increase in asphalt viscosity with aging for Shell Oil category "S" (straight run) binders *[30]*. However, the compressed time period (usually several months) of an APT test tends to exclude environmental effects seen by in-service pavements. Nevertheless, the APT test results incorporating environmental effect models may be used to predict the long-term pavement performance in the future.

Constitutive Material Models. Constitutive models are essential components in a FE simulation. A constitutive model consists of a series of mathematical functions that define the stress-strain relationship of a particular material in a numerical model. A properly selected constitutive model should be able to capture key characteristics of the material behavior while being as simple as possible because a more complicated model often runs slower and requires more parameters to be determined. The constitutive models for pavement materials (e.g., asphalt concrete, unbound aggregate, cementitiously stabilized material, subgrade soil, etc.) have been studied by researchers for decades.

Asphalt concrete materials often exhibit rate-dependency and creep behaviors. Constitutive models developed for asphalt concrete materials are often based on theories of visco-elasticity or visco-elastoplasticity *[10], [31], [32], [33], [34]*.

For unbound pavement materials, the accumulation of permanent strain under repeated loads is a key characteristic of the behavior, which is related to the prediction of rutting. Conventional elastoplastic models with isotropic hardening (e.g., Drucker-Prager model and Mohr-Coulomb model) can only simulate the permanent strain of materials under a monotonic load *[21], [22]*. The stress-strain curve from a conventional elastoplastic model with an isotropic linear-strain hardening is shown in Figure 1. Under repeated loading, these models become less effective. Plastic strains would not be generated after the first repetition if the load level is not increased. The stress-strain curve of the conventional elastoplastic model under repeated loads is shown in Figure 2.

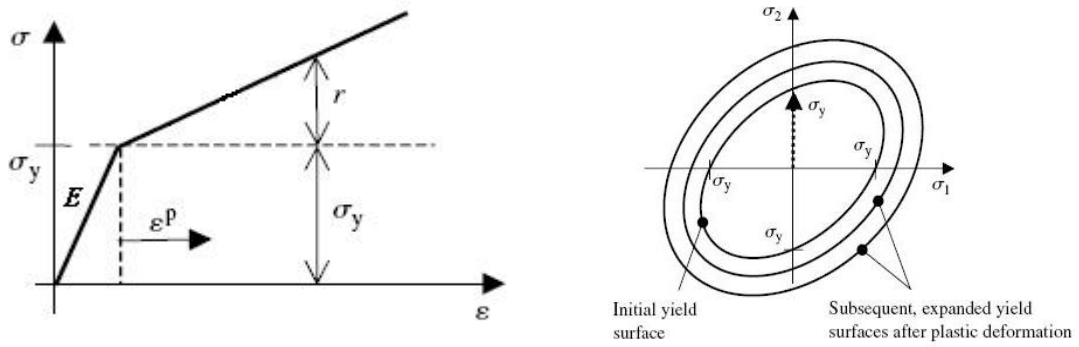

(a) Stress-strain curve for linear strain hardening **(b) Isotropic hardening**

Figure 1
Conventional elastoplastic model with linear isotropic strain hardening *[35]*

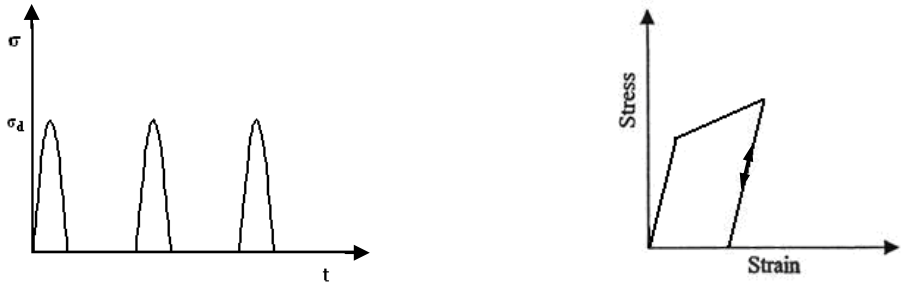

(a) Repeated loading **(b) Schematic results by conventional Elastic-plastic model**

Figure 2
Stress-strain behavior of a conventional elastoplastic model under repeated loading

A number of more sophisticated elastoplastic constitutive models were developed based on advanced plasticity theories, such as kinematic hardening, bounding surface plasticity, disturbed state concept, and shakedown theory. These constitutive models are generally able to simulate the accumulation of permanent strain under repeated loads. Elastoplastic models with kinematic hardening have been available since the 1970s but have only recently been applied to pavement modeling *[36]*. The bounding surface plasticity was originally developed by Dafalias and then extended by Dafalias and Hermann for modeling isotropic cohesive materials *[36]*, *[37]*, *[38]*. Yu et al. presented a unified bounding surface plasticity theory for modeling the stress-strain behavior of sand and clay under both drained and undrained cyclic loading conditions *[39]*. Yang and Elgamal developed a multi-surface

plasticity model for cohesionless granular materials in which the Lade-Duncan failure criterion was employed as the yield function *[40]*. Manzari and Dafalias developed a two-surface plasticity formulation in the deviatoric stress-ratio combined with the state parameter ψ arising within the critical state soil mechanics (CSSM) framework to yield a comprehensive multiaxial constitutive model for sands *[41]*. Hau et al. presented a three-surface kinematic hardening model to simulate the behavior of thinly surfaced pavements dominated by the clay subgrade *[42]*. Desai and his co-workers developed the Hierarchical Single Surface (HiSS) plasticity model, which is able to simulate elastic, plastic and creep strains, microcracking, damage and softening, cyclic fatigue failure, and stiffening under thermomechanical and environmental loadings *[43]*. Bonaquist and Witczak used the HiSS model to predict the permanent deformation response of granular materials in flexible pavements *[44]*. Huang et al. developed a thermo-viscoplastic constitutive model based on the HiSS model for hot mix asphalt mixtures *[45]*. In general, implementing these advanced elastoplastic models often requires more material parameters to be determined. For example, in the permanent deformation analysis of asphalt concrete materials, the HiSS model requires more than 14 model parameters related to mixture properties from several non-routine laboratory tests.

Very limited studies were found in the literature on the numerical simulation of chemically stabilized materials in flexible pavements. Heymsfield et al. utilized a damage model to simulate the behavior of 6 percent soil-cement mixtures under unconfined-compression tests with both monotonic and cyclic loading *[46]*. The damage model was originally developed by Valanis *[47]*. It was found that Valanis' damage model accurately captured the softening behavior of soil-cement mixtures under repeated loading. However, the plastic behavior was not considered in this damage model. Heymsfield et al. then made several modifications to Valanis' damage model: (1) unloading occurs linearly by using the material's initial Poisson's ratio; (2) material hardening during the first cycle results in residual strain and an increased elastic modulus; and (3) plastic strain increases linearly in the axial and radial directions *[48]*. Comparison showed that the modified Valanis' model better simulated the unconfined compression test results on the soil-cement samples. However, because of the limited axial strain range, the damage model does not correctly capture how much the material stiffness decreased in the radial direction *[48]*. In addition, the modified model assumed that plastic strain increases linearly in the axial and radial directions, which is inconsistent with the permanent deformation development observed from laboratory or field tests in which the permanent deformation increases more dramatically at the beginning of the test and then reaches a steady state *[49]*, *[50]*.

Permanent Deformation (P-D) Test on Stabilized/Treated Materials

The development of permanent deformation under repeated loads is an important behavior of pavement materials. The P-D test has been widely accepted to characterize the permanent deformation behavior of pavement base and subbase/subgrade materials *[49]*, *[51]*, *[52]*, *[53]*.

A P-D test was reported by Mohammad et al. in their study of laboratory characterization of rutting potential for different base and subgrade materials *[49]*. It was basically a repeated load test inside a triaxial load cell mounted in the Material Testing Systems (MTS) machine (Figure 3). During the test, a haversine load pulse of 0.1-sec. loading and 0.9-sec. resting was applied to the cylindrical sample for 10,000 repetitions, and the permanent strains that developed in the sample were continuously recorded. For base materials, a confining stress of 5 psi and a vertical stress of 15 psi were used. For subgrade materials, either treated or untreated, a confining stress of 2 psi and a vertical stress of 6 psi were used. The dimension of the cylindrical samples for base materials was 6 in. in diameter and 12 in. in height. For subgrade materials, the samples were 2.8 in. in diameter and 5.6 in. in height.

Figure 3
Setup of a permanent deformation (P-D) test

It is well recognized that for a granular material, both resilient and permanent deformations occur even under a small stress level. The stress-strain relationship is generally a nonlinear curve. Figure 4 presents a typical stress-strain curve in a P-D test. As shown in the figure, the stress-strain relationships are hysteretic loops with decreasing areas indicating energy absorption, or damping, during each complete cycle of stress reversal *[54]*. The hysteretic curve changes in each cycle more dramatically in the beginning of the test and then reaches a steady state. The dissipated energy (area enveloped by hysteretic curve) brings changes to its properties through microstructural adjustment and leads to strengthening or damaging effects to the material depending on loading levels and its initial conditions (e.g., void ratio and moisture content). As a result, a small amount of permanent strain (or plastic strain) is developed under each load repetition, which then accumulates into a larger, more visible surface permanent deformation.

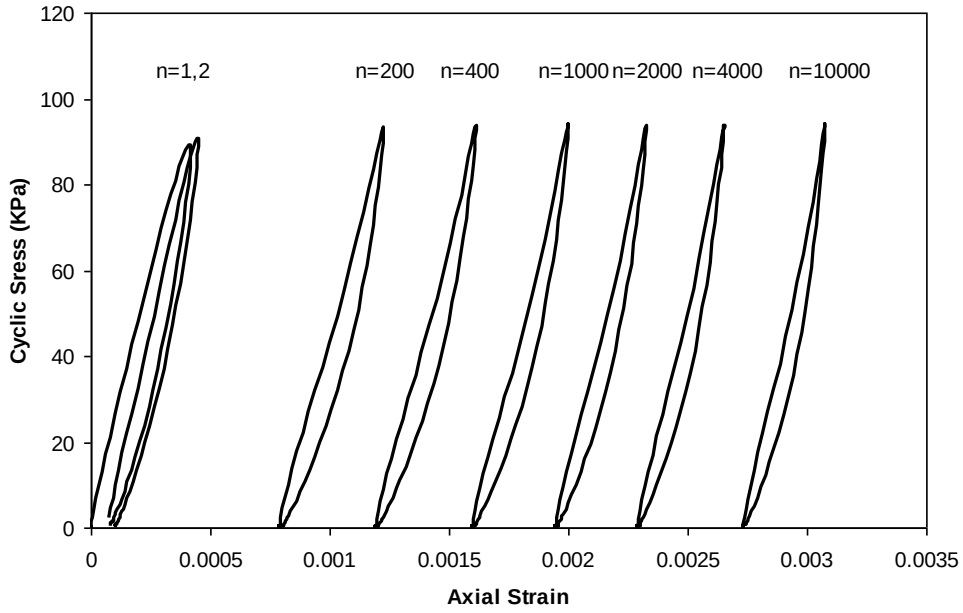

Figure 4
An example of the stress-strain curve in a P-D test

OBJECTIVE

The objective of the research was to develop a finite element model(s) to simulate pavement structural performance of stabilized base and treated subbase materials under accelerated loading, so that the performance of pavement structures with other stabilized base and subbase materials can be predicted without running additional APT tests. Validation of the developed finite element model(s) was focused on applying the results obtained from LTRC Project No. 03-2GT, or ALF Experiment 4, in which six flexible pavement sections with different types of stabilized bases and subbases were tested.

SCOPE

Three FE models were preliminarily developed to simulate pavement under APT loading: a 3-D model with a simulated moving load, a 3-D model with repeated loading, and an axisymmetric model.

A P-D material model was proposed for simulation of permanent deformation of pavement base and subgrade materials under repeated loading. The P-D test data analysis spreadsheet by Excel Macro (VBA) was developed to obtain these model parameters. The proposed P-D material model was implemented into a commercial FE program, ABAQUS, through a user-defined UMAT subroutine. Verification of the P-D model was conducted by FE simulation of laboratory P-D tests for eight materials: (1) base materials: limestone, blended calcium sulfate (BCS, a by-product of hydrofluoric acid) treated with ground granulated blast furnace slag (BCS/Slag), BCS treated with class C fly ash (BCS/Fly ash), foamed-asphalt treated blend of 50 percent recycled asphalt pavement (RAP) with 50 percent soil cement (FA50), and foamed-asphalt treated with 100 percent RAP (FA100); (2) subbase materials: lime treated soil and cement treated soil; and (3) subgrade. In addition, a sensitivity analysis was conducted to evaluate the effect of material model parameters, pavement structures, and load configurations on permanent deformation in pavement structures.

The axisymmetric and 3-D FE models with proposed material models are first developed to simulate the performance of six pavement sections used in ALF tests. Based on the preliminary APT simulation results, a suitable FE model is then selected to predict the permanent deformation of the six ALF test sections with four ALF load levels. In addition, the developed FE simulation method will be applied in the predation of permanent deformation for pavement with other stabilized materials (e.g., lime/fly ash). Also, the developed FE model is applied to predict the permanent deformation of two typical low volume pavement structures used in Louisiana.

Finally, the APT test calibrated FE model was used to develop P-D prediction models (transfer function) for pavement base and subbase/subgrade materials (e.g., stabilized base materials, unbound base materials, treated subbase/subgrade materials, and untreated subgrade soils). The developed P-D transfer functions were verified by predicting the six APT sections and two typical low volume pavement structures.

METHODOLOGY

This section contains two parts. The first describes the development, verification, and calibration of the finite element (FE) model, and the second describes the development of the P-D prediction model (transfer functions).

FE Model for the Permanent Deformation of Pavement Structures

FE models and the P-D material model are developed to simulate the permanent deformation of six APT test sections. These APT tests were conducted at LTRC's Pavement Research Facility. The APT results indicated that these test sections mainly failed due to excessive surface rutting *[50]*.

FE Model and the Effect of the Dimensionality

A commercial FE analysis software, ABAQUS, was employed to develop FE models. Three FE models were preliminarily developed to study the effects of the dimensionality: a 3-D model with a moving load, a 3-D model with a repeated load, and an axisymmetric model with a repeated load.

Three-Dimensional (3-D) Model with a Moving Load. Figure 5a shows the geometry of a 3-D model for an APT section. The section is 100-ft. long, while the length of loading portion is 39 ft. The width and the depth of the section are both 13 ft. The depth of the model is selected based on the maximum induced vertical stress at the subgrade bottom, which should be less than 0.5 percent the applied load. Due to the symmetry of the problem, only half of the test section is modeled. The FE model includes four layers: a 2-in. HMA layer, an 8.5-in. base layer, a 12-in. subbase layer, and a subgrade layer. The 20-node quadratic brick reduced integration elements (C3D20R) are selected in the FE model. Kinematic boundary conditions were applied as the horizontal movement along the vertical boundaries as well as horizontal and vertical movements along the bottom boundary were restrained by roller supports. Figure 5b presents the mesh of the FE model. A total of 19,000 elements are adopted in the model based on a mesh sensitivity analysis.

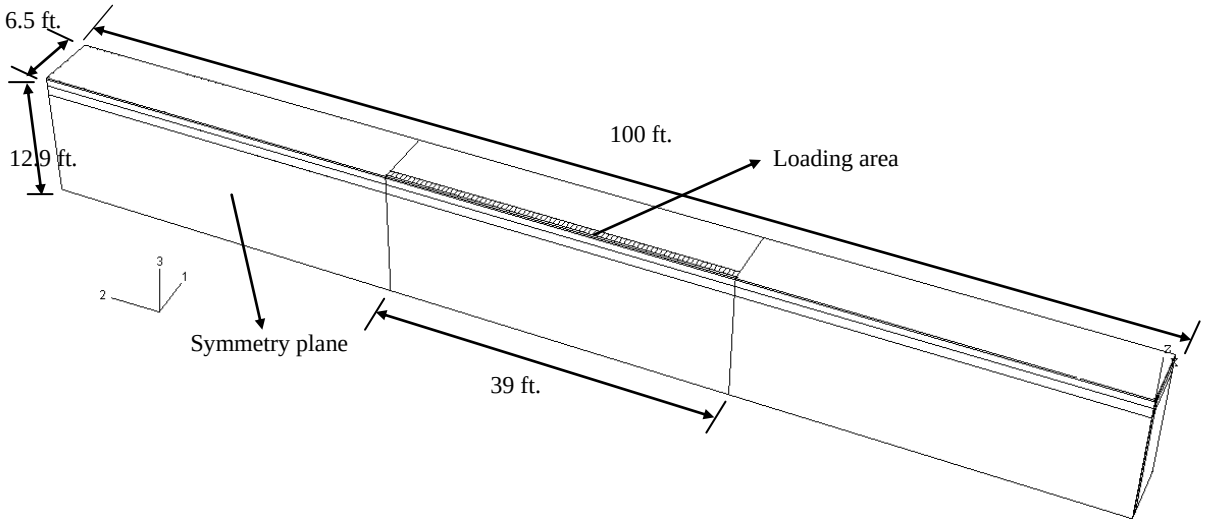

(a) Schematic geometry of ALF FE model

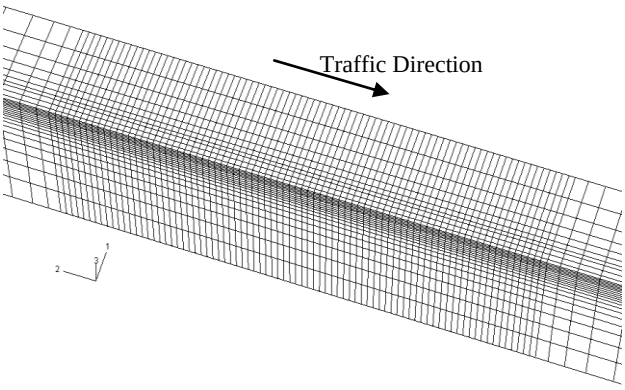

(b) 3-D finite element mesh

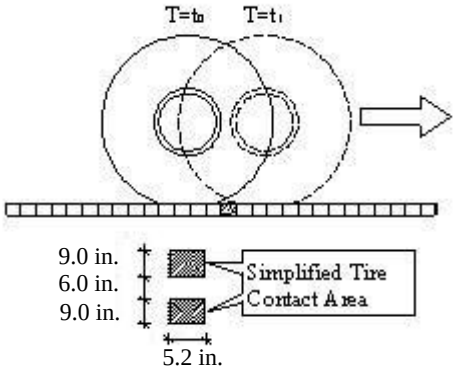

(c) Schematic moving load

Figure 5
3-D model with a moving load

As shown in Figure 5c, the tire imprint area is simulated as two rectangular shapes. In the step load function, the tire pressure was applied as a load amplitude function to the first set of elements in the wheel path for the time period. Subsequently, the load function was manually applied to the next set of elements. When the load step function was applied to the last set of elements, a single wheel pass was completed. No dynamics effect was considered during the moving load simulation. A similar approach was used by Zaghloul et al. *[20]*.

Three-Dimensional (3-D) Model with a Repeated Load. In this model, a repeated load with a triangular shape was applied at the same location to simulate the APT loading in the FE model (as shown in Figure 6b). Since the loading location did not change in this model, the FE model can be further reduced to a quarter of the problem since there were two axes of symmetry. Furthermore, the length and width of model was reduced to 6.5 ft. (as shown in Figure 6a). The depth of the model was 13 ft. Layer thicknesses and material parameters were the same as the 3-D FE model with a moving load. The APT wheel load is simulated as a triangular-shape repeated load applied on a rectangle area with a peak value of 105 psi. Kinematic boundary conditions were applied as the horizontal movements along the vertical boundaries as well as horizontal and vertical movements along the bottom boundary were restrained by roller supports.

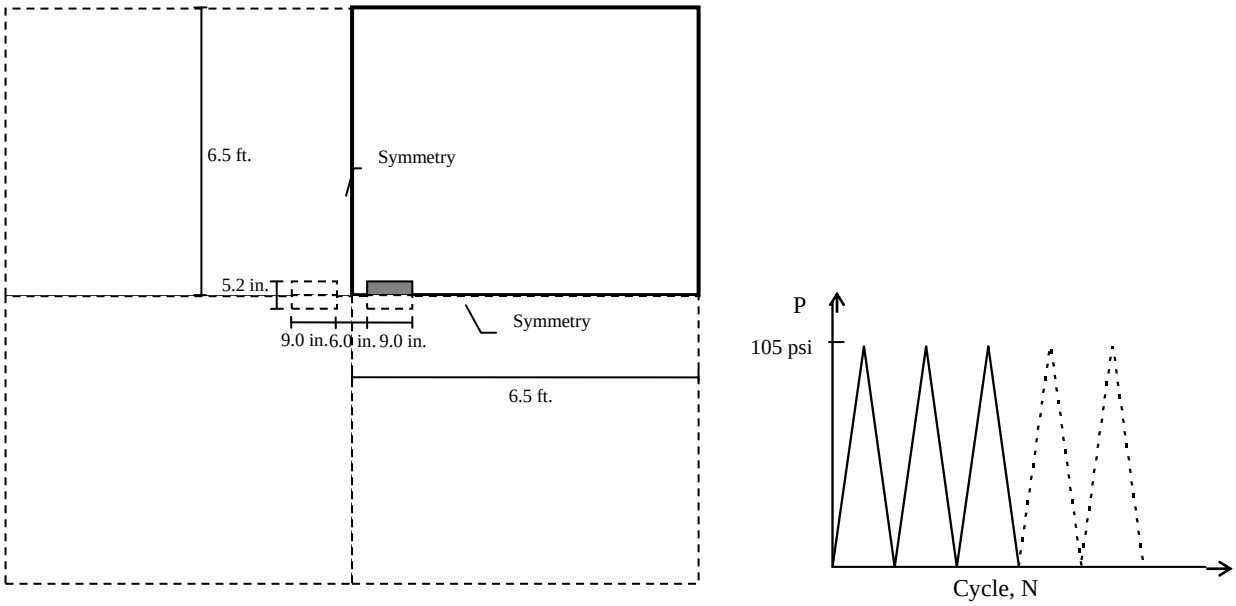

(a) Plane geometry **(b) Schematic repeated load**

Figure 6
3-D quarter-symmetric model with a repeated load

Based on the mesh sensitivity analysis, the mesh with a total of 4,752 elements was selected for the 3-D model with a repeated load. Figure 7 presents the mesh and boundaries of the developed model.

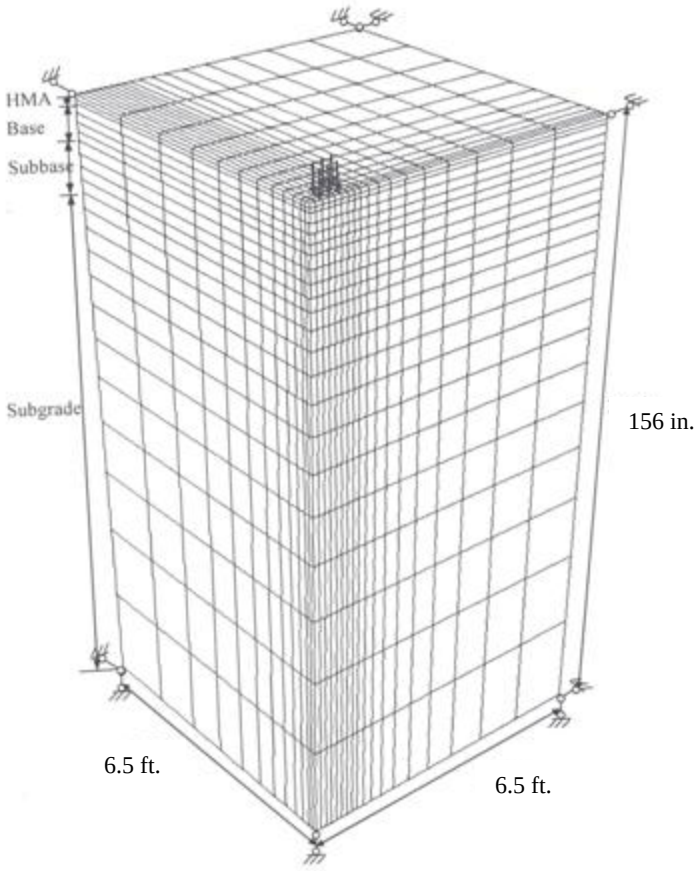

Figure 7
Mesh and boundaries of the 3-D quarter-symmetric model for APT tests

Axisymmetric Model with a Repeated Load. The axisymmetric FE model has a radius of 6.5 ft. and total depth of 13 ft. The layer thicknesses and material parameters were the same as the 3-D FE models. The eight-node biquadratic axisymmetric quadrilateral elements (CAX8R) are selected in the numerical model. Kinematic boundary conditions were applied as the horizontal movements along the two vertical boundaries as well as the horizontal and vertical movements along the bottom boundary were restrained by roller supports. The APT wheel load is simplified into a triangle-shape repeated load on a circular area with a peak value of 105 psi. Figure 8b presents the mesh of the axisymmetric model for APT tests.

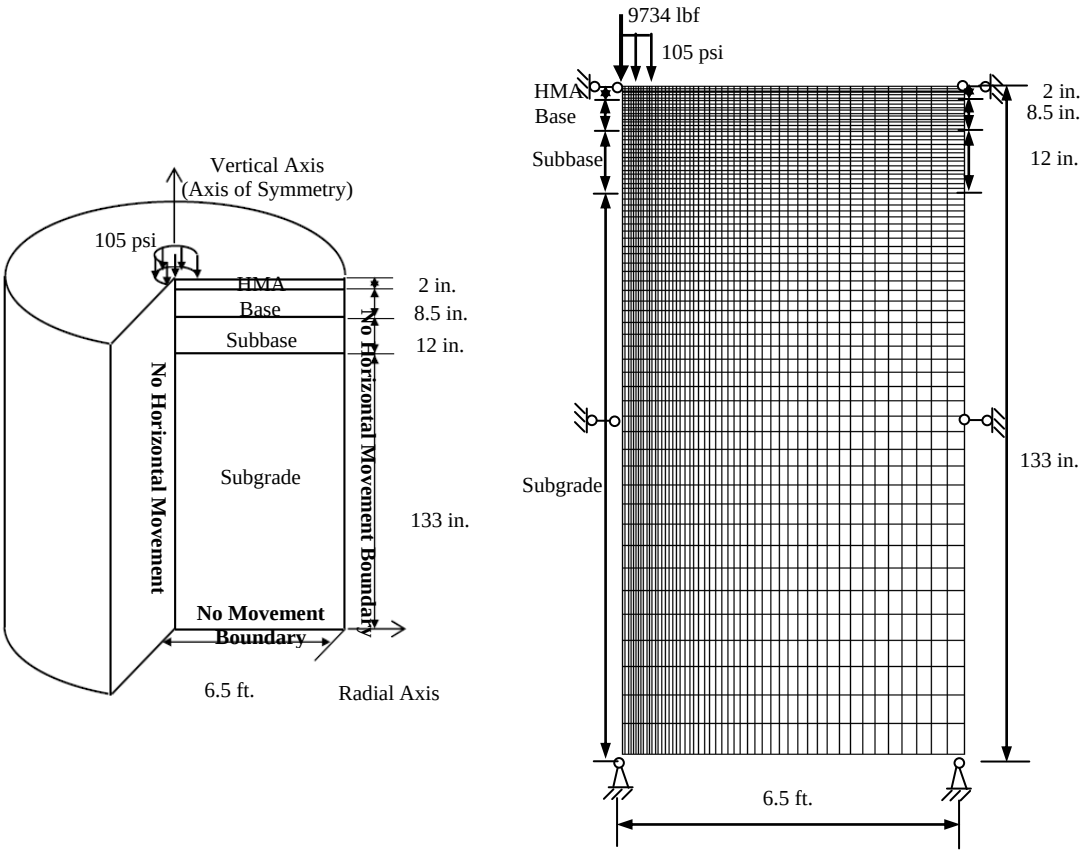

(a) Axisymmetric model **(b) Mesh of axisymmetric model**

Figure 8
Axisymmetric model for APT tests

Permanent Deformation (P-D) Model

Since no material model has been explicitly reported for the permanent deformation prediction of stabilized pavement materials, a P-D model is proposed in this study to simulate the permanent deformation behavior of flexible pavement materials, especially base and subbase/subgrade materials.

Development of P-D Model. The proposed P-D model was developed based on a general observation obtained from P-D test results (as shown in Figure 4) in which the unloading stress-strain path is usually steeper than the loading path during the same load cycle. It was also observed that the stress-strain behavior of the sample during the first load cycle is often considerably different from that during the following cycles, depending on the level of deviatoric stress applied in a P-D test. In the proposed model, the pavement material

is modeled as linear elasto-plastic during the first load cycle and linear elastic during the following cycles of loading/unloading.

During the first cycle of loading/unloading, the pavement material is modeled using a conventional elastoplastic model with the Von Mises yield criterion and linear strain hardening. The Von Mises yield criterion is expressed in equation (1):

$$f = \sigma_e - \sigma_y = \left(\frac{3}{2}\boldsymbol{\sigma}' : \boldsymbol{\sigma}'\right)^{\frac{1}{2}} - \sigma_y \tag{1}$$

where, σ_y is the initial yield stress, σ_e is the Von Mises stress, and $\boldsymbol{\sigma}'$ is the stress deviator tensor, $\boldsymbol{\sigma}' = \boldsymbol{\sigma} - \frac{1}{3}Tr(\boldsymbol{\sigma})\boldsymbol{I}$, in which $\boldsymbol{I}$ is the second order identity tensor.

The linear strain hardening function is defined as in equation (2):

$$\varepsilon^p = \frac{\sigma - \sigma_y}{h_c} \tag{2}$$

where, h_c is the hardening constant, and ε^p is the plastic strain.

Under uniaxial stress conditions, the slope of the stress-strain curve after initial yielding can be derived as:

$$\frac{d\sigma}{d\varepsilon} = E\left(1 - \frac{E_L}{E_L + h_c}\right) \tag{3}$$

If no initial yielding occurs during the first load cycle, a material element is considered to stay in the elastic range, and no plastic strain will be predicted. If initial yielding occurs during the first cycle, the element is then modeled as a linear elastic material with different loading and unloading moduli during the subsequent load cycles. By varying the elastic moduli of the material in each load cycle, a hysteresis loop observed in a P-D test can be approximated the by a series of scalene-triangle shaped open loops (as illustrated in Figure 9) without implementing complicated elastoplastic models. As shown in Figure 9, the unloading modulus is larger than the loading modulus in the same load cycle. The difference between the strain developed during loading and the strain recovered during unloading is the plastic strain accumulated in a particular load cycle. The concept of simulating the hysteretic stress-strain response by varying the elastic moduli of the material at each individual load cycle was also accepted by Yandell and Uzan *[*55*], [56]*.

Under uniaxial stress conditions, as shown in Figure 9b, the permanent strain ε_1^p developed in the first load cycle (n=1) can be written as:

$$\varepsilon_1^p = \varepsilon_1^p + \varepsilon_1^p = \frac{\sigma - \sigma_y}{h_c} + \left(\frac{d_1 - 1}{d_1}\right)\frac{\sigma}{E_L(n=1)} \tag{4}$$

where, $E_L(n=1)$ is the secant loading modulus in the first cycle, and d_1 is the secant modulus ratio between unloading and loading moduli in the first cycle $\frac{E_{UL}(n=1)}{E_L(n=1)}$.

From the second load cycle, the permanent strain will develop continuously due to the difference between the loading and unloading moduli. For the nth (n ≥ 2) cycle, the following equations can be derived:

$$\varepsilon_n^t = \varepsilon_n^p + \varepsilon_n^r \tag{5}$$

$$d_n = \frac{E_{UL}(n)}{E_L(n)} = \frac{\sigma/\varepsilon_n^r}{\sigma/\varepsilon_n^t} = \frac{\varepsilon_n^t}{\varepsilon_n^r} = \frac{TE}{DE} \tag{6}$$

$$\varepsilon_n^p = \left(\frac{d_n - 1}{d_n}\right)\frac{\sigma}{E_L(n)} \tag{7}$$

where, ε_n^t, ε_n^p, and ε_n^r are respectively the total, permanent, and resilient strains at the nth load cycle, $E_L(n)$ and $E_{UL}(n)$ are the loading modulus and unloading modulus in the nth load cycle, d_n is the ratio between $E_{UL}(n)$ and $E_L(n)$, TE is total energy induced during loading in the , and DE is dissipated energy during unloading.

By combining equations (4) and (7), the accumulative permanent strain can be written as:

$$\varepsilon_p(n) = \frac{\sigma - \sigma_y}{h_c} + \sum_{i=1}^{n}\left(1 - \frac{1}{d_i}\right)\frac{\sigma}{E_L(i)} \tag{8}$$

where, $\frac{1}{d_i} = \frac{DE}{TE}$ is the damping factor, which is the dotted area in the loop divided by the hatched area under the loading line (Figure 9c).

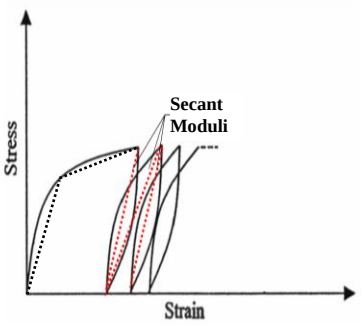

(a) Stress-strain curve under repeated loading

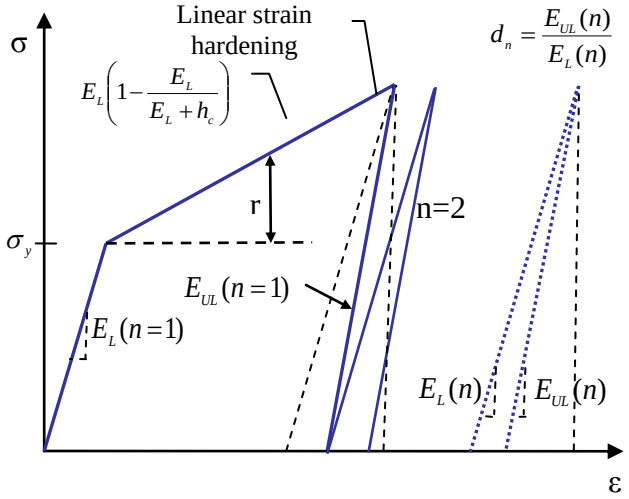

(b) Schematic representation of proposed model

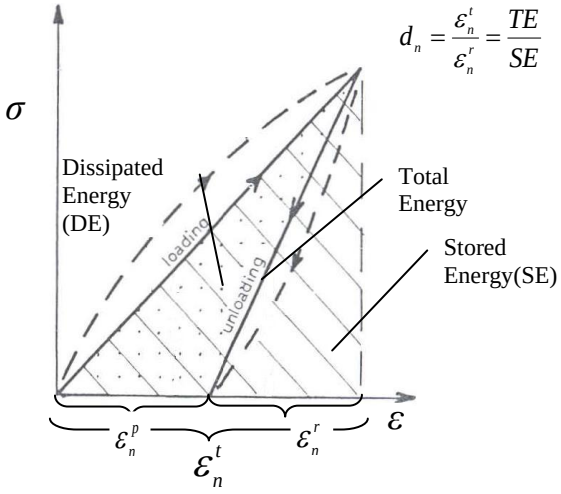

(c) Schematic representation of hysteresis loop

Figure 9
Schematic representation of the proposed P-D model

An example of determining the model parameters from the P-D test data are illustrated in Figure 10. The initial yield stress σ_y and the hardening constant h_c can be determined from the first cycle of loading (Figure 10a). The loading secant modulus E_L usually changes slightly with the number of load repetitions n. Thus a constant E_L (average value is taken) is assumed (Figure 10c). The modulus ratio d_n can be determined at each selected loading

repetition (Figure 10b). From the P-D test data (Figure 10d), d_n decreases with the load cycle n. The following function can be used to fit the variation of d_n with the number n:

$$d_n = \frac{E_{UL}(n)}{E_L} = \frac{a}{n^b} + 1 \tag{9}$$

where, *a* and *b* are the permanent deformation parameters. More details about *a* and *b* are provided in Appendix B.

A spreadsheet with a VBA Macro was developed in this study for determining model parameters from the P-D test data. The details of the spreadsheet are presented in Appendix C.

In 2-D and 3-D FE analyses, the proposed P-D model was incorporated into a commercial finite element program, ABAQUS, through a user-defined UMAT Subroutine *[57]*.

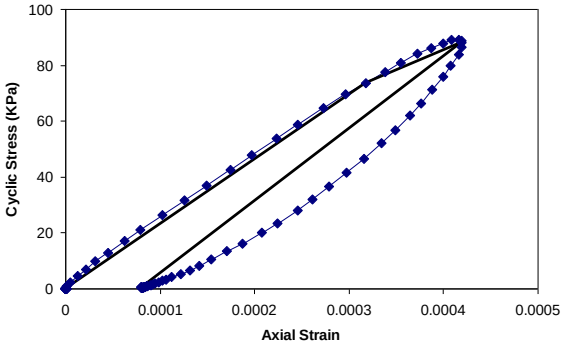

(a) First cycle of stress-strain curve

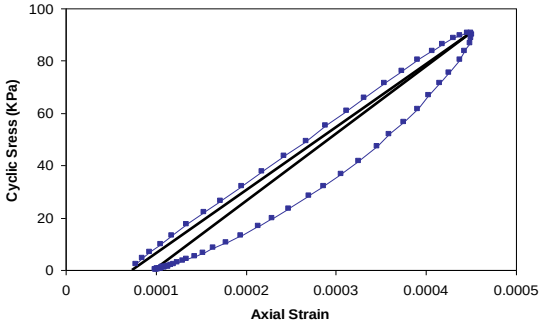

(b) Subsequent cycle of stress-strain curve

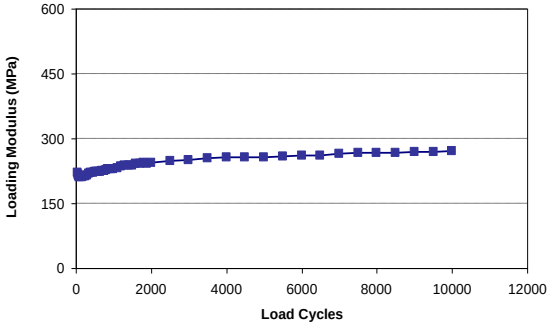

(c) Loading modulus E_L

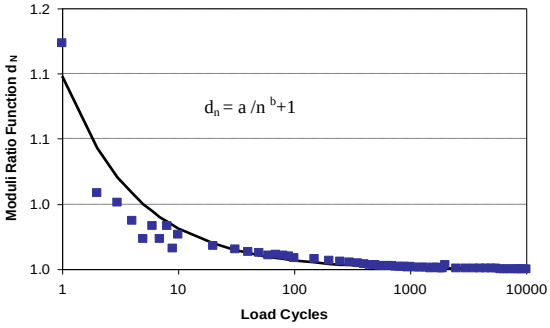

(d) Modulus ratio function d_n

Figure 10
An example of determining input parameters for the P-D model (1 psi = 6.894 kPa)

Verification of the Proposed P-D Model with Laboratory Tests. Laboratory P-D test data on eight pavement materials were used to verify of the proposed P-D model. An axisymmetric FE model (shown in Figure 11) was created to simulate the cylinder sample in a P-D test. For simplicity, this model was created with a single CAX8R element. Since the Von Mises yield criterion is a function of deviatoric stress (i.e., $\sigma_1 - \sigma_3$ in two an axisymmetric stress condition), only a vertical deviatoric stress was applied. Such a simplification will not change the predicted permanent strain results.

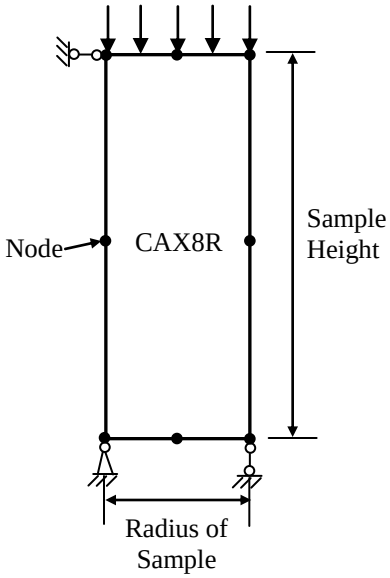

Figure 11
FE model for a P-D test

The eight tested pavement materials were (1) five base materials: limestone, BCS treated with ground granulated blast furnace slag (BCS/Slag), BCS treated with class C fly ash (BCS/Fly ash), foamed-asphalt treated blend of 50 percent recycled asphalt pavement (RAP) and 50 percent soil cement (FA/50RAP), and foamed-asphalt treated with 100 percent RAP (FA/100RAP); (2) two subbase materials: lime treated soil and cement treated soil; and (3) one subgrade material.

Sensitivity Analysis of Proposed P-D Model. After the proposed P-D model was verified with various pavement materials, a sensitivity analysis of pavement structures was conducted to evaluate the effect of material model parameters and pavement structures on the permanent deformation. The sensitivity analysis can help (1) understand how the permanent deformation prediction results will be affected by various input parameters and pavement

structures, (2) identify the significance of design or parameter for the pavement permanent deformation, and (3) aid engineers or researchers in using this model more easily.

A series of axisymmetric FE models were created to conduct the sensitivity analysis. The modeled pavement consisted of three layers: HMA, base, and subgrade. A triangle-shape repeated load on a circular area with a maximum value of 105 psi was applied. The proposed P-D model was used to simulate the HMA and the base layers, and an elastic model was used for the subgrade layer. The permanent deformation of the base layer after 30 cycles was used to analyze the sensitivity of structure thickness and material parameters to the permanent deformation. Six factors were selected to perform the sensitivity analysis (as listed in Table 1). These factors included HMA layer thickness, base layer thickness, base layer material loading modulus, and base layer permanent deformation parameters *a* and *b*.

Table 1
Selected factors and the corresponding levels for the sensitivity analysis

Level	Factor and their levels					
	P1	P2	P3	P4	P5	P6
	HMA Thickness (in.)	Base Thickness (in.)	Base Loading Modulus (ksi)	Subgrade Modulus (ksi)	Base Layer Permanent Deformation Parameter *a*	Base Layer Permanent Deformation Parameter *b*
1	2	6	25	5	0.003	0.7
2	6	9	75	10	0.1	0.57
3	10	12	125	15	0.2	0.45

The Taguchi method was employed to design the sensitivity analysis. The Taguchi method was developed as a process optimization technique by Genichi Taguchi in 1950s *[58]*. The Taguchi method utilizes a partial factorial design. Only a small fraction of all the possible combinations of interested factor levels need to be tested. Standard tables known as orthogonal arrays (OAs) are used for the design of the analysis in the Taguchi method, and the analysis of variation (ANOVA) is used to examine the relative significance of each of the factors. Based on the factors and their levels in Table 1, a total of 18 simulations were conducted for the sensitivity analysis.

The effect of load level on the permanent deformation of pavements was also investigated. Four different load levels used in APT tests were applied to the FE model. Table 2 shows that under different wheel loads, the contact area varied while the tire pressure was kept constant.

Table 2
Load parameters in the FE model for different APT load levels

Load Levels	ALF Load-I	ALF Load-II	ALF Load-III	ALF Load-IV
Load (lbf)	9,750	12,050	14,350	16,650
Pressure (psi)	105	105	105	105
Load Radius (in.)	5.44	6.04	6.60	7.10

FE Simulation of APT Tests

The six tested APT sections have the same pavement structure thickness but with various base and subbase materials. Table 3 presents the pavement structures of the APT sections.

Table 3
Pavement structures and materials of the APT sections

Section	4-1A	4-2A	4-1B	4-2B	4-3A	4-3B
2-in. HMA	Superpave -19					
8.5-in. Base	BCS/Slag	BCS/Fly ash	Limestone	Limestone	FA/50RAP	FA100/RAP
12-in. Subbase	Lime-treated Soil			Cement-treated Soil		
Subgrade	A-4					

Material Parameters of APT Sections. The proposed P-D model was applied to all pavement layers in six APT test sections. Model parameters for base, subbase, and subgrade materials were determined from laboratory P-D tests. The model inputs for the HMA layer were carefully selected by a trial-and-error process so that the calculated rut depths of the HMA layer were considerably small, similar to the field observation.

For the crushed limestone base, the in-situ modulus is stress-dependent and can be affected by the modulus of its supporting subbase layer. In this study, the laboratory determined loading modulus for limestone was modified by a modulus ratio, which was determined from falling weight deflectometer (FWD) test results *[50]*.

Temperature also has a significant effect on the modulus of asphalt materials. In this study, the loading elastic moduli of asphaltic layers (the HMA and foamed asphalt base layers) are adjusted at every 25,000 load repetitions based on the average pavement temperatures using the following model *[28]*:

$$E_{T_w} = E_{T_c}/[(1.8T_w + 32)^{2.4462} \cdot (1.8T_c + 32)^{-2.4462}] \quad (10)$$

where, E_{T_w} is the adjusted modulus of elasticity at T_w, MPa; E_{T_c} is the measured modulus of elasticity at T_c, MPa; T_w is the temperature to which the modulus of elasticity is adjusted, ºC; and T_c is the mid-depth temperature at the time of FWD data collection, ºC.

Accelerated Analysis Procedure. The FE analysis of a pavement structure is a time-consuming process especially when dealing with a large number of load cycles. Therefore, an accelerated analysis procedure is desired. In this study, an accelerated analysis procedure introduced by Desai was accepted *[59]*. The step by step procedures are described as follows:

(1) Determine material parameter B from the laboratory permanent deformation test result (as shown in Figure 12a);
(2) Run the numerical model up to the reference number N_r cycle of loading and unloading; and
(3) Extrapolate the permanent deformation curve obtained from the numerical model for each pavement layer based on equation (11) (as shown in Figure 12b).

The reference number N_r is determined by plotting permanent deformation against the number of cycle in a Log-Log scale and then selecting the point where the slope of the curve approximately equals to B.

$$PD(N) = PD(N_r)\left(\frac{N}{N_r}\right)^B \tag{11}$$

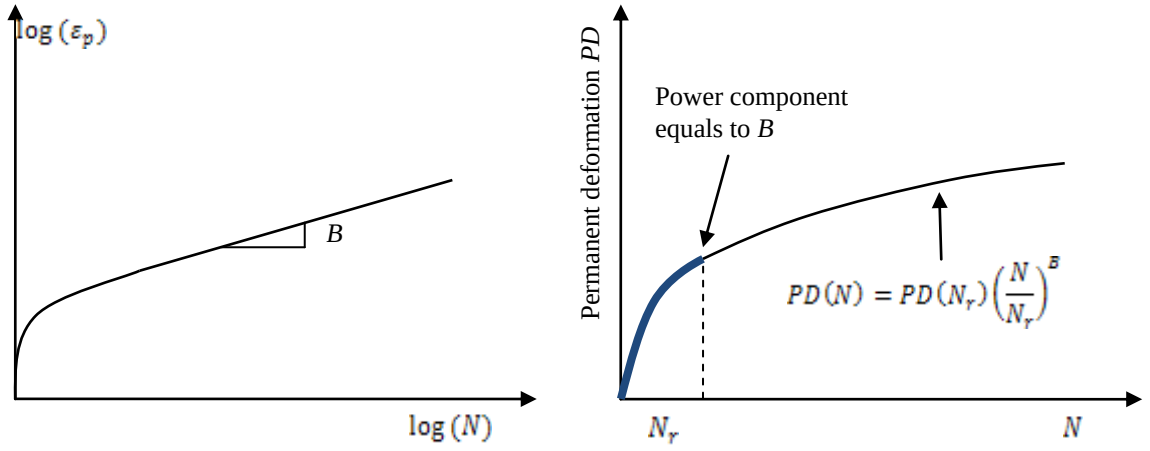

(a) Obtain *B* from permanent deformation test curve

(b) Extrapolate the numerical result

Figure 12
Schematic diagram of accelerated analysis procedure

The approach of predicting rutting progress under different temperatures is presented in Figure 13 (three temperatures are used for demonstration purposes). Temperature I, II, and III are the average temperatures measured in the pavement during load cycles 0 to 25,000, 25,001 to 50,000, and 50,001 to 75,000, respectively. As shown in Figure 13, permanent deformation curves under Temperature I, II, and III can be calculated using the accelerated analysis procedure. The predicted rutting for the first 25,000 load passes under Temperature I is represented by segment OA. The predicted rutting during load passes 25,001 to 50,000 can be found on curve Temperature II by locating point A', which has the same rut depth as point A. Segment A'B' represents the rutting development of the following 25,000 load cycles start from point A' under Temperature II. Segment A'B' is then translated horizontally to connect with the point A (as shown in segment AB). Similarly, the predicted rutting during load passes 50,001 to 75,000 under Temperature III can be found by moving segment B"C" horizontally to BC. The curve OABC will be the predicted rut progress under the three different temperatures.

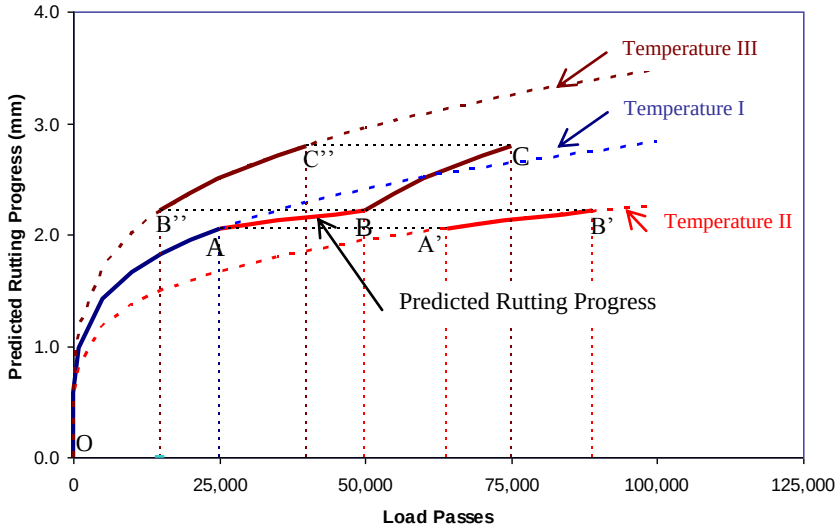

Figure 13
Approach of predicting asphaltic materials rutting progress under different temperatures (1 in. = 25.4 mm)

Different ALF Load Levels. Four different load levels were used in the APT tests (as listed in Table 4). In this study, the permanent deformation curves under different load levels were first predicted separately in different FE simulation models with an accelerated analysis procedure, and then were connected at the cycle where the load level is changed. It should be noted that the deformed mesh at the end of simulation cycles under one load level will have some effects on the subsequent prediction results under another different load level. To investigate such effects, limited cycles of FE analysis were conducted on both un-deformed and deformed mesh boundary conditions. As shown in Figure 14, the un-deformed initial boundary results are a connection of separate FE analysis results under Load I, II, and III; whereas, the deformed initial boundary results are obtained by applying different load levels in one FE analysis mesh model. The permanent deformation with deformed initial boundary is found slightly smaller (about 2 percent) than that with un-deformed initial boundary after three different load levels applied. This small difference was considered acceptable in this study when the accelerated analysis procedure was used.

Table 4
Different load levels applied for APT sections

Load Repetitions	Load Level	Load (lbf)	4-1A	4-2A	4-1B	4-2B	4-3A	4-3B
1-175,000	ALF_Load I	9,750	+	+	+	+	+	+
175,001-225,000	ALF_Load II	12,050	+	+	—	+	+	+
225,001-325,000	ALF_Load III	14,350	+	+	—	+	+	—
325,001- Fail	ALF_Load IV	16,650	+	+	—	—	—	—

Note: "+" means applied load level for APT sections;
"—"means not applicable.

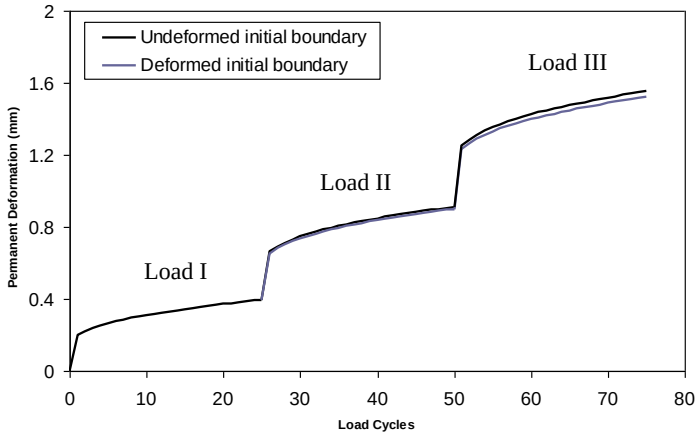

Figure 14
Predicted permanent deformation with un-deformed and deformed initial boundaries (1 in. = 25.4 mm)

Effect of Load Wander on Permanent Deformation. A normally distributed load wander was configured in the APT tests. Figure 15 presents the wander frequency distribution.

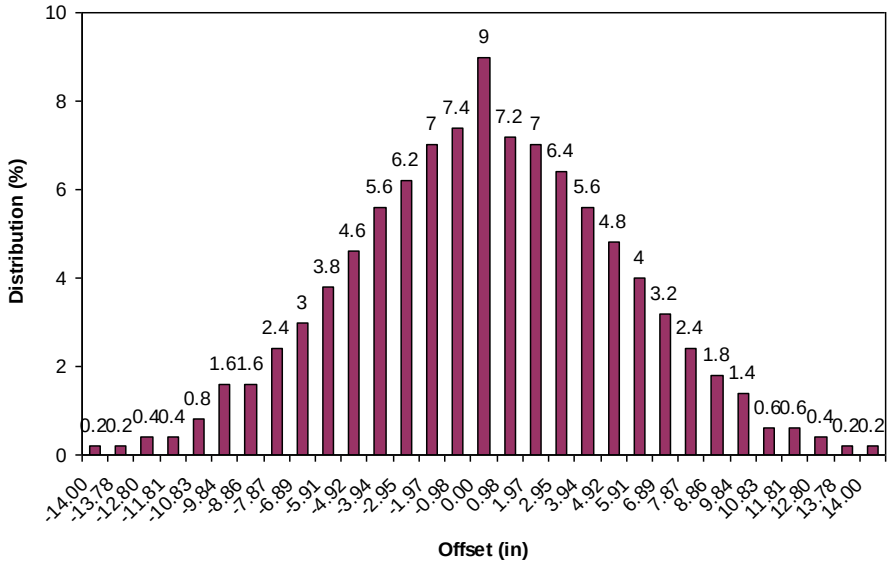

Figure 15
Load frequency of wander used at APT tests

The surface rut depths at the model central line with different load wander offsets were calculated for each section with four different load levels. In this study, the wander adjustment factor (ratio of rut depth with wander over the rut depth without wander at the central line) was calculated by the following equation:

$$R = \sum F_x \times D_x \tag{12}$$

where, R is the wander adjustment factor, x is the load offset from the center line, F_x is the load frequency with offset x, and D_x is the ratio of rut depth with load offset x over the rut depth without load offset.

Shift Factor for the Predicted Permanent Deformation. Because of the complex nature of a pavement structure and loading conditions, the FE simulation results based on the laboratory determined material parameters are usually different from those observed in the field. These condition differences can be accounted for by introducing a "shift factor." In this study, the shift factor was calibrated from the average ratios between measured and predicted permanent deformations at the same interval of 25,000 repetitions.

Prediction of Permanent Deformation with Other Materials under APT Loading

The proposed FE model and the calibrated shift factor were used to predict the permanent deformation of pavements with other materials.

Axisymmetric FE models of pavements with lime/fly ash and cement treated subbase layers were created to simulate the permanent deformation of the pavement under APT loading. The pavement structure consisted of a 2-in. HMA layer, an 8.5-in. stone base, a 12-in. treated subbase, and a subgrade. The effects of load wander and temperature change were also considered. Finally, the calibrated shift factor obtained from the six APT sections was applied to the predicted permanent deformations.

In addition, economic analysis of lime/fly ash and cement treated subbase layer was conducted. The economic analysis was conducted based on the latest "Weighted Averages" summaries published by LADOTD or Texas DOT. The material costs of cement, lime, fly ash are $215.28, $146.3, and $60/ton, respectively. The unit weights of soil, cement, lime, and fly ash are 111.4, 94, 35, and 60 lb/ft^3, respectively. The calculation of cost per linear foot of roadway is based on a pavement section of 1-ft. long, 13-ft. wide (1 lane), and 12-in. thick.

Prediction of Permanent Deformation for Typical Low Volume Pavements

The proposed FE model and the calibrated shift factor were used to predict the permanent deformation of two typical low- and medium-volume roads used in Louisiana. The predicted permanent deformations are compared with the field measured rut-depths.

Table 5 presents the general information of the two selected road projects. The project on LA10 had a length of 3.6 miles with an average daily traffic (ADT) of 721 in 1999. The project on LA28 had a length of 6.7 miles with an ADT of 5,500 in 2001. The profiles of pavement structures of the two projects are shown in Figure 16.

Table 5
General information of selected projects

Road Name	District	Parish	Project Number	ADT	Accepted Date
LA10	61	Pointe Coupee	219-30-0012	721	01/27/1999
LA28	08	Rapides	417-02-0031	5,500	02/19/2001

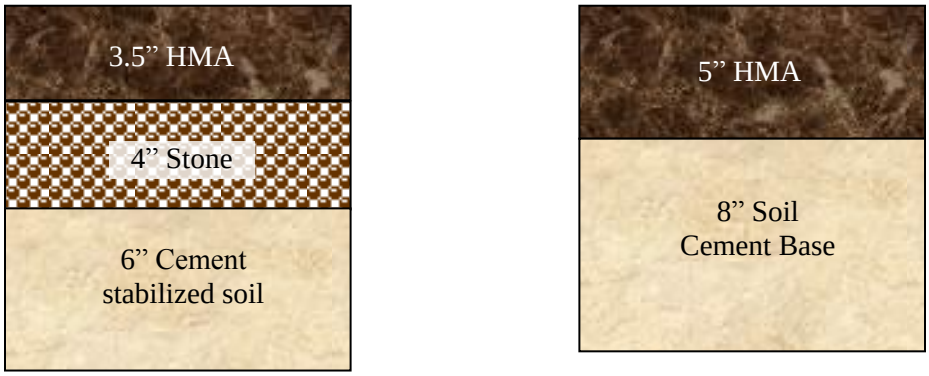

(a) LA10 **(b) LA28**

Figure 16
Pavement structures of selected projects

The axisymmetric FE models were created to simulate the rut depths of selected projects. The proposed P-D model was applied for all pavement materials. Material parameters were obtained from laboratory P-D tests. The effects of load wander and temperature change were also considered. The calculated permanent deformations were multiplied by the shift factor obtained from the six APT sections. Finally, the predicted permanent deformations were compared with field measured rut depths.

Development of P-D Prediction Models (Transfer Function) for Base and Subbase/Subgrade Materials

Although the proposed FE model can efficiently simulate the permanent deformation of APT sections, to perform such an FE analysis requires a basic understanding of the FEM and a familiarity of the ABAQUS software. To better implement the FE model developed in this study, the calibrated FE model was used to develop P-D prediction models (transfer functions) for pavement base and subbase/subgrade materials.

Transfer functions act as a link between pavement responses and performances (rutting, cracking, etc.). It assumes that pavement distresses under repeated loads are directly attributable to pavement responses under a monotonic load. The transfer function is the biggest “empirical” component of the M-E pavement design. It is important to note that because transfer functions are empirical, they are developed for a specific set of conditions, such as a range of HMA thickness, a given climate, a certain range of material properties, and a certain level of distress, etc.

In this study, the transfer function was modified from the formula of the accumulated permanent strain of the P-D model by introducing a number of calibration factors. FE simulations were performed on a large number of computer-generated pavement sections with assumed material properties. The variation of material properties were based on the laboratory P-D test data collected in this study. Calibration factors in the transfer functions were then determined by statistical analysis on the predicted permanent deformations from FE simulations.

Formula of the P-D Transfer Function

From equations (8) and (9), for laboratory P-D test, the accumulated permanent strain can be written as:

$$\varepsilon^p(n) = \frac{\sigma - \sigma_y}{h_c} + \frac{\sigma \cdot a}{E_L} \sum_{i=1}^{n} \left(\frac{1}{a + i^b} \right) \tag{13}$$

where, $\varepsilon^p(n)$ is the permanent strain after *n* load cycles, σ is the cyclic deviatoric stress, σ_y is the yield stress, h_c is the hardening constant, E_L is the constant loading modulus, a and b are the permanent deformation parameters.

The value of the parameter a of different materials are generally much smaller than the value of i^b, especially as load cycle i becomes larger. Assuming that $a + i^b \approx i^b$,

$$\varepsilon^p(n) \approx \frac{\sigma - \sigma_y}{h_c} + \frac{\sigma \cdot a}{E_L} \sum_{i=1}^{n} \left(\frac{1}{i^b} \right) \tag{14}$$

The equation (14) could be further simplified as:

$$\varepsilon^p(n) \approx \frac{\sigma - \sigma_y}{h_c} + \frac{\sigma}{E_L} \cdot \frac{a}{1 - b} [(n + 1)^{1-b} - 1] \tag{15}$$

When $b = 1$, a number that is very close to 1 (e.g., 0.9999 or 1.0001) can be assigned to equation (15). More details about the derivation of equation (15) are provided in Appendix B.

In equation (15), the permanent strain developed in the first load cycle (represented by $\frac{\sigma - \sigma_y}{h_c}$) is generally much smaller compared to the total permanent strain generated after a large number of load cycles. Therefore, this part of strains can be omitted, and equation (15) can be further simplified as:

$$\varepsilon^p(n) \approx \frac{\sigma}{E_L} \cdot a \cdot \left[\frac{(n+1)^{1-b}-1}{1-b}\right] = \varepsilon_v \cdot a \cdot \left[\frac{(n+1)^{1-b}-1}{1-b}\right] \quad (16)$$

where, ε_v can be considered as the vertical resilient strain.

In a pavement structure, the permanent deformation (rut depth) on the surface of the pavement can be calculated by summing up the permanent deformation developed in each sublayer:

$$PD = \sum \varepsilon^p \cdot \Delta h \quad (17)$$

where, PD is the accumulated vertical permanent deformation of pavement, ε^p is the accumulated vertical permanent strain at the mid-depth a sublayer, and Δh is the thickness of the sublayer.

Development of P-D Transfer Function

Obviously equations (16) and (17) cannot be directly used to predict the permanent deformation of an APT section because the conditions (e.g., temperature, load, time, etc.) between a laboratory P-D test and a field APT test are different. To account for the different conditions, equation (16) was modified by introducing a number of calibration factors. In this study, a general form of the transfer function was proposed:

$$\varepsilon^p = \beta_0(\varepsilon_v)^{\beta_1}(a)^{\beta_2}\left[\frac{(n+1)^{1-b}-1}{1-b}\right]^{\beta_3} \quad (18)$$

where, ε^p is the accumulated vertical permanent strain at the mid-depth a sublayer, ε_v is the vertical resilient strain calculated by the structural response model at the mid-depth of the sublayer, a and b are the permanent deformation parameters, and $\beta_{0,1,2,3}$ are the calibration factors.

In this study, pavement base and subgrade materials were classified into four categories: stabilized base materials (e.g., stabilized BCS materials); unbound base materials (e.g., stone); treated subbase/subgrade materials (e.g., lime, lime/fly ash, and cement treated soils); and untreated subgrade soils. For each category material, three levels of material parameters (loading modulus and permanent deformation parameters a and b) were selected to conduct the FE simulation based on the laboratory test result range.

Table 6 presents the parameters of the FE simulation for obtaining the calibration constants of the base, subbase, and subgrade materials.

Table 6
Parameters used in the FE simulation for various base and subbase/subgrade materials

Materials	Loading modulus (ksi)	Permanent deformation parameter a	Permanent deformation parameter b
Stabilized base materials	75, 115,140	0.003, 0.007, 0.01	0.55, 0.65, 0.75
Unbound base materials	15, 35, 60	0.06, 0.11, 0.16	0.60, 0.65, 0.70
Treated subbase/subgrade materials	20, 45,70	0.002, 0.006, 0.01	0.55, 0.75, 0.95
Untreated subgrade	5, 10, 15	0.02, 0.04, 0.06	0.55, 0.65, 0.75

A series of axisymmetric FE models for pavements were developed to predict the vertical permanent strains in the middle of each element (sublayer) under the centerline of the APT load. The effect of load wander on permanent strains was considered. The shift factor obtained from the six APT sections was applied. The final predicted permanent strains were treated as the "real" permanent strain in the pavement. Meanwhile, the corresponding vertical resilient strains were calculated at the middle of each sublayer under the centerline of APT load. The Statistical Analysis Software (SAS) was employed to conduct the regression to obtain the calibration constants $\beta_{0,1,2,3}$ for each category of material. A linear regression was conducted by rewriting equation (18) as:

$$\log(\varepsilon^p) = \log(\beta_0) + \beta_1 \log(\varepsilon_v) + \beta_2 \log(a) + \beta_3 \log\left[\frac{(n+1)^{1-b} - 1}{1-b}\right] \qquad (19)$$

Verification of P-D Transfer Functions

The developed P-D transfer functions were applied to simulate the permanent deformation of the APT sections and the two selected low volume pavement structures in Louisiana. The elastic vertical strains at the mid-depth of each pavement sublayer under the centerline of load were calculated by ABAQUS. (It can also be calculated by other elastic layered pavement analysis programs, e.g., BISAR and ELSYM5 etc.) The permanent deformation parameters (a and b) of pavement materials are obtained from P-D tests. The accumulated permanent strains at the mid-depth of each pavement sublayer under the center of load were calculated by developed transfer function equations. The accumulated permanent deformation is the sum of products of mid-depth permanent strain and thickness for all sublayers [see equation (18)].

DISCUSSION OF RESULTS

Verification and Sensitivity Analysis of the Proposed P-D Model

The proposed P-D model was verified by the laboratory P-D test data of eight pavement materials. A sensitivity analysis was conducted to evaluate the effect of material model parameters, pavement structures, and load configurations on the permanent deformation of pavement structures.

Verification of P-D Model with Laboratory Tests

Figure 17 presents a comparison between measured and calculated axial stress-strain curves for the first 10 cycles of load repetitions. It is shown that the proposed P-D model approximates the hysteresis loops by a series of linear loading and unloading paths. Although the nonlinearity during loading/unloading was ignored, the proposed model simulates the accumulation of permanent strain very well.

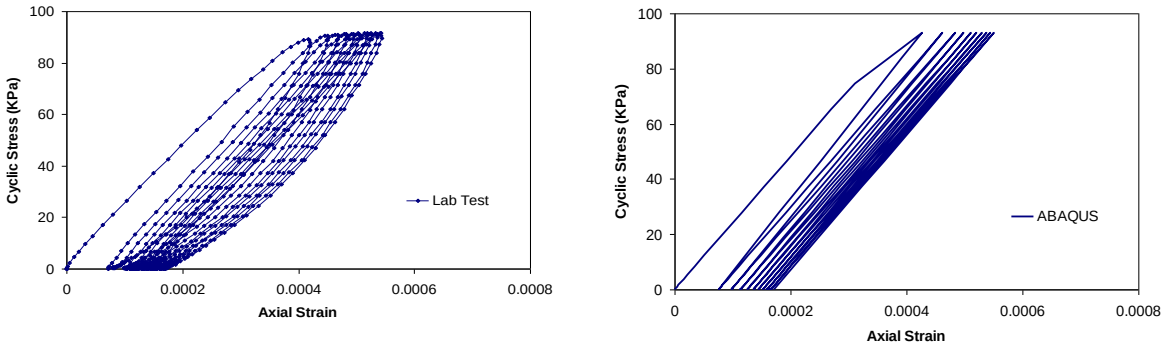

(a) Measured axial stress-strain curve **(b) Calculated axial stress-strain curve**

Figure 17
An example of axial stress-strain cyclic behavior (1 psi = 6.894 kPa)

Figure 18 presents the calculated and measured accumulated permanent strains for eight pavement materials selected in this study. The measured accumulated permanent strain after 10,000 load cycles ranged from 40 to 21,000 microstrains. Figure 18 shows that the calculated permanent strains matched well with the test data for all eight materials evaluated. The differences between the predicted and the measured strains were less than 10 percent. This result indicated that the proposed model is generally suitable for the simulating P-D tests for a variety of pavement materials.

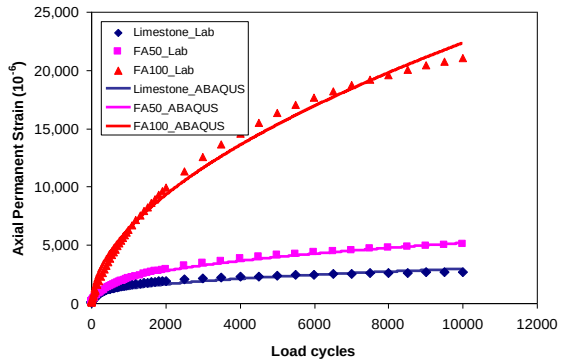

(a) limestone and foamed asphalt materials

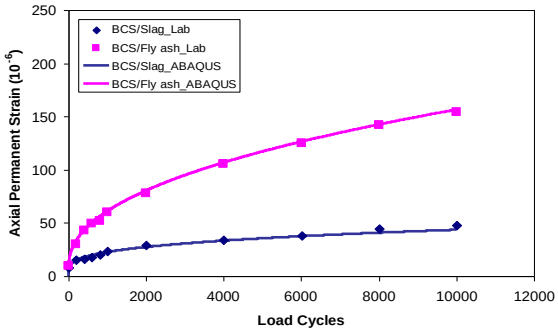

(b) BCS materials

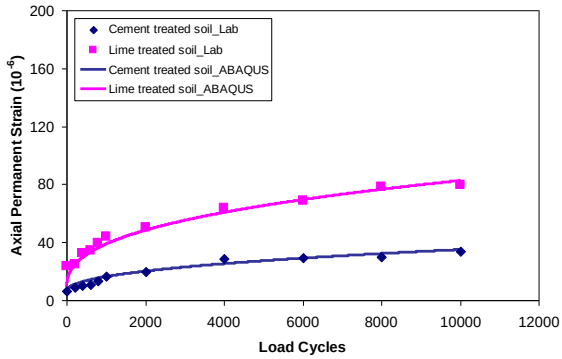

(c) treated soil materials

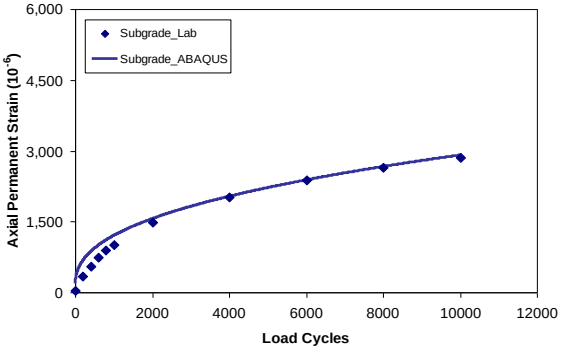

(d) subgrade soil

Figure 18
Measured and simulated axial permanent deformation of selected materials

Sensitivity Analysis of the Proposed P-D Model

Table 7 presents parameters used in the sensitivity analysis. The 18 trial cases were designed according to the Taguchi experiment design method.

Table 7
Sensitivity analysis results of base layer permanent deformation

Trail No.	P1	P2	P3	P4	P5	P6	Base Layer Permanent Deformation (in.)
	HMA Thickness (in.)	Base Thickness (in.)	Base Loading Modulus (ksi)	Subgrade Modulus (ksi)	Base Layer permanent deformation Parameter "a"	Base Layer permanent deformation Parameter "b"	
1	2	6	25	5	0.003	0.7	0.005
2	2	9	75	10	0.1	0.57	0.007
3	2	12	125	15	0.2	0.45	0.010
4	6	6	25	10	0.1	0.45	0.005
5	6	9	75	15	0.2	0.7	0.004
6	6	12	125	5	0.003	0.57	0.002
7	10	6	75	5	0.2	0.57	0.002
8	10	9	125	10	0.003	0.45	0.001
9	10	12	25	15	0.1	0.7	0.003
10	2	6	125	15	0.1	0.57	0.005
11	2	9	25	5	0.2	0.45	0.025
12	2	12	75	10	0.003	0.7	0.004
13	6	6	75	15	0.003	0.45	0.002
14	6	9	125	5	0.1	0.7	0.003
15	6	12	25	10	0.2	0.57	0.007
16	10	6	125	10	0.2	0.7	0.001
17	10	9	25	15	0.003	0.57	0.002
18	10	12	75	5	0.1	0.45	0.002

Figure 19 shows the average effects of the varying parameters on permanent deformation in the base layer. Among the six parameters investigated, HMA thickness and the permanent deformation parameters a and b have a significant influence on the calculated permanent deformation in base layer. The calculated permanent deformation decreases with an increasing HMA thickness, a decreasing a value and an increasing b value. Thus, a smaller a value and a larger b value are desirable base material properties to reduce rutting.

The other three parameters – base thickness, base modulus, and subgrade modulus – only display intermediate influences to the predicted base layer permanent deformation. Although typically a thicker base layer would reduce the total rut depth of a pavement, it may result in more permanent deformation in the base itself. On the other hand, permanent deformation is a plastic behavior of materials. Thus permanent deformation in the base layer is more

dependent on the plastic parameters (a and b), rather than the elastic loading modulus of the base layer.

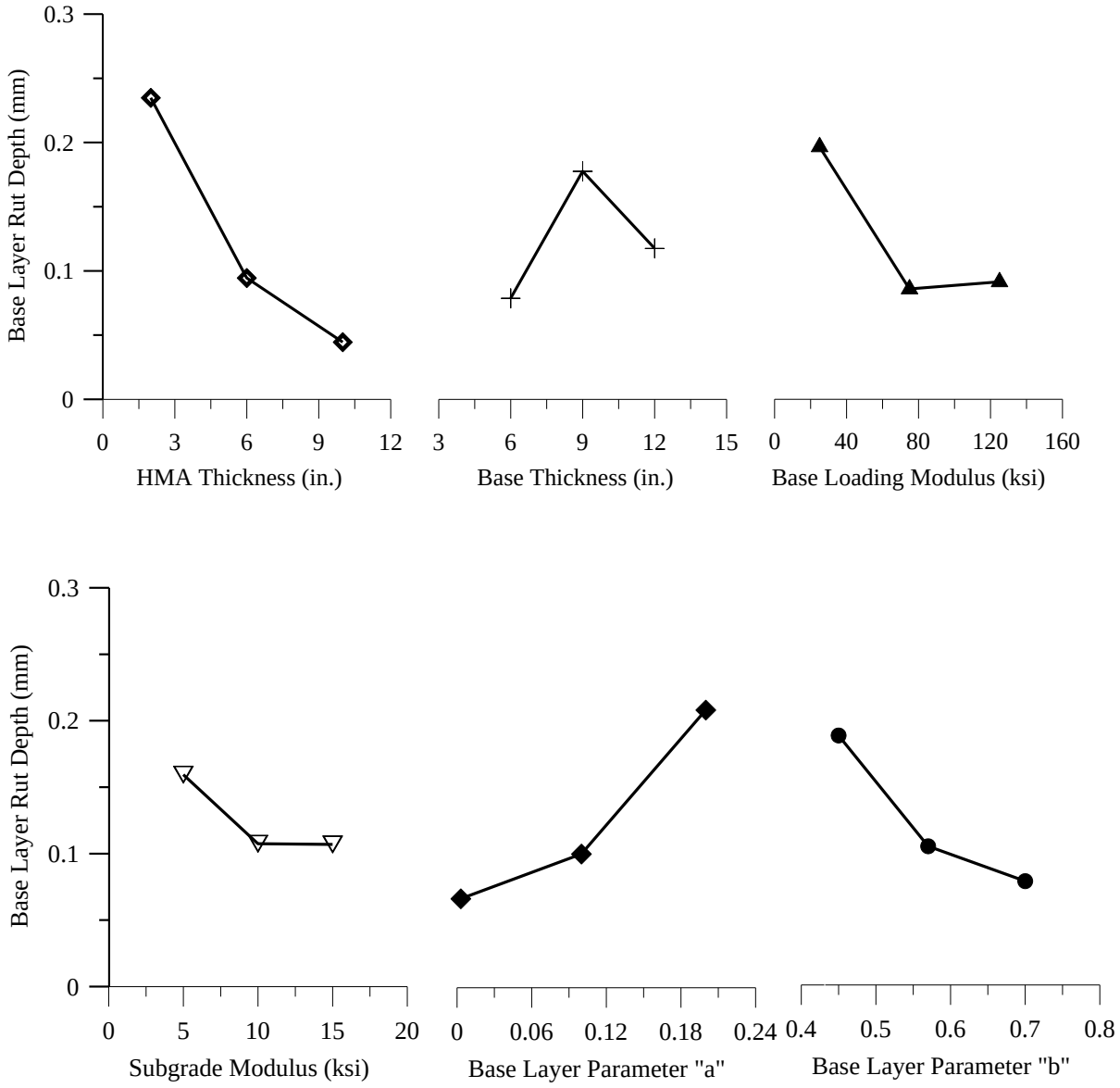

Figure 19
Effects of varying factors on base layer permanent deformation (1 in. = 25.4 mm)

Figure 20 presents the influences of the two P-D parameters (a and b) on the calculated base permanent deformation with varying the HMA thicknesses. Similar to the results in Figure 19, base layer permanent deformation decreases with an increasing HMA thickness. Figure 20 also indicates that the calculated base layer permanent deformation is more sensitive to the P-D parameters (a and b) when the HMA layer is relatively thin (less than 6 in.). This

observation suggested that the proposed P-D model would be more effective in predicting the permanent deformation for a base or subbase layer in thinly paved roads.

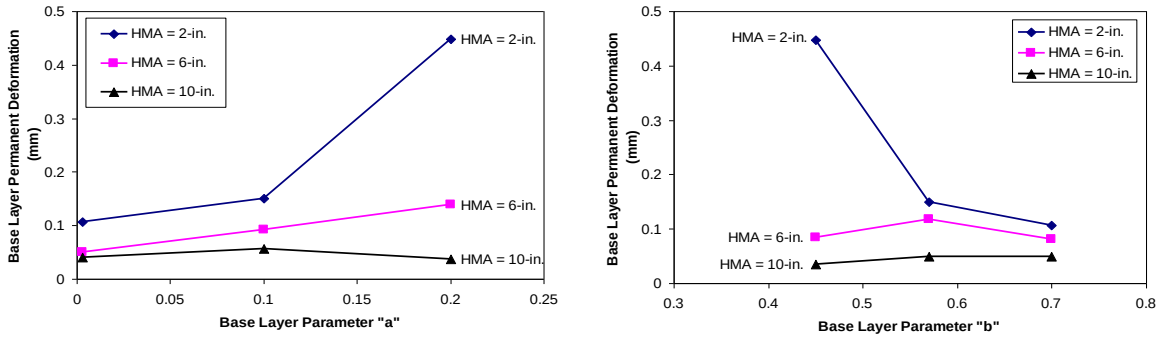

(a) (b)

Figure 20
Sensitivity analysis of parameters *a* and *b* (1 in. = 25.4 mm)

The data in Table 7 were analyzed using the ANOVA technique by the SAS program with a level of significance of 0.05 to examine the relative contribution of influential factors to the predicted base permanent deformation. The ANOVA results are presented in Table 8. A higher percentage of contribution means more contribution of the factor to the calculated base layer permanent deformation.

As shown in Table 8, HMA thickness has the greatest contribution (34.1 percent) to the base layer permanent deformation, followed by base layer parameter *a* (19.2 percent), base layer loading modulus (13.6 percent), and base layer parameter *b* (11.5 percent). The contributions of base layer thickness and subgrade modulus were less than other factors, only 8.7 and 3.2 percent, respectively.

Table 8
ANOVA results of base layer permanent deformation properties

Factor	Degree of Freedom(DF)	Sum of Squares	Mean Square	F Value	Contribution of Factors, %
HMA Thickness (in.)	2	0.11679	0.05840	8.71	34.1
Base Thickness (in.)	2	0.02979	0.01490	2.22	8.7
Base Loading Modulus (ksi)	2	0.04671	0.02335	3.48	13.6
Subgrade Modulus (ksi)	2	0.01092	0.00546	0.81	3.2
Base Layer Parameter *a*	2	0.06598	0.03299	4.92	19.2
Base Layer Parameter *b*	2	0.03929	0.01964	2.93	11.5
Error	5	0.03351	0.00670		9.8
Corrected Total	17	0.34299			100

Figure 21 presents the effects of load levels on pavement permanent deformation. It is shown that rut depths increases almost linearly with the load.

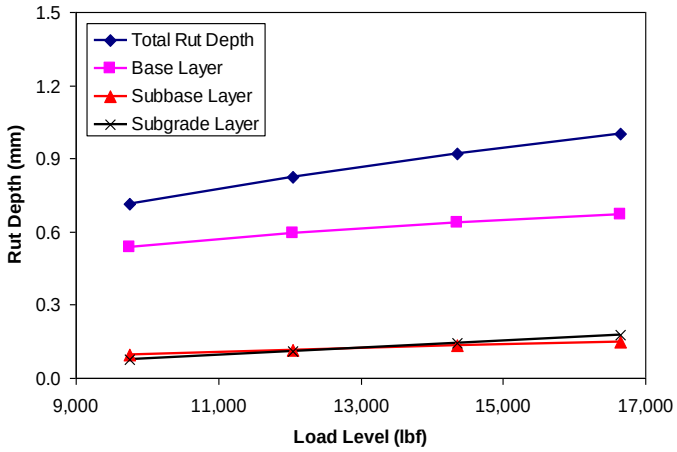

Figure 21
Effective of load configuration on permanent deformation (1 in. = 25.4 mm)

Preliminary Results of FE Simulation of APT Test

All three developed FE models (3-D model with a moving load, 3-D model with a repeated load, and axisymmetric model with a repeated load) were preliminarily compared by simulating one of the APT sections.

3-D Model with a Moving Load

The 3-D model with a moving load provides the most accurate simulation of the wheel load applied in an APT test. Figure 22 presents a deformed 3-D model with a single-axle-dual-wheel moving load. As expected, permanent deformation occurred on the path of the wheel load.

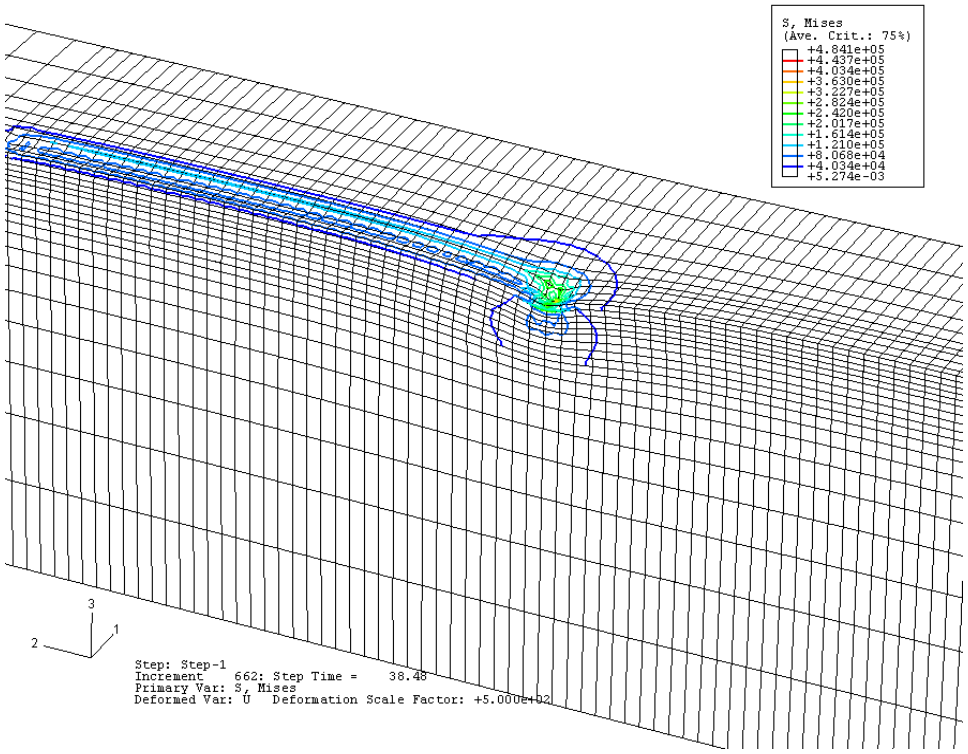

Figure 22
Deformed 3-D model with moving wheel load

Figure 23 and Figure 24 present the calculated stresses and strains at the top and bottom of the base layer, respectively. The principle directions are: 1– transverse direction, 2 – longitudinal direction, and 3 – the vertical (depth) direction. For example, "S33" means the normal vertical stress, and "S23" means the shear stress on a horizontal plane and along the longitudinal direction. As shown in Figure 23 and Figure 24, the 3-D model with a moving load can accurately simulate the stress and strain rotation induced by a moving wheel.

However, running such a model was extremely time-consuming. It took about 12 days on a PC with a Pentium Dual-core 3.2GHz central processing unit (CPU) and 2.0G memory to run

one cycle of wheel pass. It is impractical to use this model to simulate an APT test with a large number of load passes.

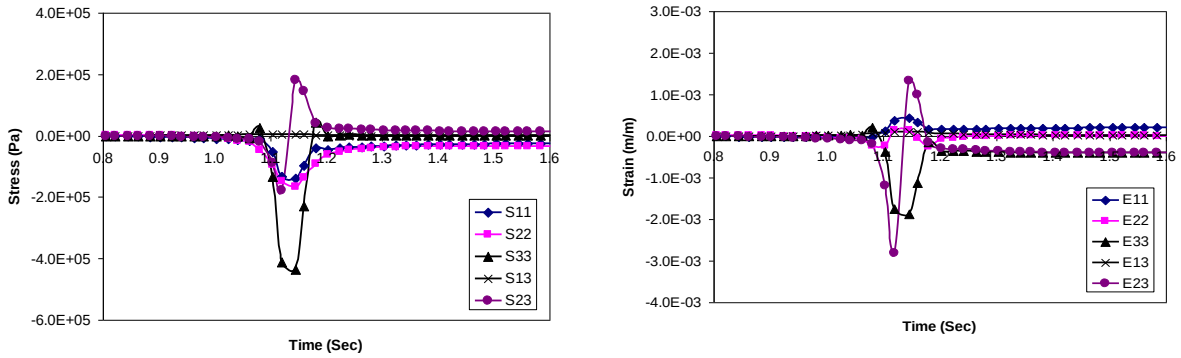

(a) Stresses **(b) Strains**

Figure 23
Predicted pavement responses at top of base layer under ALF moving load (1 in. = 0.025 m, 1 psi = 6894 Pa)

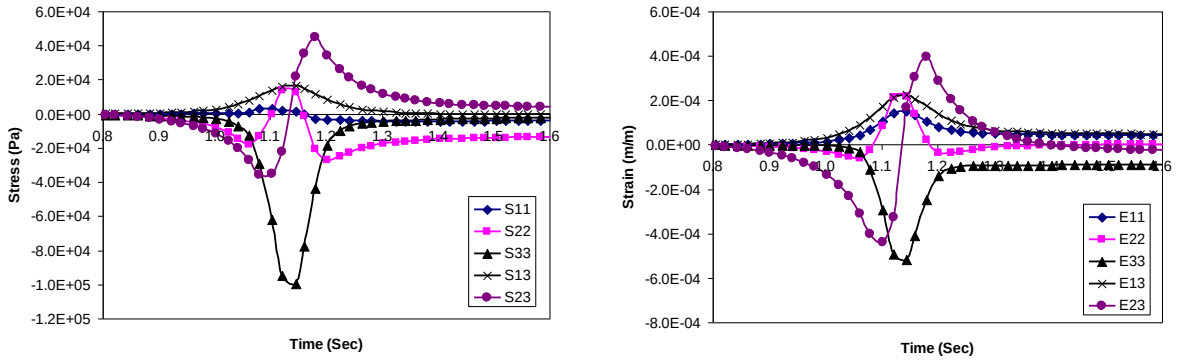

(a) Stresses **(b) Strains**

Figure 24
Predicted pavement responses at base layer bottom under ALF moving load (1 in. = 0.025 m, 1 psi = 6894 Pa)

3-D Model with a Repeated Load

When the moving load is directly above a given point, the vertical normal stress at this point is at its maximum; and when the wheel load is a considerable distance from a given point, the stresses at this point return to its at-rest value. It is therefore reasonable to assume that the stress pulse at a given point can be simulated by either sinusoidal- or triangular-shaped repeated load applied at the same position. By applying the repeated load in a static location,

the size (or the number of elements) of the numerical model can be greatly reduced. The 3-D model with repeated loading can also simulate multi-wheel configurations.

To determine the suitable mesh density for the 3-D model with a repeated load, a series of FE models were created with different numbers of elements. A linear elastic model was used in this part of the analysis. Figure 25 to Figure 28 exhibit various pavement responses with different models. Based on the mesh sensitivity analysis, the model with a total of 4,752 elements was selected.

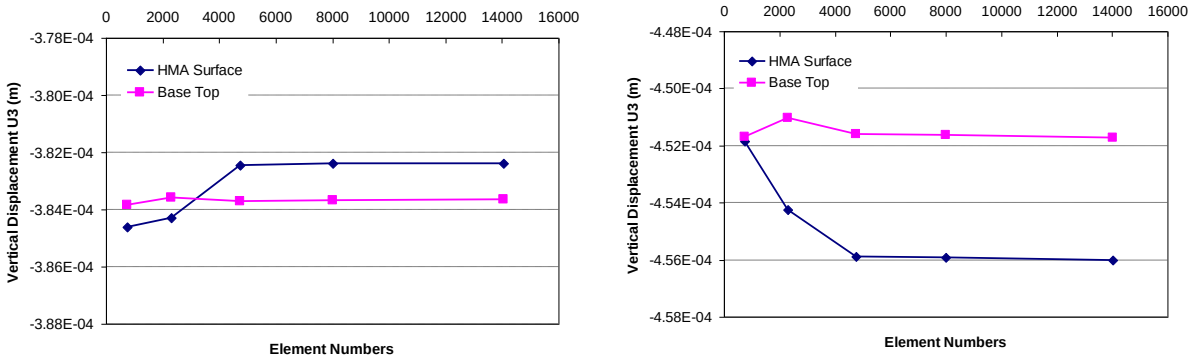

(a) axial center **(b) wheel center**

Figure 25
Vertical displacements on HMA surface and base top with different mesh sizes (1 in. = 0.025 m)

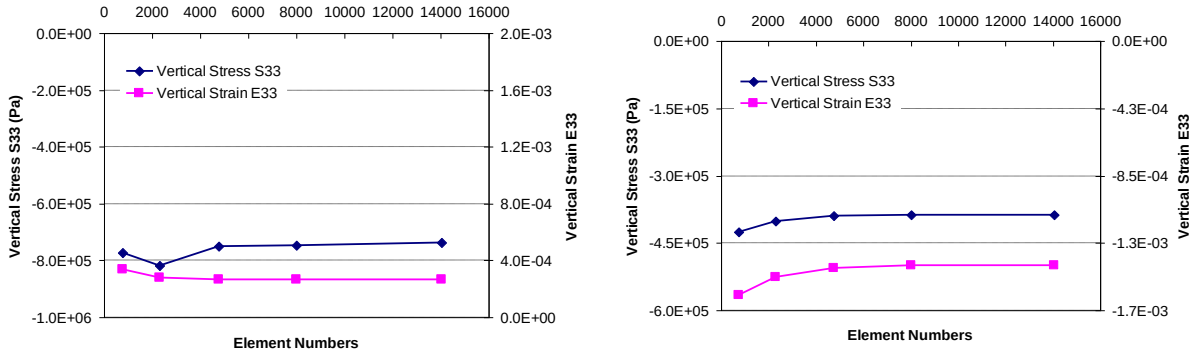

(a) HMA surface wheel center **(b) base top wheel center**

Figure 26
Vertical stress and strain on HMA surface and base top with different mesh sizes (1 psi = 6894 Pa)

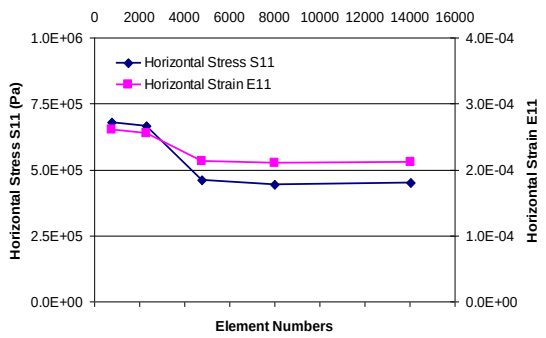

(a) axial center

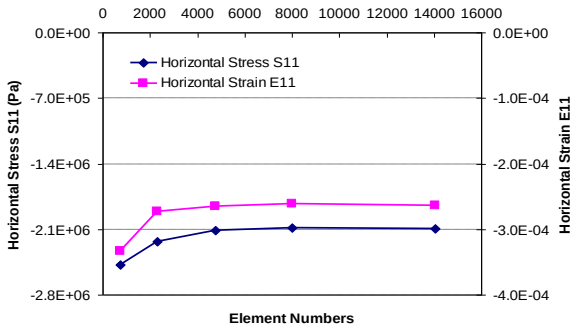

(b) wheel center

Figure 27
Horizontal stress and strain on HMA surface with different mesh sizes (1 psi = 6894 Pa)

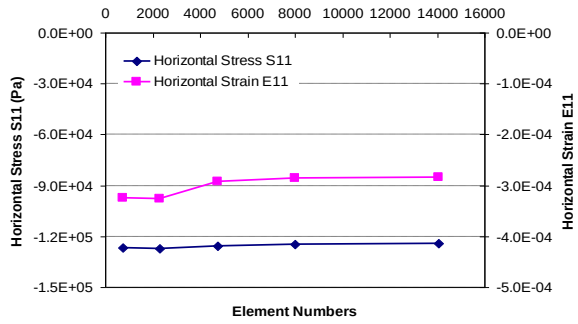

(a) axial center

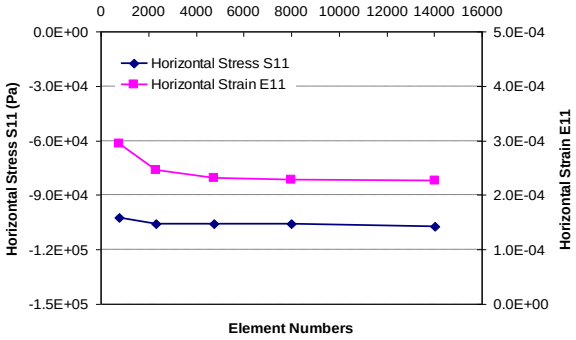

(b) wheel center

Figure 28
Horizontal stress and strain on base top with different mesh sizes (1 psi = 6894 Pa)

The selected numeric mesh was then used to simulate the six APT sections. Since this part of simulation was for comparison purposes, only a single level of load was modeled. The effects of temperature and load wander were not considered. Figure 29 presents the calculated HMA surface rut depths of the six APT sections. Sections 4-1A, 4-2A, and 4-1B were constructed with the different base materials and a lime-treated subbase. Figure 29a shows that the calculated rut depths after 3000 load cycles are 0.003 in. in section 4-1A, 0.004 in. in section 4-2A, and 0.03 in. in section 4-1B. Sections 4-2B, 4-3A, and 4-3B were constructed with the different base materials and a cement-treated subbase. Figure 29b shows that the calculated rut depths after 3000 load cycles are 0.03 in. in section 4-2B, 0.04 in. in section 4-3A, and 0.07 in. in section 4-3B.

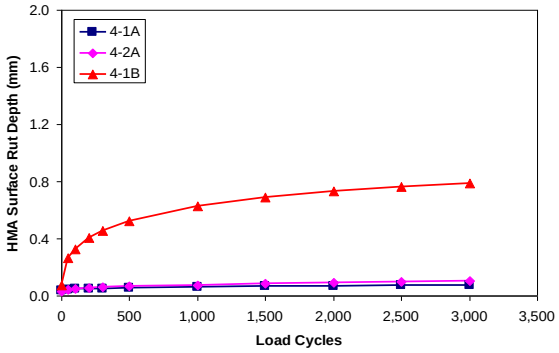

(a) sections with lime-treated soil subbase

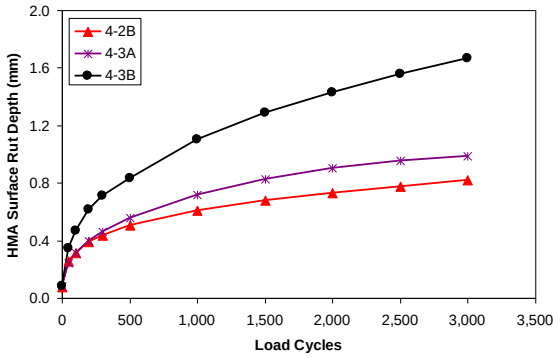

(b) sections with cement-treated soil subbase

Figure 29
Calculated rut depths by the 3-D model with a repeated load (1 in. = 25.4 mm)

With the 3-D model with a repeated load, it took about 230 to 400 hours to simulate 3,000 cycles of load on a supercomputer with four CPUs (16GB RAM) at Pelincan IBM pSeries cluster at Louisiana State University (LSU). Obviously it is still impractical to use this model to simulate APT tests.

Axisymmetric Model with a Repeated Load

An axisymmetric model simplifies a 3-D problem with a 2-D model, which uses a much smaller number of elements. To determine the suitable element size for the axisymmetric model, a series of FE models were created with different numbers of elements. Linear elastic models were used in this part of the analysis. Figure 30 and Figure 31 present various pavement responses with different models. Based on the mesh sensitivity analysis, the model with a total of 3400 elements was selected.

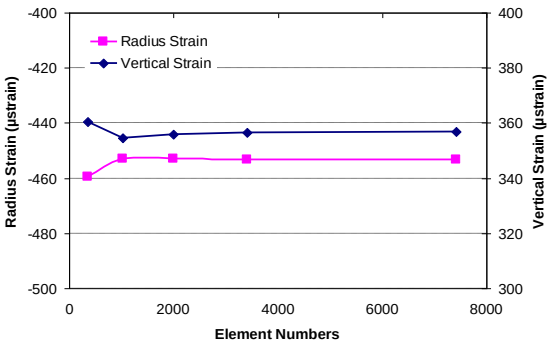

(a) radius and vertical strain

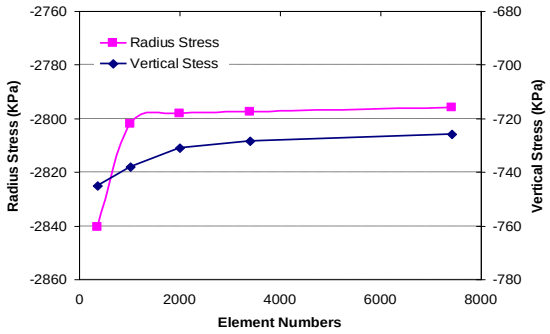

(b) radius and vertical stress

Figure 30
Strain and stress on HMA surface center with different mesh sizes (1 psi = 6.894 kPa)

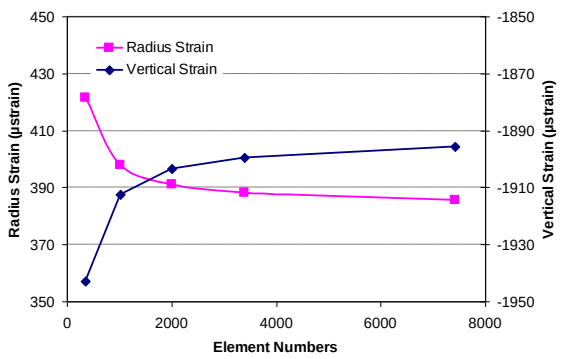

(a) radius and vertical strain

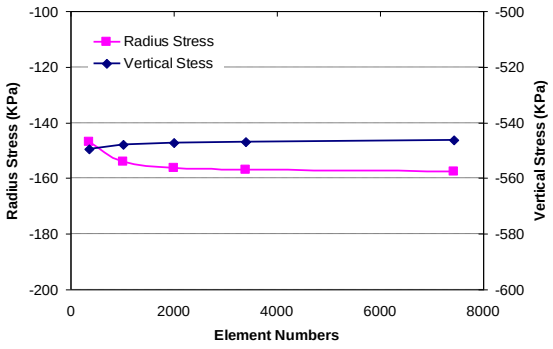

(b) radius and vertical stress

Figure 31
Strains and stresses on base surface center with different mesh sizes (1 psi = 6.894 kPa)

Since a linear elastic constitutive model was used. The calculated pavement responses by ABAQUS can be compared to those calculated by an elastic-layered pavement analysis program. Figure 32 and Figure 33 present radial and vertical stresses and strains at different depths along the center line of the model calculated by ABAQUS and BISAR. The calculated results from the two programs matched well with each other.

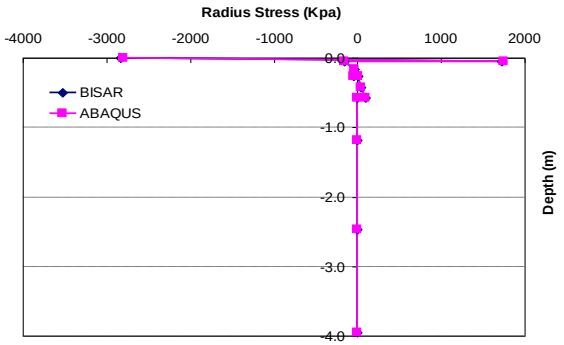

(a) radial stress

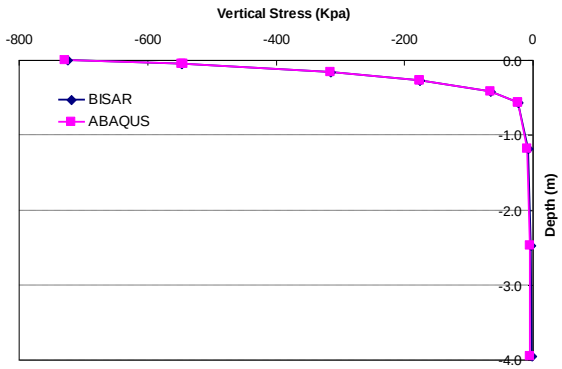

(b) vertical stress

Figure 32
Radial and vertical stresses at different depths by BISAR and ABAQUS (1 m = 3.28 ft., 1 psi = 6.894 kPa)

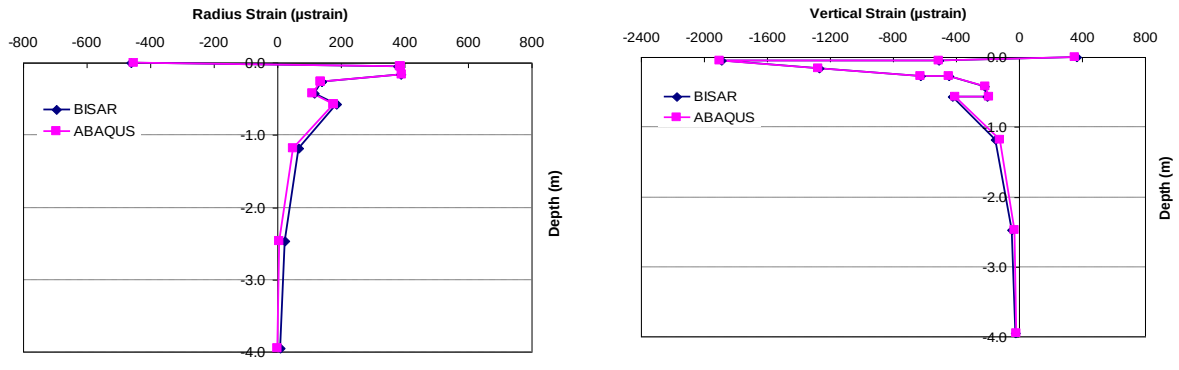

(a) radial strain **(b) vertical strain**

Figure 33
Radius and vertical strains at different depths by BISAR and ABAQUS (1 m = 3.28 ft.)

The selected numeric mesh was then used to simulate the six APT sections. Since this part of simulation was for comparison purposes, only a single level of load was modeled. The effects of temperature and load wander were not considered. Figure 34 presents the calculated HMA surface rut depths of the six APT sections. Figure 34a shows that the calculated rut depths after 10,000 load cycles are 0.005 in. in section 4-1A, 0.007 in. in section 4-2A, and 0.06 in. in section 4-1B. Sections 4-2B, 4-3A, and 4-3B were constructed with different base materials and a cement-treated subbase. Figure 34b shows that the calculated rut depths after 10,000 load cycles are 0.06 in. in section 4-2B, 0.08 in. in section 4-3A, and 0.13 in. in section 4-3B.

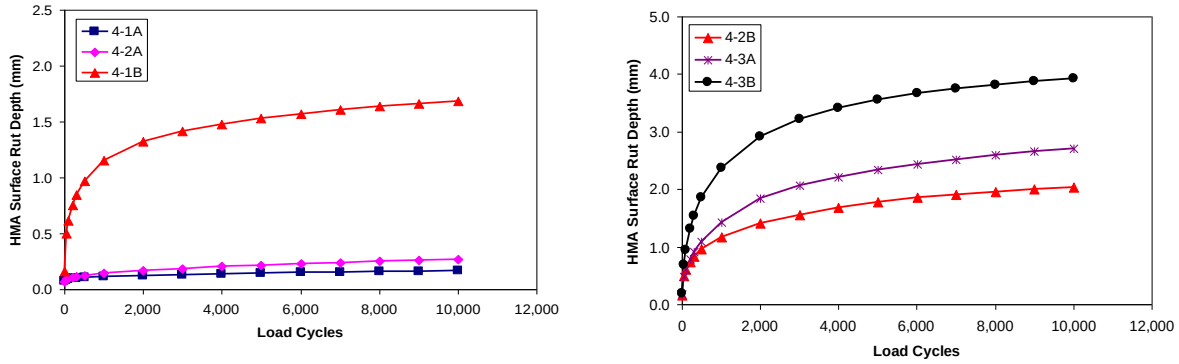

(a) sections with lime-treated soil subbase **(b) sections with cement-treated soil subbase**

Figure 34
Calculated rut depths by the axisymmetric model with a repeated load (1 in. = 25.4 mm)

The main advantage of an axisymmetric model is its computational efficiency. For example, to complete 100 cycles of simulation, it only needed about 1.5 to 3 hours by a personal

computer with a Pentium Dual-core 3.2GHz CPU and 2.0G memory, while for 10,000 cycles of simulation, it needed about 150 to 200 hours by a supercomputer with 4 CPUs (16GB RAM) at Pelincan IBM pSeries cluster at LSU, which was about half the time consumed by the 3-D model with repeated loading to finish 3,000 cycles.

When the accelerated analysis procedure was adopted, which only needed to be simulated about 100 cycles, the axisymmetric model became practical to conduct on a personal computer. Thus, this model was selected to predict the permanent deformation of the APT test sections after preliminary simulations.

Comparison between the Axisymmetric Model and the 3-D Model with a Repeated Load

In the 3-D model with a repeated load, the ALF dual wheel load was simulated as two distributed loads in two rectangular areas. In the axisymmetric model, the effect of multi-wheel configuration cannot be explicitly considered because the ALF load was simplified to a circular distributed load. In order to estimate the pavement response under multi-wheel load configurations, the numerical result from an axisymmetric model has to be interpreted by a superposition process, which is often adopted in the current MEPDG. Figure 35 presents the surface vertical displacement profiles from the 3-D model and the axisymmetric model (after superposition). It is shown that the numerical results from the 3-D and the axisymmetric models were comparable to each other.

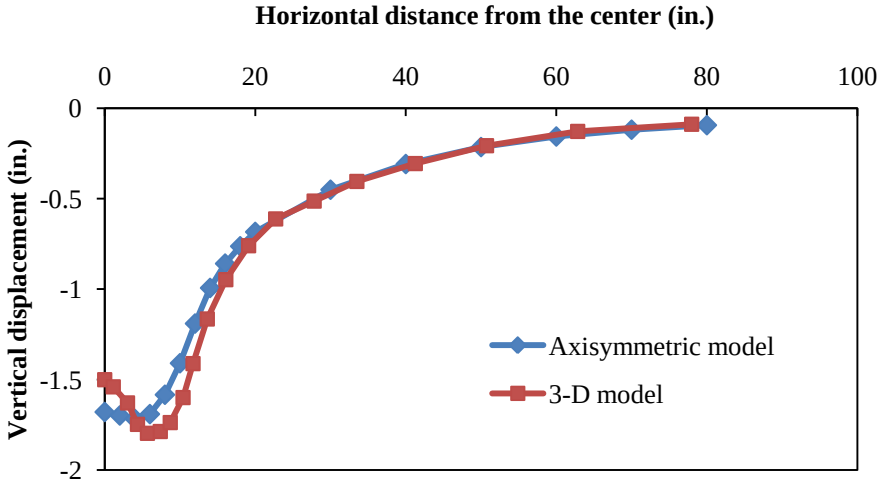

Figure 35
Vertical displacements of one circular load and two rectangular loads

Conclusions of Preliminary FE Simulation

The preliminary results of the APT simulation suggested that the developed FE models with the P-D materials model had the potential to predict the permanent deformation of the APT sections. In consideration of the computational efficiency, the axisymmetric model was finally selected for the further studies described in the following sections.

Results of FE Simulation of APT Tests

Material Parameters of the APT Sections

Table 9 presents the material parameters used for calculating permanent deformation of the APT sections.

Table 9
Field modified material parameters for APT test sections

Materials	Parameters for P-D model						Accelerated analysis parameter B
	E_L (ksi)	σ_y (psi)	h (ksi)	$d=a/N^b+1$		Poisson's Ratio	
				a	b		
HMA	100*	13	189	0.0100	0.60	0.35	0.2
BCS/Slag	128	12.6	155	0.0059	0.67	0.3	0.31
BCS/Fly ash	86	12.2	149	0.0073	0.56	0.3	0.41
Stone (4-1B)	19	10.7	71	0.1200	0.62	0.3	0.31
Stone (4-2B)	33	10.7	71	0.0960	0.64	0.3	0.31
FA50	28**	10.2	46	0.1250	0.62	0.35	0.32
FA100	25**	10.0	49	0.1560	0.63	0.35	0.32
Cement-treated soil	65	5.0	67	0.0027	0.56	0.3	0.24
Lime-treated soil	30	4.6	98	0.0052	0.63	0.3	0.36
Subgrade	7	4.2	7	0.0340	0.59	0.45	0.47

Note: * For Section 4-3A and 4-3B, E_L of HMA layer will be adjusted by field temperature; see Table 10.
** E_L of FA base layer will be adjusted by field temperature; see Table 10.

Table 10 presents the modified moduli of asphalt materials at sections 4-3A and 4-3B.

Table 10
Moduli of HMA layer and foamed asphalt base at sections 4-3A and 4-3B

Load Cycles	4-3A			4-3B		
	Temperature adjustment factor	HMA Modulus (ksi)	FA50% Modulus (ksi)	Temperature adjustment factor	HMA Modulus (ksi)	FA100% Modulus (ksi)
1-25,000	1.61	161	45	2.64	264	67
25,001-50,000	1.89	189	52	1.80	180	46
50,001-75,000	2.66	266	74	1.45	145	37
75,001-100,000	2.02	202	56	1.51	151	38
100,001-125,000	2.40	240	67	1.31	131	33
125,001-150,000	1.54	154	43	1.13	113	28
150,001-175,000	1.34	134	37	1.01	101	25
175,001-200,000	1.13	113	31	0.91	91	23
200,001-225,000	1.01	101	28	0.89	89	23
225,001-228,000	0.89	89	25	-	-	-

Effects of Load Wander on Permanent Deformation

Figure 36 presents an example of surface permanent deformations at the center line with different load wander offsets under ALF_Load I. As can be seen, a larger load wander offset would produce a smaller surface permanent deformation at the center line.

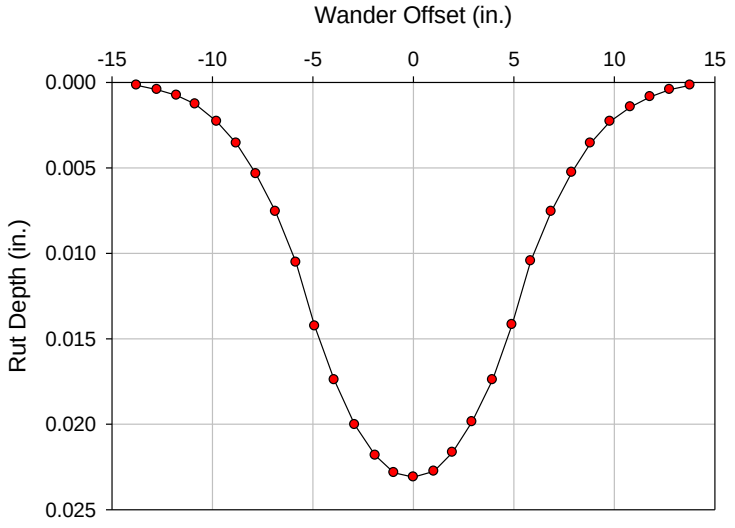

Figure 36
Example of surface permanent deformation at central line with different load wander offsets

Figure 37 presents the percentages of permanent deformation with wander to without wander at different load wander offsets under ALF_Load I. Table 11 presents the calculation of the wander adjustment factor for APT sections under ALF_Load I. The wander adjustment factors ranged from 68.3 to 71.6 percent under ALF_Load I.

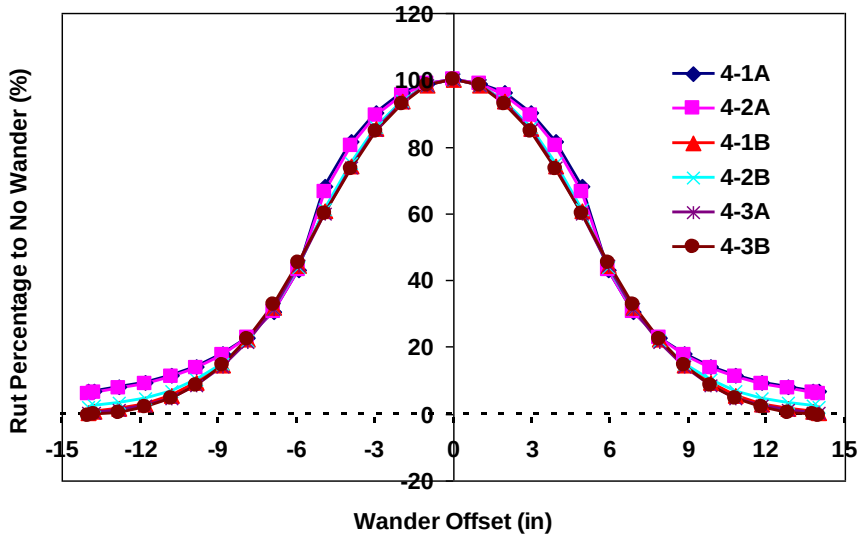

Figure 37
Wander adjustment factor under ALF_Load I

Table 11
Calculation of the wander adjustment factors for APT sections under ALF_Load I

Load Offset	Load Frequency	Ratio of rut depth with load offset x over offset zero, (D_x, %)					
in	(%)	4-1A	4-2A	4-1B	4-2B	4-3A	4-3B
-14.00	0.2	0.01	0.01	0.00	0.00	0.00	0.00
-13.78	0.2	0.01	0.01	0.00	0.00	0.00	0.00
-12.80	0.4	0.03	0.03	0.01	0.01	0.00	0.00
-11.81	0.4	0.04	0.04	0.01	0.02	0.01	0.01
-10.83	0.8	0.09	0.09	0.04	0.05	0.04	0.04
-9.84	1.6	0.23	0.22	0.15	0.16	0.14	0.14
-8.86	1.6	0.29	0.28	0.24	0.24	0.22	0.23
-7.87	2.4	0.55	0.55	0.53	0.53	0.52	0.54
-6.89	3	0.91	0.91	0.96	0.94	0.95	0.98
-5.91	3.8	1.64	1.63	1.69	1.67	1.68	1.71
-4.92	4.6	3.13	3.06	2.79	2.82	2.76	2.75
-3.94	5.6	4.58	4.49	4.17	4.20	4.12	4.10
-2.95	6.2	5.60	5.54	5.30	5.32	5.26	5.24
-1.97	7	6.72	6.67	6.54	6.55	6.52	6.51

(continued)

-0.98	7.4	7.33	7.31	7.28	7.28	7.27	7.27
0.00	9	9.00	9.00	9.00	9.00	9.00	9.00
0.98	7.2	7.13	7.11	7.08	7.09	7.08	7.07
1.97	7	6.72	6.67	6.54	6.55	6.52	6.51
2.95	6.4	5.78	5.72	5.47	5.49	5.43	5.41
3.94	5.6	4.58	4.49	4.17	4.20	4.12	4.10
4.92	4.8	3.26	3.19	2.91	2.94	2.88	2.87
5.91	4	1.72	1.72	1.78	1.76	1.77	1.80
6.89	3.2	0.98	0.97	1.02	1.00	1.01	1.04
7.87	2.4	0.55	0.55	0.53	0.53	0.52	0.54
8.86	1.8	0.32	0.31	0.27	0.27	0.25	0.26
9.84	1.4	0.20	0.19	0.13	0.14	0.12	0.12
10.83	0.6	0.07	0.07	0.03	0.04	0.03	0.03
11.81	0.6	0.06	0.05	0.02	0.03	0.01	0.01
12.80	0.4	0.03	0.03	0.01	0.01	0.00	0.00
13.78	0.2	0.01	0.01	0.00	0.00	0.00	0.00
14.00	0.2	0.01	0.01	0.00	0.00	0.00	0.00
Sum	**100.0**	**71.6**	**70.9**	**68.7**	**68.9**	**68.3**	**68.3**

Table 12 presents the wander adjustment factors for APT sections under four different load levels. The wander adjustment factor increased as the load level increased. When the load level increased from ALF_Load I (9,750 lbf) to ALF_Load IV (16,650 lbf), the average wander adjustment factor for APT sections increased from 69.4 to 78.6 percent.

Table 12
Wander adjustment factors for APT sections

Load Level	4-1A	4-2A	4-1B	4-2B	4-3A	4-3B	**Avg.**
ALF_LoadI	71.6	70.9	68.7	68.9	68.3	68.3	**69.4**
ALF_LoadII	76.3	75.8	72.2	72.8	71.6	71.2	**73.3**
ALF_LoadIII	79.7	79.1	75.0	75.9	74.4	73.7	**76.3**
ALF_LoadIV	82.2	81.6	77.2	78.2	76.6	75.7	**78.6**

Results of Predicted Permanent Deformation of APT Sections

Figure 38 presents the measured and predicted surface permanent deformations of the six APT sections. Note that the field measured surface permanent deformations were the average values from eight measurement stations. As shown in Figure 38, the predicted permanent deformations were in a reasonably good agreement with the field measured results. The shift factors for the six APT sections ranged from 0.8-1.6.

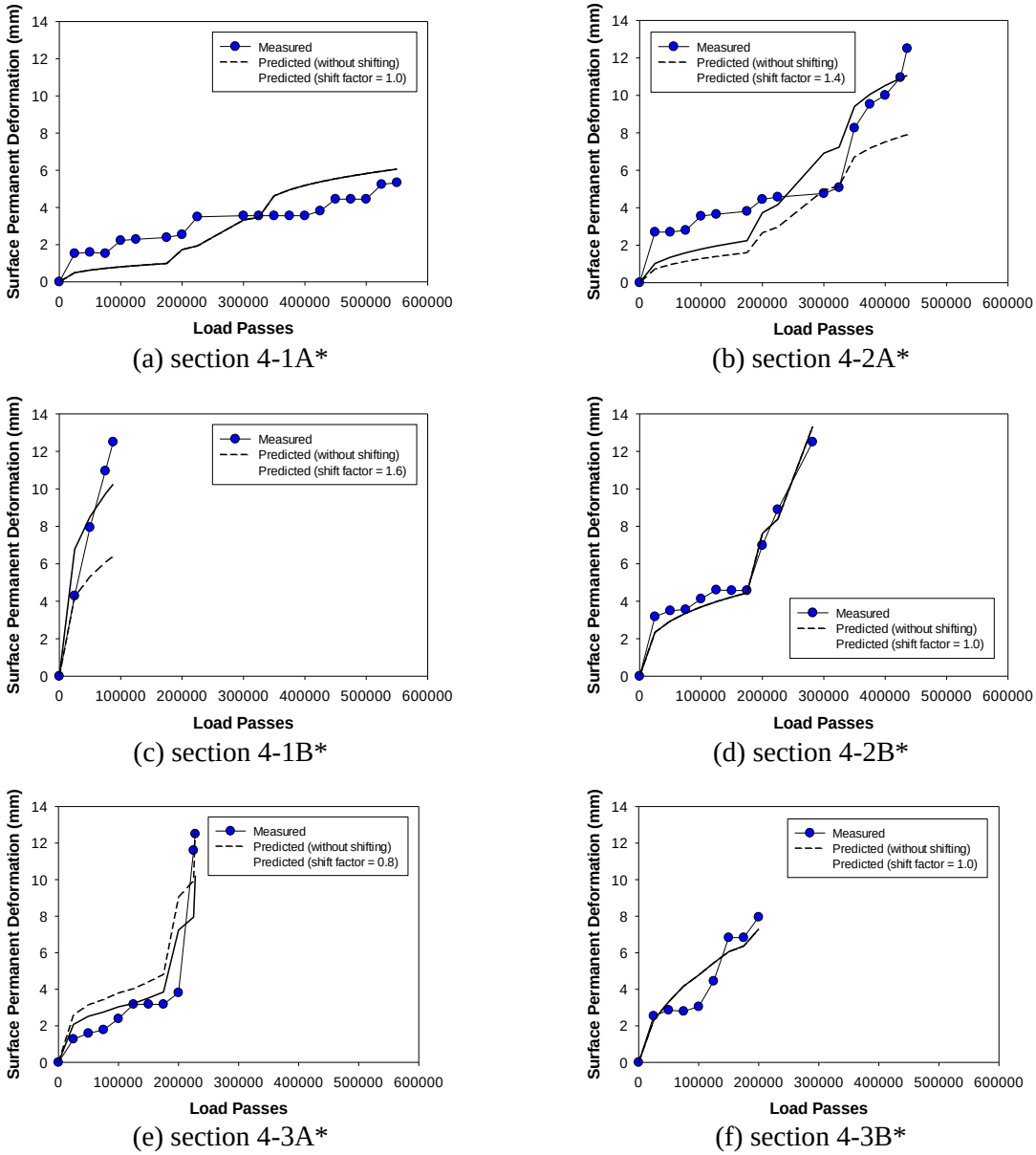

(a) section 4-1A*

(b) section 4-2A*

(c) section 4-1B*

(d) section 4-2B*

(e) section 4-3A*

(f) section 4-3B*

*The pavement structure and materials of each section are described in Table 2

Figure 38
Measured and predicted surface permanent deformation of APT test sections (1 in. = 25.4 mm)

Figure 39 presents the measured (from multi-depth deflectometer [MDD] stations) and calculated percentages of the total permanent deformation contributed by each layer. Note that the HMA layer deformations were not measured by MDDs. As shown in Figure 39, the calculated results closely match the measured results. The differences were generally less

than 11 percent except for the subbase layer in section 4-3A, where the difference was about 17 percent.

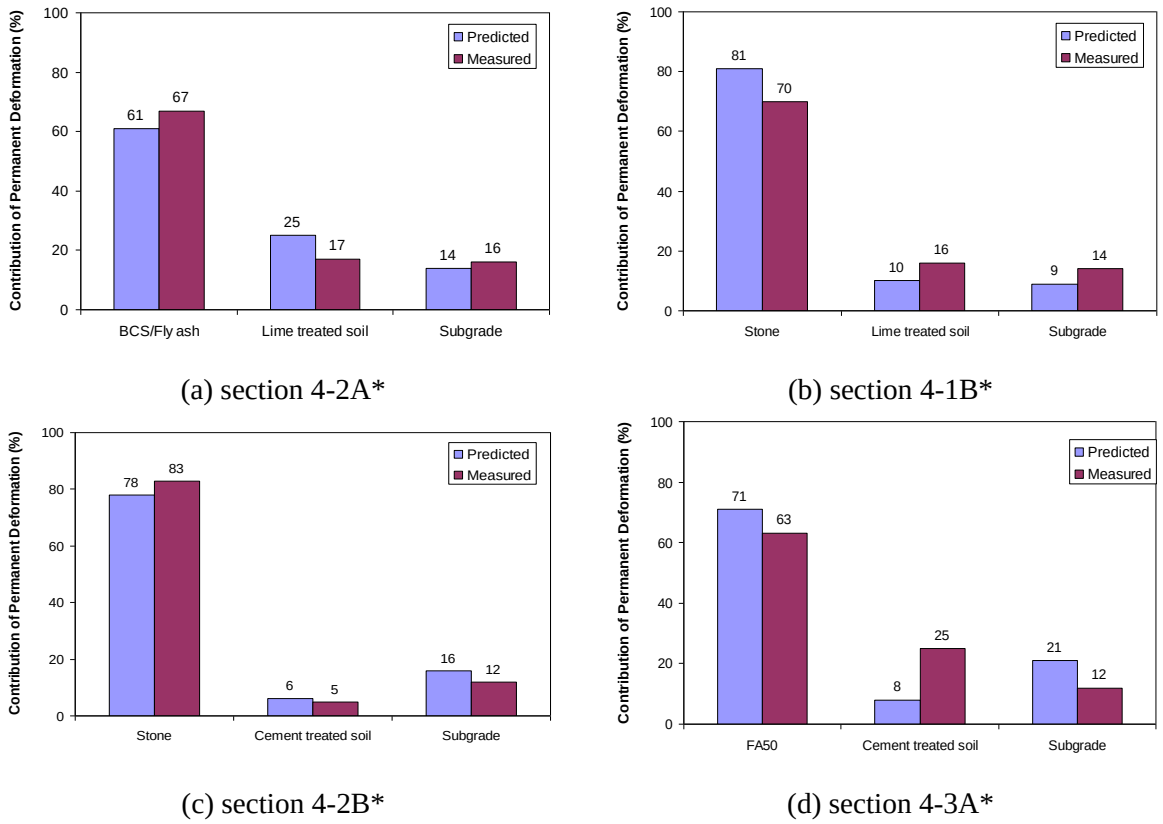

(a) section 4-2A*

(b) section 4-1B*

(c) section 4-2B*

(d) section 4-3A*

*The pavement structure and materials of each section are described in Table 2

Figure 39
Measured and predicted layer contribution of permanent deformation

Shift Factor for Predicted to Measured Permanent Deformation

The shift factors calibrated from the APT sections are summarized in Table 13. The average of the shift factor was 1.13, and the coefficient of variation was 26.6 percent.

Table 13
Shift factors for APT sections

Sections	4-1A	4-2A	4-1B	4-2B	4-3A	4-3B
Shift Factor	1.0	1.4	1.6	1.0	0.8	1.0
Avg.	1.13					
Stdev.	0.30					
Cov (%)	26.6					

Results of Prediction of Permanent Deformation with Other Materials

Material Parameters

The designed lime/fly ash content (by weight) was 2.6 percent lime/6 percent fly ash to achieve a seven-day UCS strength of 150 psi. To achieve a similar UCS strength, the cement content (by weight) was between 2 and 4 percent. The contents of 3 percent (interpolated) and 4 percent cement treated soils were selected to compare with 2.6 percent lime/6 percent fly ash to treat soil. More detail of laboratory design and P-D tests results are provided in Appendix D.

Table 14 presents the material parameters for lime/fly ash and cement treated soils obtained from the P-D tests.

Table 14
Material parameters for lime/fly ash and cement treated sandy clay

Materials		Proposed Permanent Deformation Model					Accelerated analysis parameter B
		E_L (ksi)	σ_y (psi)	h (ksi)	$d=a/N^b+1$		
					a	b	
Lime/Fly Ash	#1	60.5	4.7	49.9	0.061	0.83	0.19
	#2	79.9	4.8	41.1	0.064	0.74	0.21
	Ave.	70.2	4.7	45.5	0.063	0.78	0.20
3% Cement	#1	55.4	4.7	37.6	0.088	0.85	0.19
	#2	84.4	4.5	47.1	0.256	0.95	0.20
	Ave.	69.9	4.6	42.3	0.172	0.90	0.20
4% Cement	#1	79.0	4.6	55.4	0.123	0.92	0.19
	#2	101.2	5.0	45.3	0.037	0.76	0.15
	Ave.	90.1	4.8	50.4	0.080	0.84	0.17

FE Simulation Results

Figure 40 presents the predicted permanent deformation development of pavement with cement and lime/fly ash treated subbase under APT loading. Table 15 shows the predicted layer permanent deformation after 700,000 cycles. Based on the prediction results, the stone base layer contributes the most permanent deformation for all three pavement structures, followed by the subgrade and treated subbase layer. The 2-in. HMA layer contributed negligible permanent deformation. This trend was consistent with the finished ALF4 APT tests *[49]*. For the treated subbase layer, the 3 percent cement treated subbase developed the largest permanent deformation, followed by 2.6 percent lime/6 percent fly ash and 4 percent cement treated subbase layers. The treated subbase layer also had an influence on the permanent deformation of the base and subgrade. The ranking of surface permanent

deformation from high to low was the pavement with 3 percent cement treated, 2.6 percent lime/6 percent fly ash treated, and 4 percent cement treated subbase layer.

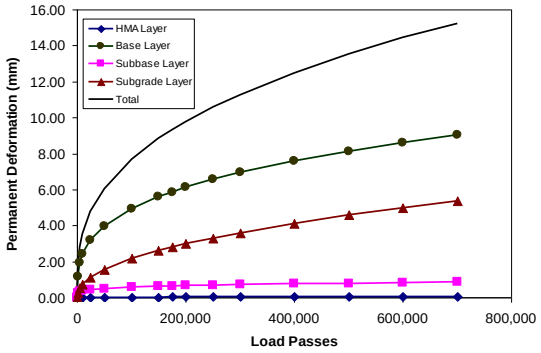

(a) 3% cement

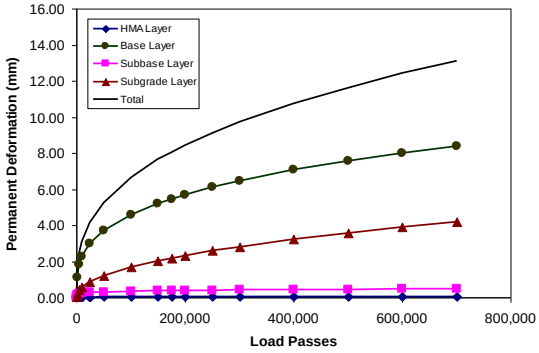

(b) 4% cement

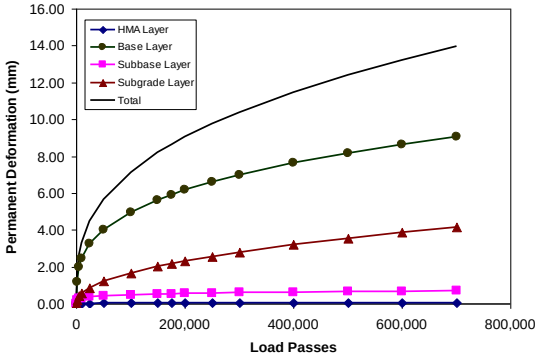

(c) 2.6% lime/ 6% fly ash

Figure 40
Predicted layer permanent deformation with lime/fly ash and cement treated subbase layer (1 in. = 25.4 mm)

Table 15
Predicted permanent deformation with lime/fly ash and cement treated subbase layer

Pavement Layer	Rut Depth After 700,000 cycles, unit: in.		
	3% Cement	4% Cement	2.6% Lime/6% Fly ash
HMA Layer	0.001	0.002	0.002
Base Layer	0.36	0.33	0.36
Subbase Layer	0.03	0.02	0.03
Subgrade Layer	0.21	0.17	0.16
Total	0.6	0.52	0.55

Figure 41 presents the predicted average and upper and lower bounds of permanent deformation for pavements with lime/fly ash and cement treated subbase. Table 16 presents the pavement life when the predicted surface average permanent deformation reached 0.5 in. (12.5mm). The predicted pavement life for pavements with 3 percent cement, 2.6 percent lime/6 percent fly ash, and 4 percent cement subbase layer were 401,000; 509,000; and 612,000 cycles, respectively. Based on the predicted permanent deformation, the performance of the 2.6 percent lime/6 percent fly ash treated subbase would be similar to that of a 3.5 percent cement treated subbase.

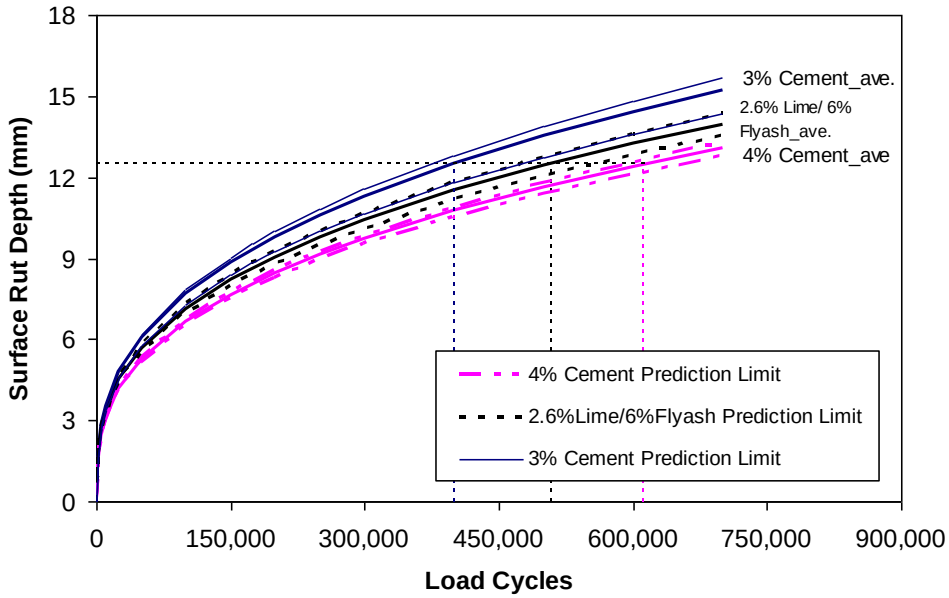

Figure 41
Predicted surface permanent deformation with lime/fly ash and cement treated subbase layer (1 in. = 25.4 mm)

Table 16
Predicted pavement life with lime/fly ash and cement treated subbase layer

Subbase Material	3% Cement	4% Cement	2.6% Lime/6% Flyash
Pavement Life @ 0.5 in.	401,000	612,000	509,000

Figure 42 presents the predicted or tested surface permanent deformation for pavements with various subbase materials under APT loading. All these pavements share the same pavement structure: 2-in. HMA layer, 8.5-in. stone base layer, 12-in. treated subbase layer, and subgrade. The APT loading was 9750 lbf, and the tire pressure was 105 psi. The permanent deformation of sections 4-1B with 3.2 percent lime (by weight) treated subbase and section 4-2B with 6.9 percent cement (by weight) treated subbase were measured during APT testing

at every 25,000 cycles. The predicted surface permanent deformation of pavements with 2.6 percent lime/6 percent fly ash and 3 and 4 percent cement treated subbase were larger than those of section 4-2B, but smaller than those of section 4-1B.

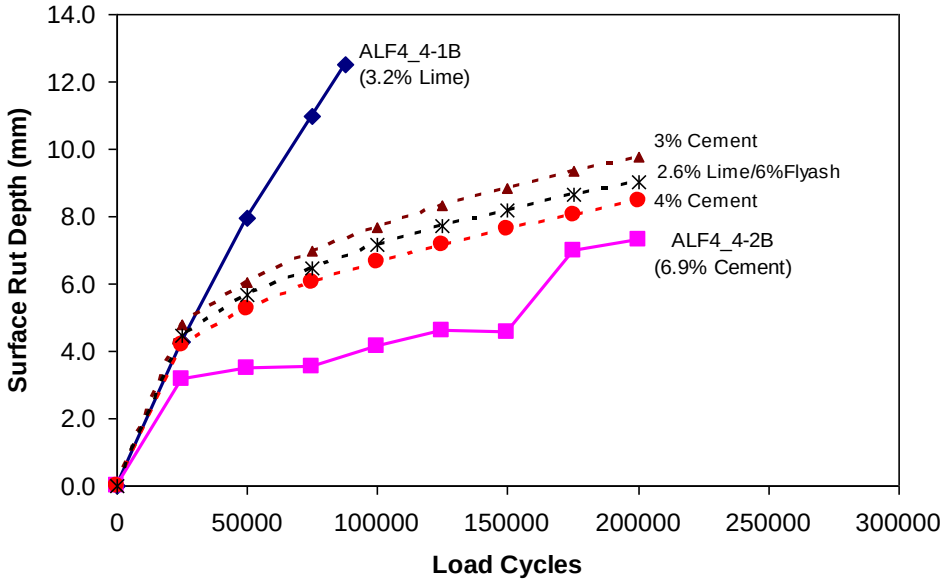

Figure 42
Predicted or tested surface permanent deformation for various subbase materials (1 in. = 25.4 mm)

Economic Analysis

Table 17 presents the economic analysis results of lime/fly ash and cement treated subbase layers. For subbase layers treated by 2.6 percent lime/6 percent fly ash and 3.5 percent cement, which have a similar performance based on predicted pavement life, material linear foot costs were 5.36 and 5.46 dollars/linear ft., respectively. The analysis showed that lime/fly ash treated soil could be a viable alternative to cement treated subbase.

Table 17
Economic analysis of lime/fly ash and cement treated soils

Materials		Content in volume (%)	Weight per linear ft. (lb/linear ft.)	Material Cost (dollars/linear ft.)	
2.6% Lime/6% Fly ash	Lime	8.3	37.8	2.76	**5.36**
	Fly ash	11.1	86.6	2.6	
3% Cement	cement	3.6	44		4.74
4% Cement		4.7	57.4		6.18
3.5% Cement		4.15	50.7		**5.46**

Results of Predicted Permanent Deformation of Typical Low Volume Pavement

Table 18 presents the traffic information for the selected project on LA28. The equivalent single axle loads (ESALs) after 1.9, 3.9, and 5.8 years were 131,173; 271,897; and 408,224; respectively. Table 19 presents the traffic information for the selected project on LA10. The ESALs after 1.8, 3.7, 5.6, and 8.1 years were 10,859; 22,641; 34,760; and 51,237; respectively. As shown in Table 18 and Table 19, although the percentages of vehicle type 9 were small in ADT percentages (4.5 percent for LA28 and 3.0 percent for LA10), the vehicle type 9 contributed the largest part of ESALs for both projects, which were about 60 percent in these two projects.

Table 18
Traffic information for the project on LA28

Vehicle Type	Percentage (%)	Annual Growth (%)	ESALs		
			1/13/2003 (1.9 Years)	1/17/2005 (3.9 Years)	11/22/2006 (5.8 Years)
1	0.2	1.0	2	3	5
2	56.7	1.0	435	901	1,352
3	31.5	1.0	9,078	18,817	28,252
4	0.5	1.0	1,481	3,069	4,608
5	4.0	1.0	11,846	24,555	36,867
6	1.0	1.0	6,277	13,012	19,536
7	0.1	1.0	628	1,301	1,954
8	1.1	1.0	14,862	30,807	46,253
9	4.5	1.0	75,880	157,285	236,146
10	0.1	1.0	2,223	4,607	6,917
11	0.1	1.0	2,821	5,847	8,778
12	0.1	1.0	2,821	5,847	8,778
13	0.1	1.0	2,821	5,847	8,778
Total	100		**131,173**	**271,897**	**408,224**

Table 19
Traffic information for the project on LA10

Vehicle Type	Percentage (%)	Annual Growth (%)	ESALs			
			10/28/2000 (1.8 Years)	10/16/2002 (3.7 Years)	8/27/2004 (5.6 Years)	2/25/2007 (8.1 Years)
1	0.2	1.5	0	0	1	1
2	54.4	1.5	52	108	166	245
3	35	1.5	1,254	2,615	4,015	5,919
4	0.5	1.5	184	384	589	869
5	5.6	1.5	2,063	4,300	6,602	9,732
6	1.3	1.5	1,015	2,116	3,249	4,788
7	0.0	1.5	0	0	0	0
8	0.0	1.5	0	0	0	0
9	3.0	1.5	6,291	13,117	20,137	29,683
10	0.0	1.5	0	0	0	0
11	0.0	1.5	0	0	0	0
12	0.0	1.5	0	0	0	0
13	0.0	1.5	0	0	0	0
Total	100		**10,859**	**22,641**	**34,760**	**51,237**

The permanent deformations for selected projects were measured about every two years by a laser profilemeter, and the interval of measurement stations was 0.1 mile. For the project on LA28, permanent deformations were measured on 01/13/2003, 01/17/2005, and 11/22/2006. For the project on LA10, permanent deformations were measured on 10/28/2000, 10/16/2002, 08/27/2004, and 02/25/2007. Table 20 presents the measured permanent deformations of the selected projects.

Table 20
Measured rut depths for selected projects

LA28			LA10		
Date	Rut Depth (in.)		Date	Rut Depth (in.)	
	Avg.	Std.		Avg.	Std.
01/13/2003	0.106	0.026	10/28/2000	0.104	0.010
01/17/2005	0.196	0.054	10/16/2002	0.118	0.020
11/22/2006	0.191	0.059	08/27/2004	0.150	0.042
—	—	—	02/25/2007	0.208	0.079

Note: "—"means not applicable.

Table 21 presents the material parameters used for two selected projects.

Table 21
Material parameters for the selected projects

Materials	Proposed Permanent Deformation Model						Accelerated analysis parameter "B"
	E_L (ksi)	σ_y (psi)	h (ksi)	$d=a/N^b+1$		Poisson's Ratio	
				A	b		
HMA	100	13	189	0.0100	0.6	0.35	0.2
Soil Cement Base	65	10.9	67	0.0090	0.55	0.3	0.24
Crushed Stone Base	33	10.7	71	0.0960	0.64	0.3	0.31
Cement Stabilized Base	65	5.0	67	0.0027	0.56	0.3	0.24
Subgrade	7	4.2	7	0.0340	0.59	0.45	0.47

The load wander effect and the shift factor of 1.13 obtained from the APT sections were used in the FE simulation. Figure 43 presents the predicted and measured permanent deformations of the selected projects. Overall, the predicted permanent deformations matched well with measured deformations. Figure 44 presents the predicted permanent deformations in each pavement layer.

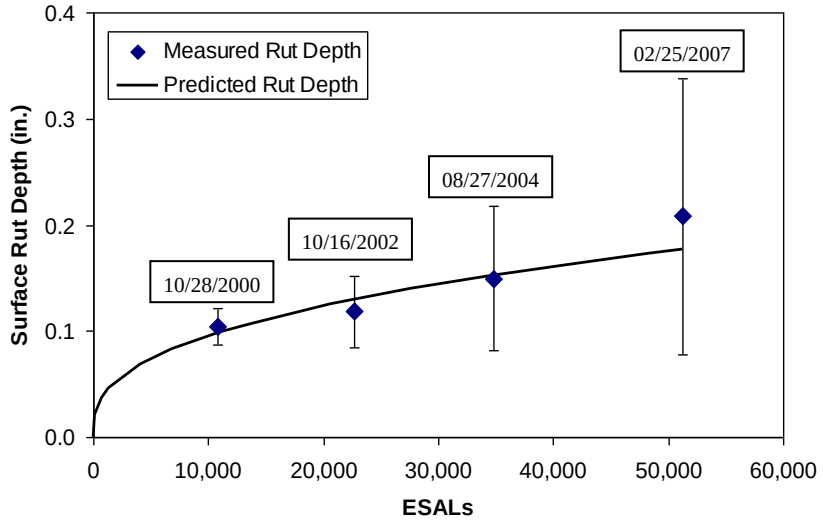

(a) LA10

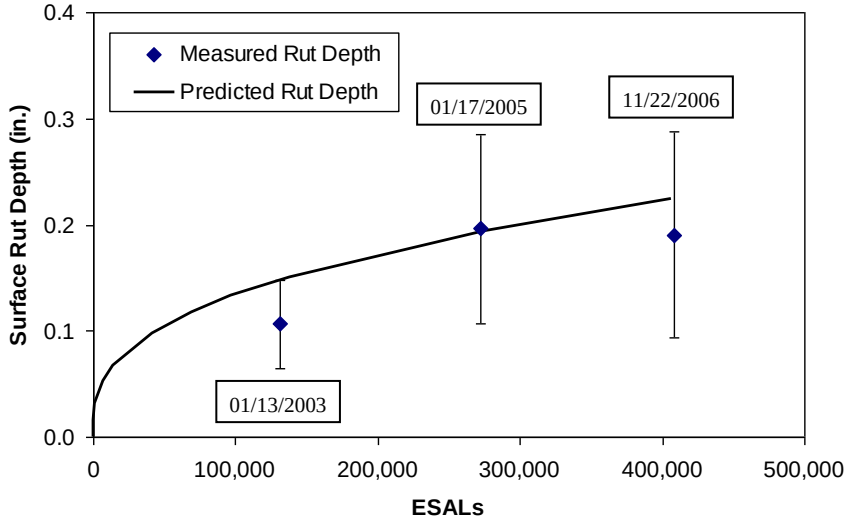

(b) LA28

Figure 43
Predicted and measured permanent deformations for selected projects

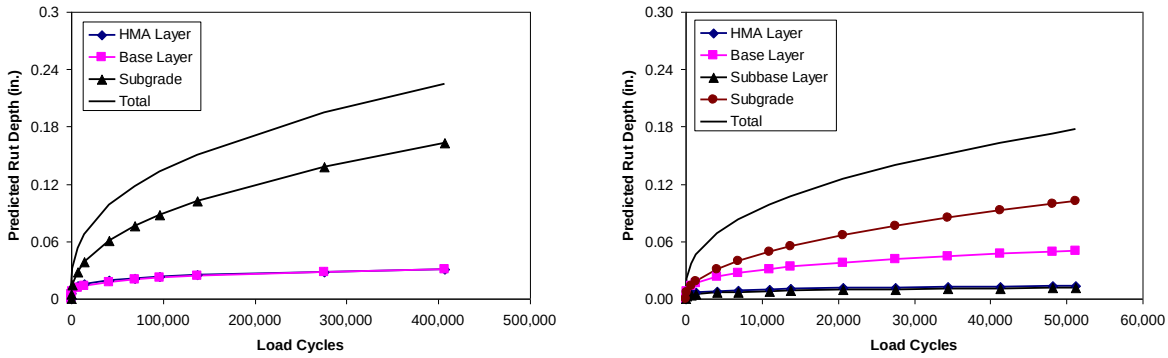

(a) LA28 (b) LA10

Figure 44
Predicted layer rut depths for selected projects

P-D Prediction Models (Transfer Function) for Base and Subbase/Subgrade Materials

Development of P-D Transfer Function

The P-D prediction models (transfer functions) for four categories of pavement base and subbase/subgrade materials were developed based on the FE simulation. Table 22, Table 23, Table 24, and Table 25 present the results of the regression analysis for P-D transfer functions of these materials. The regressive transfer functions have R-Squares higher than 0.90. The F-test indicated the all three independent variables (Log(ε_v), Log(a), and Log$\left[\frac{(n+1)^{1-b}-1}{1-b}\right]$) have a significant influence on the dependent variable Log(ε^p).

Table 22
Regression analysis for transfer function of stabilized base materials

Dep. Var. = Log (ε^p)	N = 3384	R-Square = 0.9848	Adjusted R-Square = 0.9848			
Root MSE = 0.05015	Dependent Mean = -2.63499	Coeff. Var. = -1.90320				
Variable	Coefficient	STD error	STD Coef.	Tolerance	Type II SS	F Value
Intercept	-2.82054	0.01937	0	.	53.32705	21204.1
Log(ε_v)	0.46816	0.00503	0.20240	0.94709	21.75146	8648.88
Log(a)	0.12250	0.00445	0.05982	0.95180	1.90940	759.22
$\text{Log}\left[\frac{(n+1)^{1-b}-1}{1-b}\right]$	0.89856	0.00210	0.92646	0.95916	461.5609	183527

Analysis of Variance

Source	DF	Sum of Squares	Mean Square	F Value	Pr > F
Regression	3	552.13975	184.04658	73181.1	< 0.0001
Residual	3380	8.50052	0.00251		
Corrected Total	3383	560.64026			

Table 23
Regression analysis for transfer function of unbound base materials

Dep. Var. = Log (ε^p)	N = 4,872	R-Square = 0.9611	Adjusted R-Square = 0.9610			
Root MSE = 0.08293	Dependent Mean = -2.09502	Coeff. Var. = -3.95854				
Variable	Coefficient	STD error	STD Coef.	Tolerance	Type II SS	F Value
Intercept	-0.68039	0.01548	0	.	13.27941	1930.77
Log(ε_v)	0.85216	0.00464	0.52123	0.99511	232.4201	33792.9
Log(a)	0.58708	0.00703	0.23700	0.99350	47.97490	6975.35
$\text{Log}\left[\frac{(n+1)^{1-b}-1}{1-b}\right]$	0.78918	0.00286	0.78097	0.99807	523.3389	76091.3

Analysis of Variance

Source	DF	Sum of Squares	Mean Square	F Value	Pr > F
Regression	3	826.22362	275.40787	40043.2	< 0.0001
Residual	4868	33.48102	0.00688		
Corrected Total	4871	859.70463			

Table 24
Regression analysis for transfer function of treated subbase/subgrade materials

Dep. Var. = Log (ε^p) N = 2,033 R-Square = 0.9308 Adjusted R-Square = 0.9307
Root MSE = 0.10188 Dependent Mean = -3.03005 Coeff. Var. = -3.36233

Variable	Coefficient	STD error	STD Coef.	Tolerance	Type II SS	F Value
Intercept	0.27772	0.03935	0	.	0.51712	49.82
$\text{Log}(\varepsilon_v)$	1.03095	0.01371	0.53829	0.66566	58.71689	5656.97
$\text{Log}(a)$	0.43255	0.01190	0.25736	0.68002	13.71097	1320.96
$\text{Log}\left[\frac{(n+1)^{1-b}-1}{1-b}\right]$	0.59982	0.00479	0.74137	0.97395	162.9604	15700.1

Analysis of Variance

Source	DF	Sum of Squares	Mean Square	F Value	Pr > F
Regression	3	283.36483	94.45494	9100.09	< 0.0001
Residual	2029	21.06012	0.01038		
Corrected Total	2032	304.42495			

Table 25
Regression analysis for transfer function of untreated subgrade

Dep. Var. = Log (ε^p) N = 1,596 R-Square = 0.9031 Adjusted R-Square = 0.9029
Root MSE = 0.20457 Dependent Mean = -3.37127 Coeff. Var. = -6.06806

Variable	Coefficient	STD error	STD Coef.	Tolerance	Type II SS	F Value
Intercept	5.74466	0.15636	0	.	54.49084	1349.86
Log (ε_v)	3.02187	0.03501	0.68911	0.95506	311.7597	7449.59
Log (a)	0.37620	0.04164	0.07392	0.90954	3.41589	81.626
$\text{Log}\left[\frac{(n+1)^{1-b}-1}{1-b}\right]$	0.99161	0.01153	0.68880	0.94929	309.5893	7397.73

Analysis of Variance

Source	DF	Sum of Squares	Mean Square	F Value	Pr > F
Regression	3	620.77090	206.92363	4944.50	< 0.0001
Residual	1592	66.62402	0.04185		
Corrected Total	1595	687.39492			

From the regression analysis, the P-D transfer functions of base materials can be written as:
Stabilized base materials:

$$\varepsilon^p = 0.00151(\varepsilon_v)^{0.46816}(a)^{0.1225}\left[\frac{(n+1)^{1-b}-1}{1-b}\right]^{0.89856} \quad R^2 = 0.98 \qquad (20)$$

Unbound base materials:

$$\varepsilon^p = 0.20874(\varepsilon_v)^{0.85216}(a)^{0.58708}\left[\frac{(n+1)^{1-b}-1}{1-b}\right]^{0.78918} \quad R^2 = 0.96 \qquad (21)$$

Treated Subbase/Subgrade materials:

$$\varepsilon^p = 1.89548(\varepsilon_v)^{1.03095}(a)^{0.43255}\left[\frac{(n+1)^{1-b}-1}{1-b}\right]^{0.59982} \quad R^2 = 0.93 \qquad (22)$$

Untreated Subgrade:

$$\varepsilon^p = 10^{5.74466}(\varepsilon_v)^{3.02187}(a)^{0.3762}\left[\frac{(n+1)^{1-b}-1}{1-b}\right]^{0.99161} \quad R^2 = 0.90 \qquad (23)$$

Figure 45 to Figure 48 present the comparison between “measured” and predicted permanent strain for pavement materials. Here, the “measured” permanent stains are obtained by FE simulation; whereas, the “predicted” permanent strains are predicted by the developed transfer functions. It can be found that the “measured” and predicted permanent strains are reasonably close.

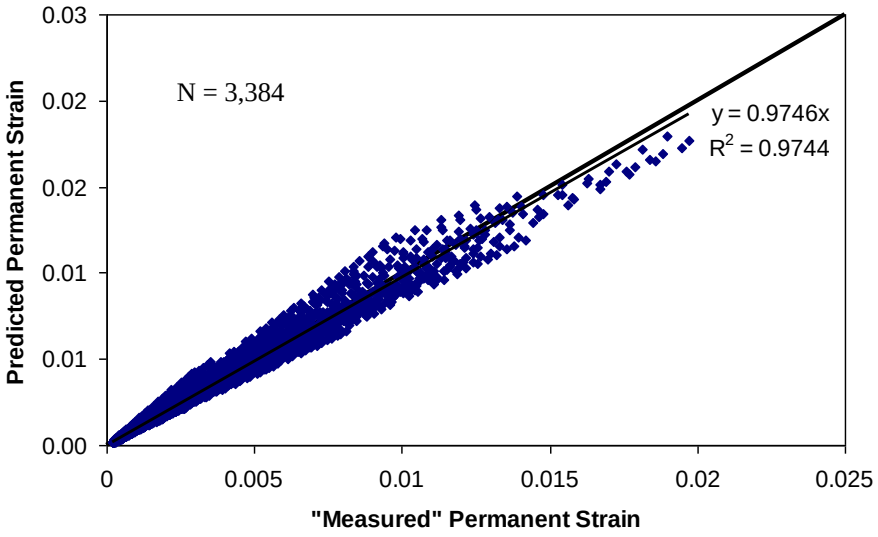

Figure 45
Comparison between "measured" and predicted permanent strains for stabilized base materials

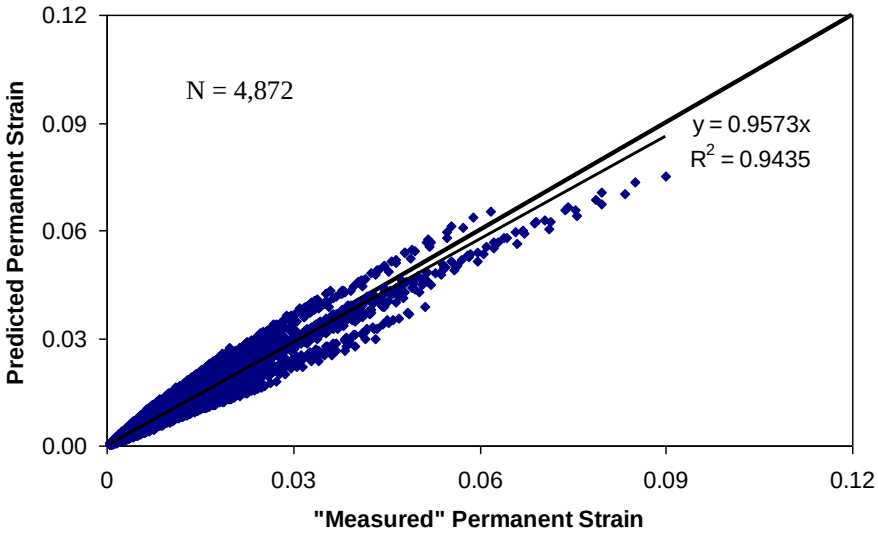

Figure 46
Comparison between "measured" and predicted permanent strains for unbound base materials

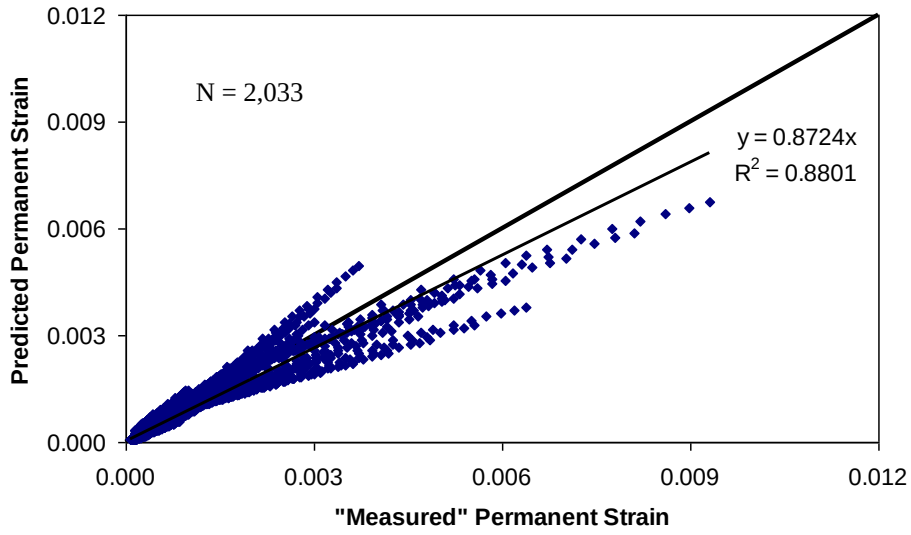

Figure 47
Comparison between "measured" and predicted permanent strains for treated subbase/subgrade materials

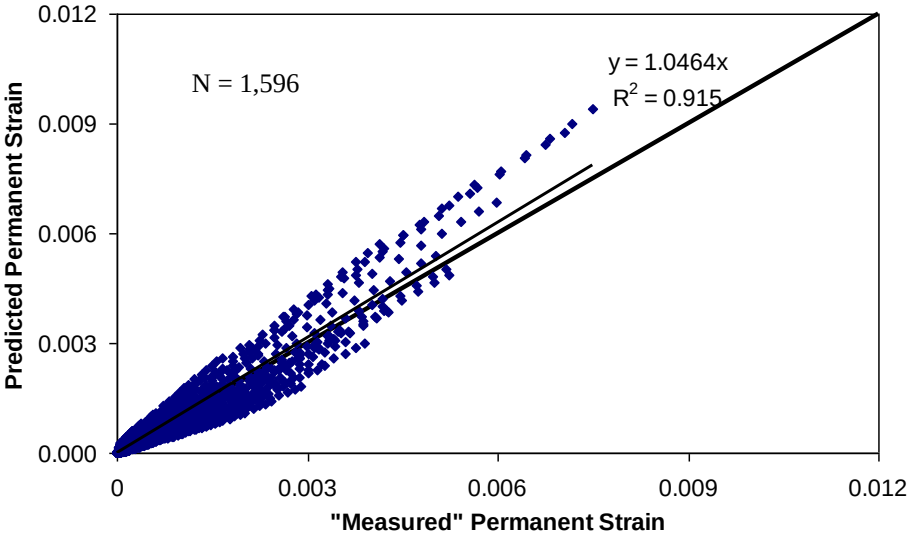

Figure 48
Comparison between "measured" and predicted permanent strains for untreated subgrade

Verification of P-D Transfer Functions

Prediction of Permanent Deformation of APT Sections by Prediction Model. The developed P-D transfer functions were utilized to predict the permanent deformation of six

APT test sections. Figure 49, Figure 50, and Figure 51 present the comparison between predicted and measured permanent deformations of the base, subbase, and subgrade layer of six APT sections, respectively. Figure 52 presents the comparison between predicted and measured total permanent deformations under HMA layer of six APT sections. It can be found that the permanent deformations predicted by transfer functions are in good agreement with measured ones.

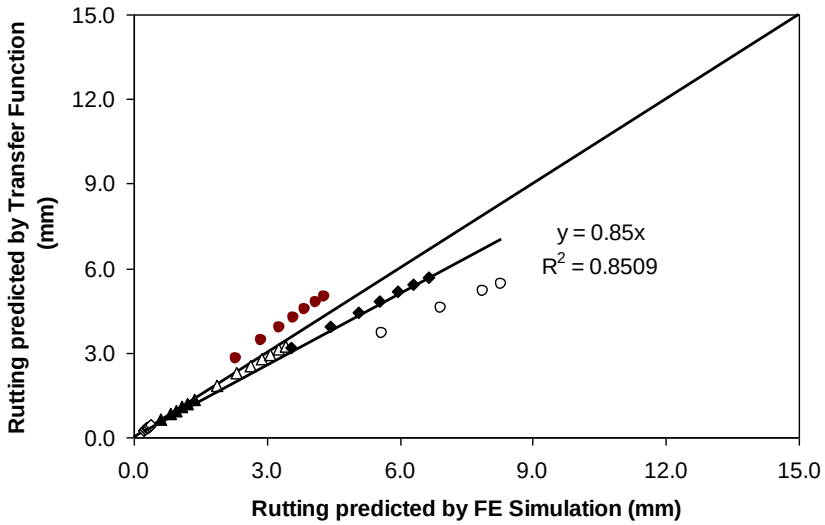

Figure 49
Comparison between predicted and measured base layer permanent deformations of APT test sections (1 in. = 25.4 mm)

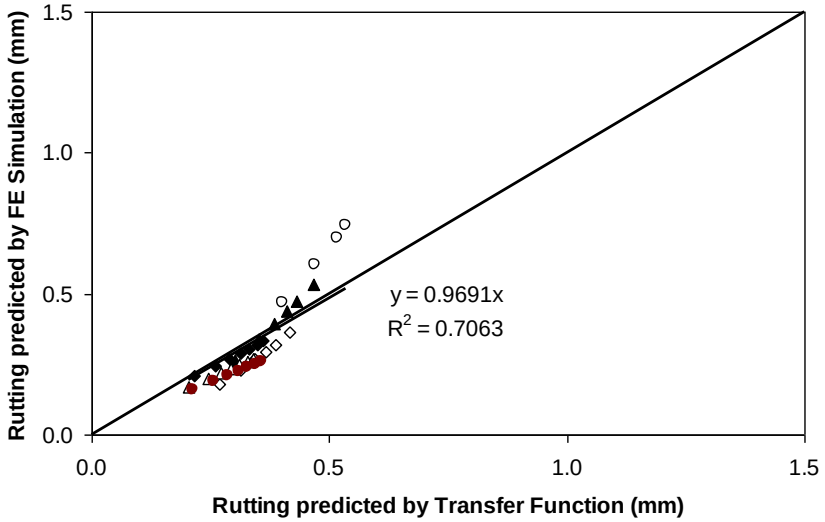

Figure 50
Comparison between predicted and measured subbase layer permanent deformations of APT test sections (1 in. = 25.4 mm)

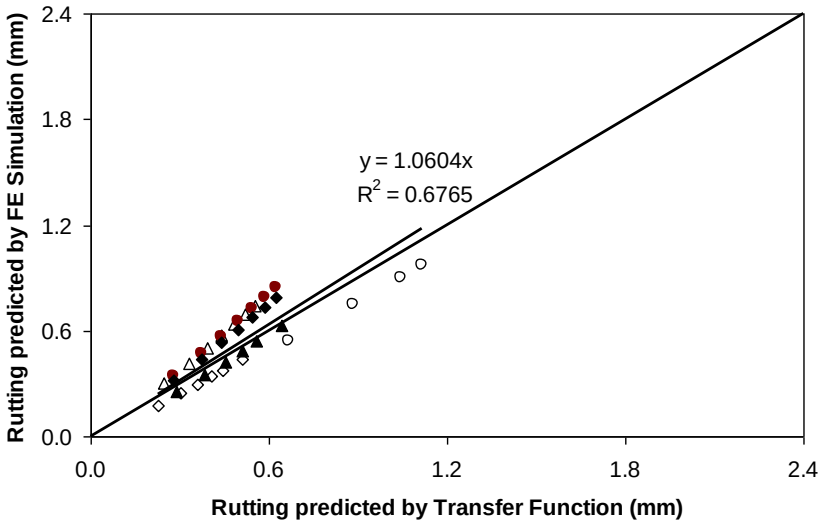

Figure 51
Comparison between predicted and measured subgrade layer permanent deformations of APT test sections (1 in. = 25.4 mm)

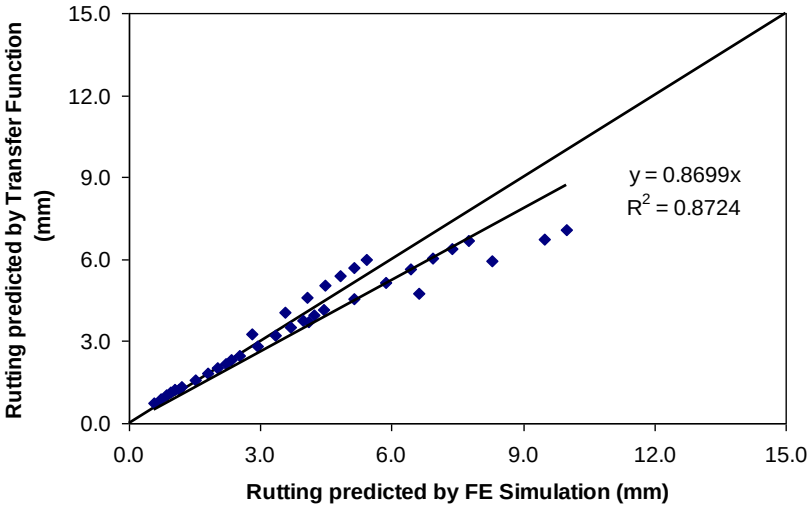

Figure 52
Comparison between predicted and measured total permanent deformations under HMA layer of APT test sections (1 in. = 25.4 mm)

Prediction of Permanent Deformation of Low Volume Pavements. Since only transfer functions for base and subbase/subgrade materials were developed in this study, the permanent deformations under the HMA layer were calculated. Figure 53 presents the predicted and measured permanent deformation under the HMA layer for the two selected

projects. To obtain an estimate of the true field permanent deformation under the HMA layer, the percentage from the FE predicted permanent deformation under the HMA layer was multiplied by the average total permanent deformation. As shown in Figure 53, the predicted permanent deformations match well with measured ones for project LA10, which had a similar four-layer pavement structure with ALF sections. The transfer function slightly over-predicted permanent deformations for project LA28, which had a three-layer pavement structure. It should be noted that for LA28, the predicted permanent deformation after 275,500 ESALs was within the 90 percent confidence limit; whereas, the measured average permanent deformation after 406,500 ESALs was smaller than that after 275,500 ESALs for some unknown reasons. On the other hand, since the transfer function was developed based on ALF section structures, further calibration is recommended when it is applied to other pavement structures.

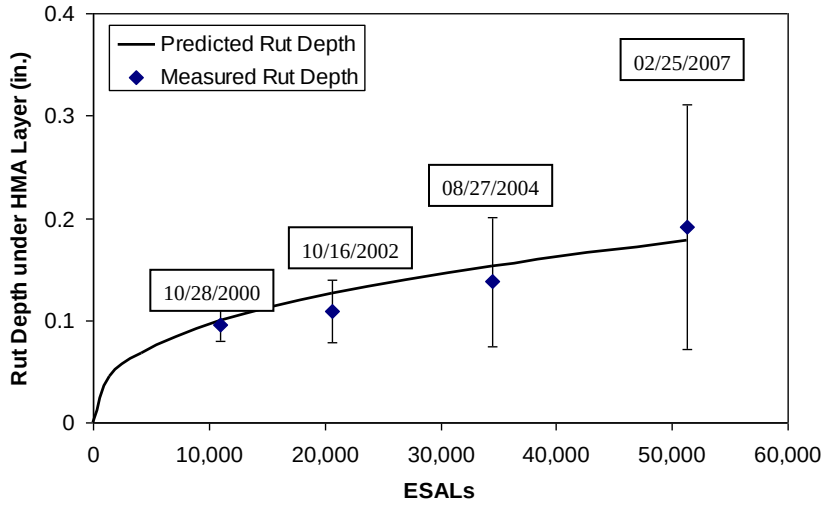

(a) LA10

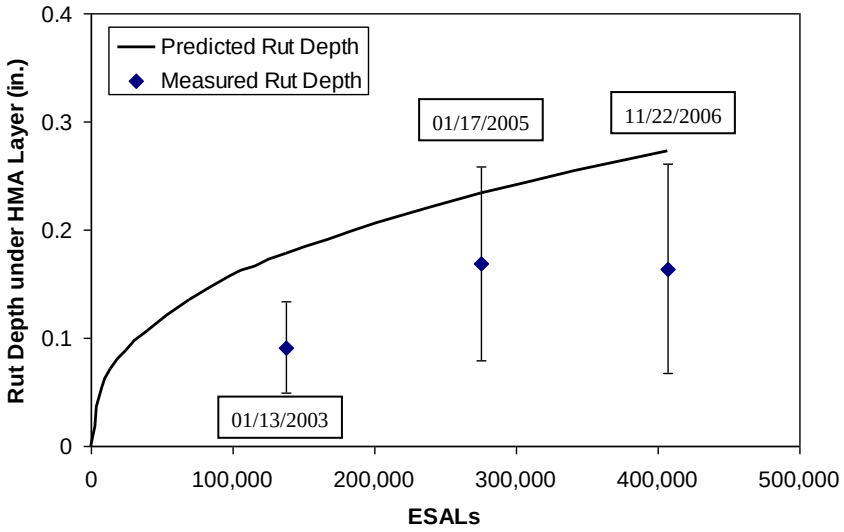

(b) LA28

Figure 53
Predicted and measured permanent deformation under HMA layer for selected projects

CONCLUSIONS

A P-D material model was proposed in this study for simulation of pavement base and subgrade materials under repeated loading. This model was modified from a conventional elastoplastic model with linear strain hardening. The permanent deformation behavior of materials under repeated loading was approximated by varying the loading and unloading moduli in the constitutive model. The proposed P-D model contains four sets of input model parameters. All model parameters can be obtained from a single laboratory P-D test. A P-D test data analysis spreadsheet by Excel Macro (VBA) was developed to obtain these model parameters from the P-D test data.

The P-D model was verified by simulating the laboratory P-D tests on eight pavement base and subbase/subgrade materials. A sensitivity analysis was conducted to evaluate the effects of material model parameters, pavement structures, and load configurations on permanent deformation in the pavement structure. The proposed P-D material model was implemented into a commercial FE program, ABAQUS, through a user-defined UMAT subroutine. FE models were created to simulate the permanent deformation of the six APT test sections and two low-volume road pavements in Louisiana.

The following conclusions can be drawn from this study:

- Comparison showed that the axisymmetric model has the best computational efficiency and meanwhile produces compatible results compared with the more “realistic” 3-D model.

- The sensitivity analysis results indicated that the proposed P-D model could effectively predict the permanent deformation for different pavement structures.

- By simulating the permanent deformation of the six APT test sections, a shift factor of 1.13 was calibrated to account for the condition differences between the laboratory P-D test and the field.

- Based on the FE predicted permanent deformation, the performance of 2.6 percent lime/6 percent fly ash (by weight) treated sandy clay subbase would be similar to that of 3.5 percent cement (by weight) treated the same soil subbase. The analysis also showed that lime/fly ash treated soil could be a viable alternative to cement treated soil.

- The developed FE model and the calibrated shift factor (1.13) were applied to predict the permanent deformation of two typical low volume pavement structures used in Louisiana. Overall, the predicted permanent deformations matched well with the measured data.

- The APT test calibrated FE model was used to develop P-D prediction models (transfer functions) for pavement base and subbase/subgrade materials. The predicted permanent deformations based on transfer functions also matched well with field measured data.

RECOMMENDATIONS

It is recommended that the developed FE model may be used in one of the following application areas:

- Determination of the APT permanent deformation performance of other stabilized base or subbase materials to be used in a similar pavement structure as those of the ALF 4 without the need of actual running APT tests.

- As a pre-analysis tool in the selection process of APT test sections for a new APT experiment in which test sections with different combinations of materials and layer thicknesses may be proposed and the preliminary performance for each proposed section may be predicted using the FE model developed and compared to each other.

- As a comparison tool to the DARWin-ME (or MEPDG) in the prediction of permanent deformation for stabilized base and subbase materials, and use the comparison results in the development of pavement design manual for LADOTD.

In addition, the developed permanent deformation prediction models (or transfer functions) for various pavement materials are also recommended to be used in the prediction of the permanent deformation of pavement structures under accelerated loading. However, the developed transfer functions are limited only to those materials considered in the ALF4 experiment of this study. Therefore, developing transfer functions for other pavement materials is recommended to be considered in the future. In the mean time, the calibration constants of developed transfer functions may be further calibrated by more field projects.

ACRONYMS, ABBREVIATIONS, AND SYMBOLS

2-D	Two Dimensions
3-D	Three Dimensions
AASHTO	American Association of State Highway and Transportation Officials
ADT	Average Daily Traffic
AI	Asphalt Institution
ALF	Accelerated Loading Facility
ANOVA	Analysis of Variation
APT	Accelerated Pavement Testing
BCS	Blended Calcium Sulfate
C3D20R	The 20-node Quadratic Brick Reduced Integration Elements
CAX8R	The Eight-node Biquadratic Axisymmetric Quadrilateral Element
CPU	Central Processing Unit
CSSM	Critical State Soil Mechanics
DEM	Discrete Element Method
DSC	Disturbed State Concept
E-P	Elastic-Plastic
ESAL	Equivalent Single Axle Loads
FA	Foamed asphalt
FDM	Finite Difference Method
FE	Finite Element
FEM	Finite Element Method
FLEXPASS	Flexible Pavement Analysis Structural System
FWD	Falling Weight Deflectometer
Hiss	Hierarchical Single Surface
HMA	Hot-mix Asphalt
HVS	Heavy Vehicle Simulator
ICM	Integrated Climatic Model
LADOTD	Louisiana Department of Transportation and Development
LAPMS	Louisiana Pavement Management Systems
LEF	Load Equivalency Factor
LTPP	Long Term Pavement Performance
LTRC	Louisiana Transportation Research Center
LSU	Louisiana State University
MDD	Multi Depth Deflectometer
MEPDG	Mechanistic-Empirical Pavement Design Guide

MTS	Material Testing Systems
NCHRP	National Cooperative Highway Research Program
OA	Orthogonal Arrays
P-D	Permanent Deformation
PDE	Partial Differential Equation
PRF	Pavement Research Facility
RAP	Recycled Asphalt Pavement
SAS	Statistical Analysis Software
UCS	Unconfined Compressive Strength
UMAT	User-defined Material Subroutine
USCS	Unified Soil Classification System
VBA	Visual Basic for Applications

REFERENCES

1. Duncan, J. M., Monismith, C. L., and Wilson, E. L. "Finite Element Analysis of Pavements." *Highway Research Record 228*, Highway Research Board, 1968, pp. 18-33.
2. Raad, L., and Figueroa, J. L. "Load Response of Transportation Support Systems." *Journal of Transportation Engineering*, Vol. 106, No. 1, 1980, pp. 111-128.
3. Harichandran, R. S., Baladi, G. Y., and Yeh, M. *Development of a Computer Program for Design of Pavement Systems Consisting of Bound and Unbound Materials*. Report No. FHWA-MI-RD-89-02. Michigan Department of Transportation, 1989.
4. Lytton, R. L., and Tseng, K. H. "Fatigue Damage Properties of Asphaltic Concrete Pavements." In *Transportation Research Record 1286*, Transportation Research Board, Washington, D.C., 1990, pp. 150-163.
5. White, T. D. "Application of Finite Element Analysis to Pavement Problems." *Finite Element for Pavement Analysis and Design, Proceedings of the First National Symposium on 3D Finite Element Modeling for Pavement Analysis & Design*, Charlston, W. Virginia, November 8-10, 1998.
6. Huang, B., Mohammad, L. N., and Rasoulian, M. "3-D Numerical Simulation of Asphalt Pavement at Louisiana Accelerated Loading Facility (ALF)." In *Transportation Research Record 1764*, Transportation Research Board, Washington, D.C., 2001, pp. 44-58.
7. Al-Qadi, I. M., Yoo, P. J., Elseifi, M. A, and Janajreh, I. "Characterization of Pavement Damage Due to Different Tire Configurations." *Journal of Association of Asphalt Paving Technologists*, Vol. 74, 2005, pp. 921-962.
8. Desai, C. S. "Unified DSC Constitutive Model for Pavement Materials with Numerical Implementation." *International Journal of Geomechanics*, Vol. 7, No. 2, 2007, pp. 83-101.
9. Howard, I. L., and Warren, K. A. "Finite-Element Modeling of Instrumented Flexible Pavements under Stationary Transient Loading." *Journal of Transportation Engineering*, ASCE, Vol. 135, No. 2, 2009, pp. 53-61.
10. Erkens, S. M. J. G., Liu, X., and Scarpas, A. "3D Finite Element Model for Asphalt Concrete Response Simulation." *The International Journal of Geomechanics*, Vol. 2, No. 3, 2002, pp. 305-330.
11. Desai, C.S. "Mechanistic Pavement Analysis and Design Using Unified Material and Computer Models." 3rd International Symposium on 3D Finite Elements for Pavement Analysis, Amsterdam, Netherlands, 2002, pp. 1-63.
12. Kim, D., Salgado, R., and Altschaeffl, A. G. "Effects of Supersingle Tire Loadings on Pavements." *Journal of Transportation Engineering*, Vol. 132, No. 10, 2005, pp. 732-743.

13. Wu, Z. *Finite Element Simulation of Rutting on Superpave Pavements*. Ph.D. Dissertation, Kansas State University, Manhattan, Kansas, 2001.
14. White, T. D., Haddock, J. E., Hand, A. J. T., and Fang, H. *Contributions of Pavement Structural Layers to Rutting of Hot Mix Asphalt Pavements.* NCHRP Report No. 468. Transportation Research Board of the National Academics, Washington, D.C., 2002.
15. Cho, Y., McCullough, B. F., and Weissmann, J. "Considerations on Finite-Element Method Application in Pavement Structural Analysis." In *Transportation Research Record 1539*, Transportation Research Board, Washington, D.C., 1996, pp. 96-101.
16. Hornych, P., and El Abd, A. *Selection and Evaluation of Models for Prediction of Permanent Deformation of Unbound Granular Materials in Road Pavements*, Work Package 5, Performance-based Specifications, Sustainable and Advanced Materials for Road Infrastructure (SAMARIS), Competitive and Sustainable Growth (GROWTH) Programme, 2004.
17. Helwany, S., Dyer, J., and Leidy, J. "Finite-element Analyses of Flexible Pavements." *Journal of Transportation Engineering*, Vol. 124, No. 5, pp. 491-499.
18. Kim, D. *Effects of Super-Single Tire Loading on Subgrade*. Ph.D. Dissertation, Purdue University, West Lafayette, Indiana, 2002.
19. Saad, B., Mitri, H., and Poorooshasb, H. "Three-Dimensional Dynamic Analysis of Flexible Conventional Pavement Foundation." *Journal of Transportation Engineering*, Vol. 131, No. 6, 2005, pp. 460-469.
20. Zaghloul, S. M., White, T. D., and Kuczek, T. "Use Of Three-Dimensional, Dynamic, Nonlinear Analysis to Develop Load Equivalency Factors for Composite Pavements." In *Transportation Research Record 1449*, Transportation Research Board, Washington, D.C., 1994, pp. 199-208.
21. Kirkner, D. J., Caulfield, P. N., and McCann, D. M. "Three-Dimensional Finite Element Simulation of Permanent Deformations in Flexible Systems." In *Transportation Research Record 1448*, Transportation Research Board, Washington, D.C., 1994, pp. 34-39.
22. Kirkner, D. J., Shen, W., Hammons, M. I., and Smith D. M. "Numerical Simulation of Permanent Deformation in Flexible Pavement Systems Subjected Moving Loads." *Proceeding of the 11th Engineering Mechanics Conference*, ASCE, New York, NY, 1996, pp. 430-433.
23. Dang Van, K., and Maitournam, M. H. "Steady-State Flow in Classical Elasto-Plasticity: Applications to Repeated Rolling and Sliding Contact." *Journal of Mechanics and Physics of Solids*, Vol. 41, No. 11, 1993, pp. 1691-1710.
24. Nazzal, M. D. *Laboratory Characterization and Numerical Modeling of Geogrid Reinforced Bases in Flexible Pavements*. Ph.D. Dissertation, Louisiana State University, 2007.

25. Terrel, R. L., Awad, I. S., and Foss, L. R. "Techniques for Characterizing Bituminous Materials Using a Versatile Triaxial Testing System." *Fatigue and Dynamic Testing of Bituminous Mixtures, ASTM STP 561*, American Society for Testing and Materials, Philadelphia, 1974, pp. 47-66.
26. Desai, C. S., and Whitenack, R. "Review of Models and the Disturbed State Concept for Thermomechanical Analysis in Electronic Packaging." *Journal of Electronic Packaging*, vol. 123, No. 1, 2001, pp. 19-33.
27. Marek, C. R., and Dempsey, B. J. "A Model Utilizing Climatic Factors for Determining Stresses and Deflections in Flexible Pavement Systems." *Proceedings of the Third International Conference on Structural Design of Asphalt Pavements*, London, England. 1972, pp. 101-114.
28. Chen, D., Lin, H., Bilyeu, J., and Murphy, M. "Temperature Correction on FWD Measurements." In *Transportation Research Record 1716*, Transportation Research Board, Washington, D.C., 2000, pp. 30-39.
29. Verhasselt, A. F., and Choquet, F. S. "Comparing Field and Laboratory Ageing of Bitumens on a Kinetic Basis." In *Transportation Research Record 1391*, Transportation Research Board, Washington, D.C., 1993, pp. 30-38.
30. Mirza, M. W., and Witczak, M. W. "Development of a Global Aging System for Short and Long Term Aging of Asphalt Cements." *Journal of the Association of Asphalt Paving Technologists*, Vol. 64, 1995, pp. 393-430.
31. Seibi, A. C. *Development of Constitutive Relations for Asphalt Concrete under High Rates of Loading*. Ph.D. Dissertation, Pennsylvania State University, 1993.
32. Long, F. M. *Permanent Deformation of Asphalt Concrete Pavements: A Nonlinear Viscoelastic Approach to Mix Analyses and Design*. Ph.D. Dissertation, University of California, Berkeley, 2001.
33. Bahuguna, S. *Permanent Deformation and Rate Effects in Asphalt Concrete: Constitutive Modeling and Numerical Implementation*. Ph.D. Dissertation, Case Western Reserve University, 2003.
34. Hornych, P., Chazallon, C., Allou, F., and Abd, A. E. "Prediction of Permanent Deformations of Unbound Granular Materials in Low Traffic Pavements." *Road Material and Pavement Design*, Vol. 8, No. 4, 2007, pp. 643-666.
35. Dunne, F., and Petrinic, N. *Introduction to Computational Plasticity*. Oxford University Press, Oxford, New York, 2005.
36. Dafalias, Y. F. *On Cyclic and Anisotropic Plasticity*. Ph.D. Dissertation, University of California at Berkeley, 1975.
37. Dafalias, Y. F., and Hermann, L. R. *Bounding Surface Formulation of Soil Plasticity*. Soil Mechanics-Transient and Cyclic Loads, Chapter 10, John Wiley and Sons, Ltd.,

1982, pp. 253-282.
38. Dafalias, Y. F., and Hermann, L. R. "Bounding Surface Plasticity. II: Application to Isotropic Cohesive Soils." *Journal of Engineering Mechanics*, ASCE, Vol. 112, No. 12, 1986, pp. 1263-1291.
39. Yu, H. S., Khong, C., and Wang, J. "A Unified Plasticity Model for Cyclic Behavior of Clay and Sand." *Mechanics Research Communications*, Vol. 34, 2007, pp. 97-114.
40. Yang, Z., and Elgamal, A. "A Multi-surface Plasticity Sand Model Including the Lode Angle Effect." *17th ASCE Engineering Mechanics Conference*, June 13-16, 2004, University of Delaware, Newark, DE., 2004.
41. Manzari, M. T., and Dafalias, Y. F. "A Critical State Two-surface Plasticity Model for Sands." *Geotechnique*, Vol. 47, No.2, 1997, pp. 255-272.
42. Hau, K. W., McDowell, G. R., Zhang, G. P., and Brown, S. F. "The Application of a Three-Surface Kinematic Hardening Model to Repeated Loading of Thinly Surface Pavements." *Granular Matter*, Vol. 7, 2005, pp. 145-156.
43. Desai, C. S., Somasundaram, S., and Frantziskonis, G. "A Hierarchical Approach for Constitutive Modeling of Geologic Materials." *International Journal for Numerical and Analytical Methods in Geomechanics*, Vol. 10, 1986.
44. Bonaquist, R.T., and Witczak, M.W. *A Comprehensive Constitutive Model for Granular Materials in Flexible Pavement Structures*, Proc., 8th Intl. Conf. On Asphalts Pavements, Seattle, Washington, 1997, pp. 783-802.
45. Huang, B.; Mohamad, L.; and Wathugala, W. *Development of a Thermo-Viscoplastic Constitutive Model for HMA Mixtures*, Journal of AAPT, 2002, pp. 594-650.
46. Heymsfield, E., Wahl, R. E., and Hodo, W. D. "Development of a Damage Model for Stabilized Soil Layers Subjected to Repetitive Aircraft Loadings." *Proceedings of the 2006 Airfield and Highway Pavement Specialty Conference*, ASCE, Atlanta, GA, 2006, pp. 260-271.
47. Valanis, K. C. "A Theory of Damage in Brittle Materials." *Engineering Fracture Mechanics*, Vol. 36, No. 3, 1990, pp.403-416.
48. Heymsfield, E., Hodo, W. D., and Wahl, R. E. "Development of Damage Model to Analyze Stabilized Soil Layers Subjected to Repetitive Aircraft Loadings." In *Transportation Research Record 1990*, Transportation Research Board, Washington, D.C., 2007, pp. 23-31.
49. Mohammad, L., Herath, A., Rasoulian, M., and Zhang, Z. "Laboratory evaluation of untreated and treated pavement base materials from a repeated load permanent deformation test." The 85th Transportation Research Board Annual Meeting, *CD-ROM*, National Research Council, Washington, D.C., 2006.
50. Wu, Z., Zhang, Z., King, B., and Mohammad, L. "Evaluating Structural Performance of

Base/Subbase Materials at the Louisiana Accelerated Pavement Research Facility." The 86th Transportation Research Board Annual Meeting, *CD-ROM*, National Research Council, Washington, D.C., 2007.

51. Vuong, B. *Permanent Deformation and Resilient Behavior of a Victorian Crushed Rock Using the Repeated Load Triaxial Test*. Report AIR 403-6, Australian Rd. Res. Board, Melbourne, 1985.
52. Bayomy, F. M., Abduljauwad, S. N., and Al-Shaikh, A. "Effect of Geotextile on Permanent Deformation in Salt Encrusted Subgrade Soils." In *Transportation Research Record 1534*, Transportation Research Board, Washington, D.C., 1996, pp. 40-49.
53. Puppala, A. J., Mohammad, L. N., and Allen, A. "Permanent Deformation Characterization of Subgrade Soil from RLT Test." *Journal of Materials in Civil Engineering*, Vol. 11, No.4, 1999, pp. 274-282.
54. Mitchell, J. K. *Fundamentals of Soil Behavior (Second Edition)*, John Wiley & Sons, Inc., 1993.
55. Yandell, W. O. "Prediction of the Behaviour of Elastoplastic Roads During Repeated Rolling Using the Mechano-Lattice Analog." *Highway Research Record 374*, Highway Research Board, National Research Council, Washington, D.C., 1971, pp. 29-41.
56. Uzan, J. "Permanent Deformation in Flexible Pavements." *Journal of Transportation Engineering*, Vol. 130, No. 1, 2004, pp. 6-13.
57. HKS. *ABAQUS User's Manual, Version 6.4*. Hibbit, Karlsson & Sorensen, Inc., Pawtucket, RI, 2003.
58. Ranjit, K. R. *A Primer on the Taguchi Method*. Van Nostrand Reinhold, New York, 1990.
59. Desai, C. S. "Unified DSC constitutive model for pavement materials with numerical implementation." *International Journal of Geomechanics*, Vol. 7, No. 2, 2007, pp. 83-101.

APPENDIX

Appendix A Procedure for Prediction of Pavement Permanent Deformation
Appendix B More Information on the Proposed Permanent Deformation (P-D) Model
Appendix C P-D Test Data Analysis Spreadsheet User's Manual
Appendix D Laboratory Test Results of Lime/Fly Ash and Cement Treated Soils

APPENDIX A

In this study, two approaches of permanent deformation prediction were developed: FE method and prediction model (transfer function) method.

Procedure for FE Method

The pavement permanent deformation can be predicted by FE method by following steps:

(1) Development of FE Model. The axisymmetric modeling is suggested in the permanent deformation simulation considering the computational efficiency. The size and the mesh density of the FE model should be determined by sensitivity analyses. It is suggested that finer mesh be assigned near the surface load. Element of CAX8R in ABAQUS is suggested. The load can be simplified as a circular uniform pressure. A repeated load with a triangle-shape can be applied sequentially to simulate the repeated load.

(2) Material Model and Parameters. The proposed P-D model is applied for pavement layers in the developed axisymmetric FE model. The material parameters are determined by the laboratory P-D test. The user-defined UMAT FORTRAN subroutine for the proposed P-D model was developed in this study. The details about the parameter determination are provided in Appendix C in this report.

(3) ABAQUS FE Simulation. The developed FE model with UMAT subroutine is run in ABAQUS for a reference number of cycles (around 100 cycles). FE simulation with each load level and temperature level needs to be run separately.

(4) Accelerated Analysis Procedure. Based on the predicted permanent deformation developed for a reference number of cycles, the accumulation of permanent deformation is extrapolated via equation (11). If the pavement is subjected to several load and temperature levels, the permanent deformation is first extrapolated separately and then connected as described in this report.

(5) Effect of Wander. The wander adjustment factor for the predicted permanent deformation is calculated by equation (12). For pavements with similar wander as the ALF tests in this study, the wander adjustment factors can be found in Table 12.

(6) Shift Factor for the Predicted Permanent Deformation. The predicted permanent deformations from the previous steps need to be adjusted by a shift factor of 1.13 calibrated from the six APT sections in this study. This shift factor is suggested being further calibrated with more simulation cases in the future.

Procedure for Prediction Model (Transfer Function) Method

The permanent deformation of pavement can also be predicted by the transfer function method with the following steps:

(1) Calculation of Elastic Vertical Strain. The elastic vertical strains at the mid-depth of each pavement sublayer under the center of load are calculated by ABAQUS or other elastic-layered pavement analysis programs (e.g., CHEVRON, DAMA, DISAR, ELSYM5, and KENLAYER etc.)

(2) Material P-D Parameters. The P-D parameters (a and b) of pavement materials are determined by laboratory P-D tests.

(3) Calculation of Permanent Vertical Strain. The accumulated permanent vertical strains at the mid-depth of each pavement sublayer under the center of load are calculated by transfer function equations (20) to (23).

(4) Calculation of Permanent Deformation. The accumulated permanent deformations of pavement under the center of load are calculated by equation (17), which is the sum of products of the mid-depth permanent strain and the thickness for all sublayers.

APPENDIX B

Implicit Integration of Proposed P-D Model

The UMAT is written in a FORTRAN code, and the flowchart for developing the FORTRAN Subroutine is presented in Figure 54. The integration scheme for the model is an implicit scheme called radial return method. More details of the radial return method may be referred elsewhere *[35]*. It is important to note that in the implicit scheme, all quantities are written at the end of the time increment. This ensures that, the yield condition is satisfied at the end of the time increment, therefore avoiding "drift" from the yield surface that can occur in the explicit scheme *[35]*.

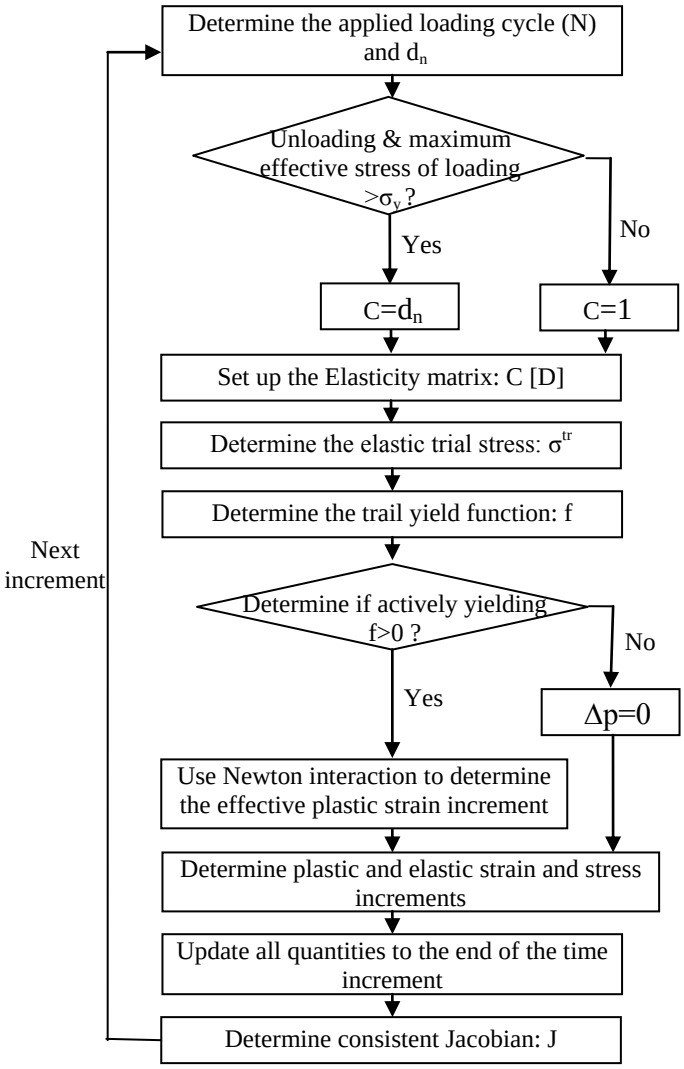

Figure 54
Flow chart of proposed model

In the flow chart, the elasticity matrix is given as:

$$C[D] = C\begin{bmatrix} \lambda+2\mu & \lambda & \lambda & 0 & 0 & 0 \\ \lambda & \lambda+2\mu & \lambda & 0 & 0 & 0 \\ \lambda & \lambda & \lambda+2\mu & 0 & 0 & 0 \\ 0 & 0 & 0 & \mu & 0 & 0 \\ 0 & 0 & 0 & 0 & \mu & 0 \\ 0 & 0 & 0 & 0 & 0 & \mu \end{bmatrix} \tag{24}$$

where, $C = d_N$when unloading, and the maximum effective stress during loading at the same cycle is larger than the initial yield stress, otherwise, $C = 1.0$; and $\lambda = \frac{E\nu}{(1+\nu)(1-\nu)}$ and $\mu = G = \frac{E}{2(1+\nu)}$ are the Lame constants.

The elastic trial stress is given as:

$$\sigma_e^{tr} = \sigma_t + 2G\Delta\varepsilon + \lambda \boldsymbol{I}\Delta\varepsilon : \boldsymbol{I} \tag{25}$$

The trail yield function can be written as:

$$f = \sigma_e^{tr} - r - \sigma_y = \left(\frac{3}{2}\sigma^{tr'} : \sigma^{tr'}\right)^{\frac{1}{2}} - r - \sigma_y \tag{26}$$

where, $\sigma_e^{tr}$is the effective trial stress, $\sigma^{tr'}$ is the deviatoric trial stress, and r is the linear hardening function.

When the material yields, the effective plastic strain increment can be determined by the Newton interaction:

$$r^{(k)} = r_t + h\Delta p \tag{27}$$

$$d\Delta p = \frac{\sigma_e^{tr} - 3G\Delta p^{(k)} - r^{(k)} - \sigma_y}{3G + h} \tag{28}$$

$$\Delta p^{(k+1)} = \Delta p^{(k)} + d\Delta p \tag{29}$$

The plastic and elastic strain and stress increments can be written as:

$$\Delta\varepsilon^p = \frac{3}{2}\Delta p\frac{\sigma'}{\sigma_e} = \frac{3}{2}\Delta p\frac{\sigma^{tr'}}{\sigma_e^{tr}} \tag{30}$$

$$\Delta\varepsilon^e = \Delta\varepsilon - \Delta\varepsilon^p \tag{31}$$

$$\Delta\sigma = 2G\Delta\varepsilon^e + \lambda \boldsymbol{I}\Delta\varepsilon^e : \boldsymbol{I} \tag{32}$$

The consistent Jacobian is given as:

$$J = \frac{\partial\Delta\sigma}{\partial\Delta\varepsilon} \tag{33}$$

where, $\Delta\sigma = 2GQ\frac{\sigma^{tr'}}{\sigma_e^{tr}}\frac{\sigma^{tr'}}{\sigma_e^{tr}} : \Delta\varepsilon^e + 2GR\Delta\varepsilon + \left(K - \frac{2}{3}GR\right) II : \Delta\varepsilon$ in which $Q = \frac{3}{2}\left(\frac{1}{1+(3G/h)} - \right.$ $\sigma e \sigma etr$, $R = \sigma e \sigma etr$, and $K = E3(1-2\nu)$.

Physical Meaning of P-D Parameters *a* and *b*

In the proposed P-D model, material permanent deformation property can be characterized by the modulus ratio function $d_n = \frac{a}{N^b} + 1$. The value of d_n changes with load cycle (N). The P-D parameter a can be written as:

$$a = d_1 - 1 = \frac{\varepsilon_1^t}{\varepsilon_1^r} - 1 = \frac{\varepsilon_1^t - \varepsilon_1^r}{\varepsilon_1^r} = \frac{\varepsilon_1^p}{\varepsilon_1^r} \tag{34}$$

where, ε_1^t, ε_1^p, and ε_1^r are the total strain, permanent strain, and resilient strain at the 1st cycle, respectively; and d_1 is modulus ratio at the 1st cycle.

The physical meaning of P-D parameter a is the initial ratio of permanent strain over resilient strain. Figure 55 presents materials with different parameter a values. The material with a higher a value has a larger d_n value and permanent strain (ε_p).

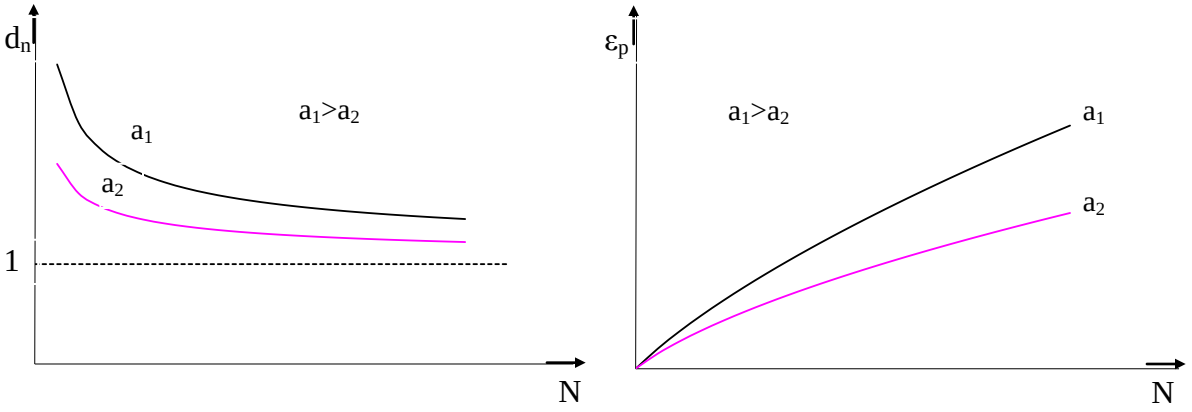

(a) d_n with cycle number N **(b) ε_p with cycle number N**

Figure 55
Schematic representation of materials with different parameter *a* values

Figure 56 presents a schematic representation of materials with parameter $a = 0$. In this case, d_n has a constant value of 1, and the stress-strain curve of materials is the same as a conventional elastoplastic model. The material becomes elastic after the first repetition, and the no permanent strain will be developed in the succeeding repetitions if the stress level does not increase.

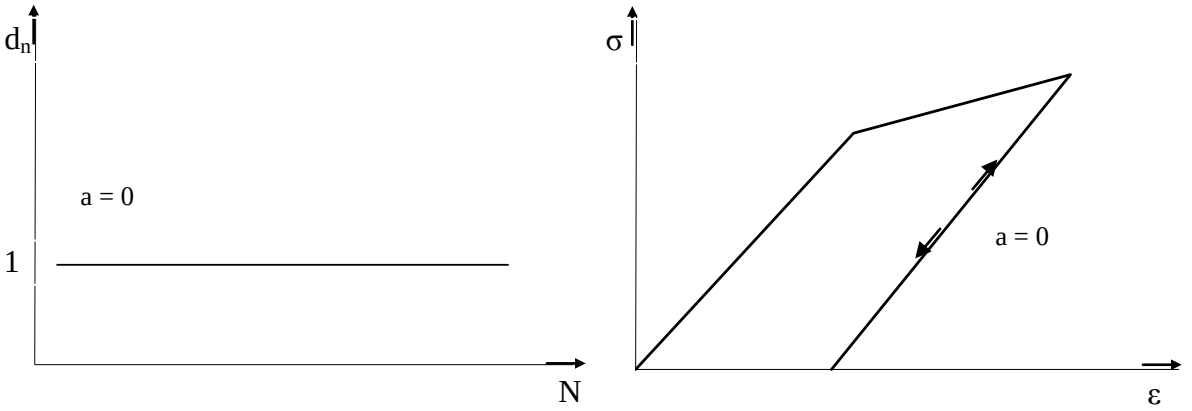

(a) d_n with cycle number N **(b) stress-strain curve**

Figure 56
Schematic representation of materials with parameter $a = 0$

Figure 57 presents a schematic representation of materials with parameter $a \rightarrow +\infty$. In this case, all strains are permanent strain, and no elastic stain will be found under repeated

loading. The permanent strain of material would increase linearly after first cycle.

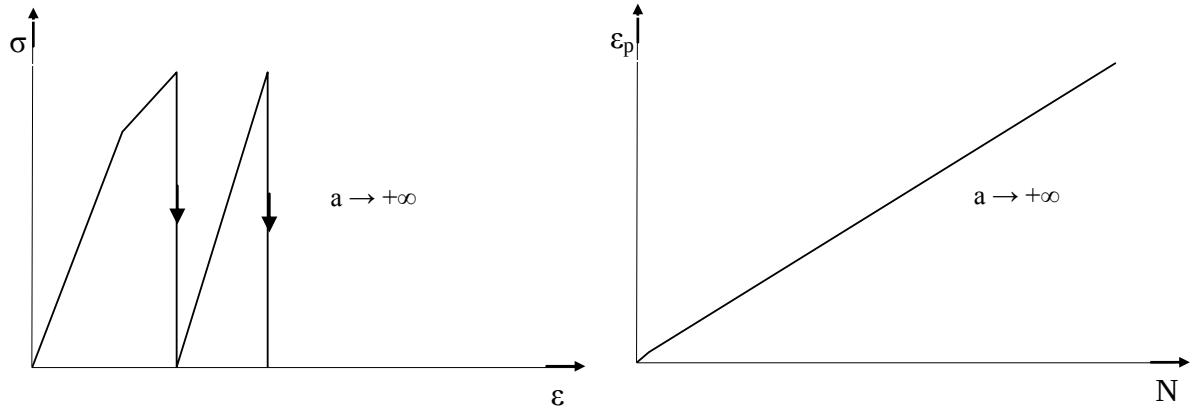

(a) d_n with cycle number N **(b) ε_p with cycle number N**

Figure 57
Schematic representation of materials with parameter $a \rightarrow +\infty$

Figure 58 presents equation (9) in log-log figure. As shown in Figure 58, the $\log(a)$ is the intercept of $(d_n - 1)$ and N at log-log figure, while the regression parameter b is the slope of (d_n-1) and N at log-log figure, which reflects the attenuation rate of d_n.

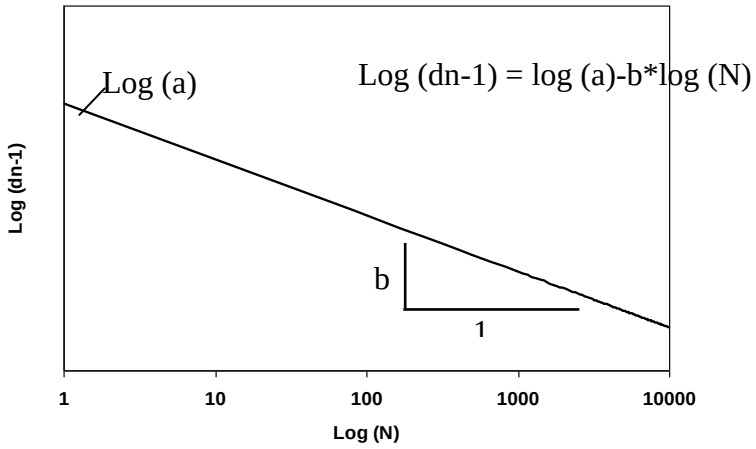

Figure 58
Modulus ratio function d_n and parameters *a* and *b*

P-D parameter b can be written as:

$$b = \frac{\log\left(\frac{\varepsilon_1^p}{\varepsilon_1^r}\frac{\varepsilon_n^r}{\varepsilon_n^p}\right)}{\log(N)} = -\frac{\log\left(\frac{\varepsilon_n^p}{\varepsilon_n^r}\right) - \log\left(\frac{\varepsilon_1^p}{\varepsilon_1^r}\right)}{\log(N) - \log(1)} \tag{35}$$

where, ε_1^p and ε_1^r are the permanent strain and resilient strain at the 1st cycle, and ε_n^p and ε_n^r are the permanent strain and resilient strain at the Nth cycle.

Figure 59 presents materials with different parameter b values. The material with a larger b value has smaller d_n value and permanent strain (ε_p).

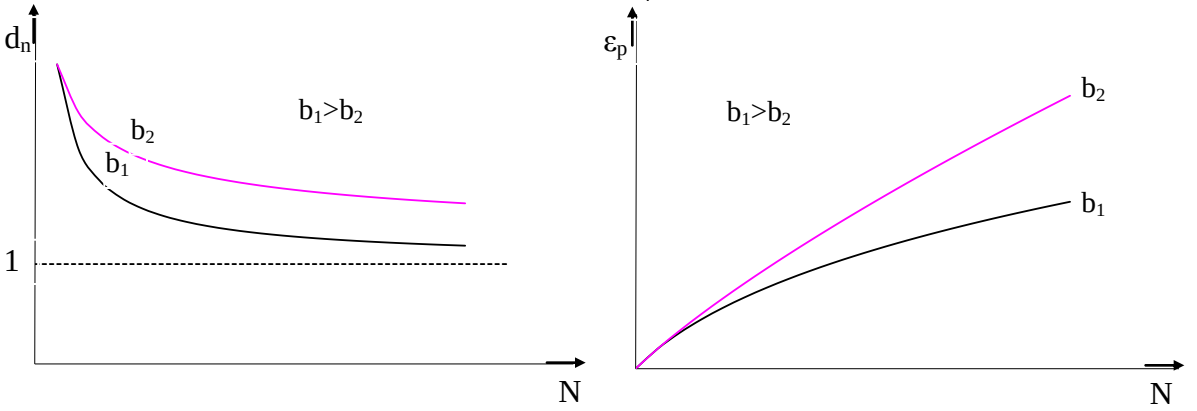

(a) d_n with cycle number N **(b) ε_p with cycle number N**

Figure 59
Schematic representation of materials with different parameter *b* values

Figure 60 presents a schematic representation of materials with parameter $b = 0$. In this case, the d_n value equals to $a + 1$. The material would produce same permanent strain in each cycle after the first one, and the permanent strain would increase linearly.

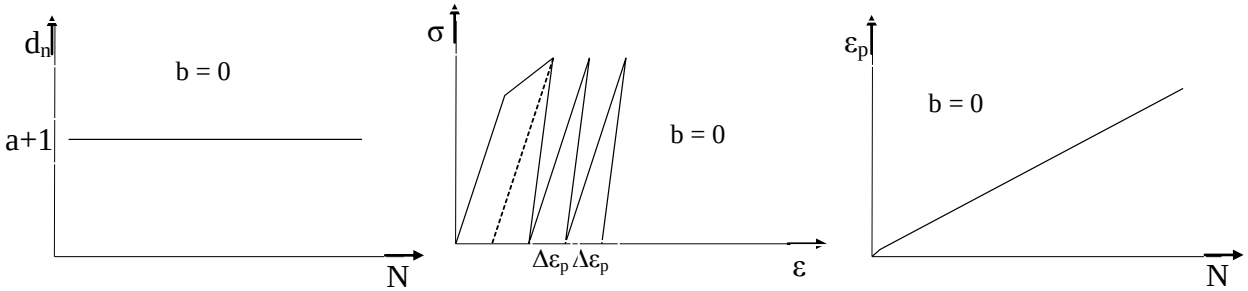

(a) d_n with cycle number N **(b) stress-strain curve** **(c) ε_p with cycle number N**

Figure 60
Schematic representation of material with parameter *b* = 0

Figure 61 presents a schematic representation of materials with parameter $b \rightarrow +\infty$. In this case, the d_n value is a + 1 at the first repetition and equal to one from the second repetition. The material becomes elastic after the first repetition, and the permanent strain will not be predicted in succedent repetitions if the stress level held as a constant.

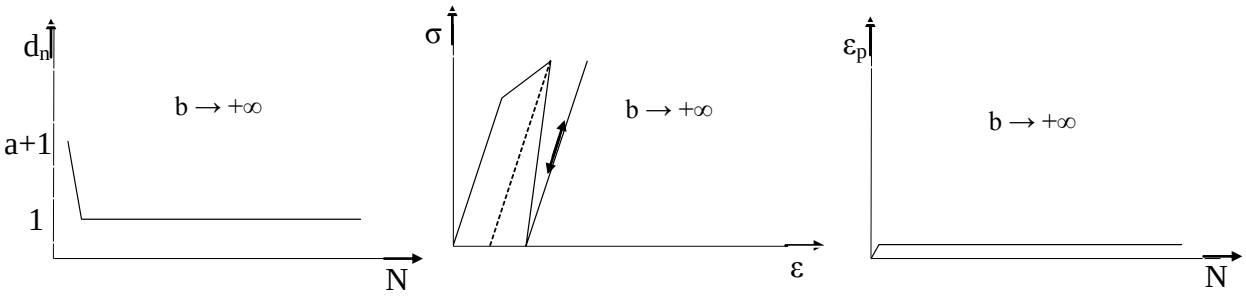

(a) d_n with cycle number N **(b) stress-strain curve** **(c) ε_p with cycle number N**

Figure 61
Schematic representation of material with parameter *b*→ + ∞

Effects of Other Parameters on Permanent Strain

Figure 62 presents the effect of modulus parameter E_L on the permanent strain. As shown in the figure, the permanent strain decreases with an increasing E_L value.

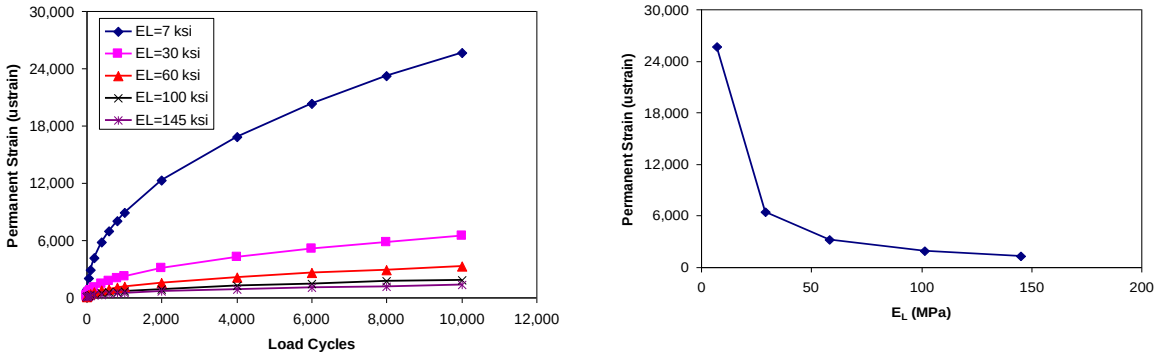

(a) permanent strain with varying modulus E_L **(b) effect of modulus E_L on permanent strain**

Figure 62
Effect of modulus E_L on permanent strain (1 ksi. = 6.894 MPa)

In a P-D test, initial yielding stress will affect the permanent strain at first cycle. Figure 63 exhibits the effect of initial yielding stress on the first cycle permanent strain. A higher yield stress will produce a smaller permanent strain in the first cycle.

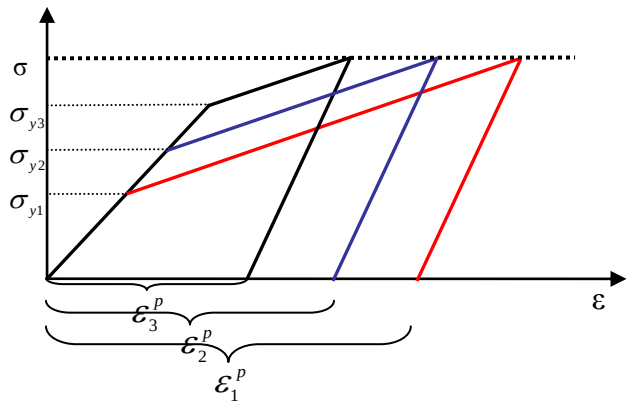

Figure 63
Effect of initial yield stress on the first cycle permanent strain

The hardening constant will affect the first cycle permanent strain as well. Figure 64 shows the effect of the hardening constant on the permanent strain in the first cycle ($h_{c1} < h_{c2} < h_{c3}$). A higher hardening constant will produce a smaller permanent strain in the first cycle.

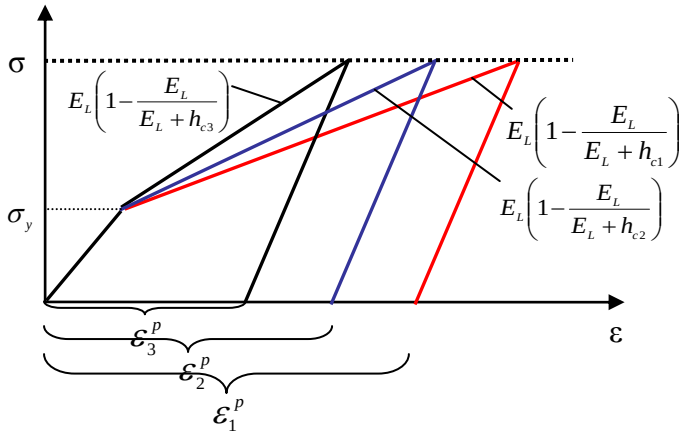

Figure 64
Effect of hardening constant on the first cycle permanent strain

Simplifying the P-D Formula

The purpose of simplifying the P-D formula is to find a simple relationship form among laboratory permanent strain, elastic stress and/or strain, material parameters, and load cycles for developing the P-D prediction model (transfer function) for pavement base and subbase/subgrade materials. This relationship is selected as the basic formula of transfer function. Then, the selected formula of transfer function can be calibrated to account for the differences between laboratory and field tests.

As shown in equation (8), for the permanent deformation test, the accumulated permanent strain is:

$$\varepsilon^p(n) = \frac{\sigma - \sigma_y}{h_c} + \sum_{i=1}^{n}\left(1 - \frac{1}{d_i}\right)\frac{\sigma}{E_L(i)} = \frac{\sigma - \sigma_y}{h_c} + \frac{\sigma}{E_L}\sum_{i=1}^{n}\left(1 - \frac{1}{d_i}\right) \tag{36}$$

then,

$$\varepsilon^p(n) = \frac{\sigma - \sigma_y}{h_c} + \frac{\sigma \cdot a}{E_L}\sum_{i=1}^{n}\left(\frac{1}{a + i^b}\right) \tag{37}$$

In this study, *a* values of all tested materials are relatively small compared to i^b, especially when the load cycle (i) becomes large. Assuming: $a + i^b \approx i^b$,

$$\varepsilon^p(n) \approx \frac{\sigma - \sigma_y}{h_c} + \frac{\sigma}{E_L}\sum_{i=1}^{n}\left(\frac{a}{i^b}\right) = \frac{\sigma - \sigma_y}{h_c} + \frac{a \cdot \sigma}{E_L}\sum_{i=1}^{n}\left(\frac{1}{i^b}\right) \tag{38}$$

The error of assuming $a + i^b$ as i^b is:

$$\left|\frac{\frac{1}{a + i^b} - \frac{1}{i^b}}{\frac{1}{a + i^b}}\right| = \frac{a}{i^b} \tag{39}$$

From equation (39), the highest *a* value and lowest *b* value will produce the largest error. In this study, of the eight tested materials, the maximum *a* value of 0.156 and the minimum *b* value of 0.44 will produce the largest error. As shown in Table 26, the error of assuming $a + i^b$ as i^b decreases as the load cycle (i) increases. At the 10^{th} cycle, the error was about 5.7 percent, while at the 100^{th} cycle, the error was only 0.13 percent. It is acceptable in practice since pavement life is much longer than this value.

Table 26
Error of assuming a + i^b as i^b

Load cycles (i)	1	10	100	1,000	10,000	100,000
Error (%)	15.6	5.7	0.13	0.048	0.017	0.006

For $\sum_{i=1}^{n} \frac{1}{i^b}$, when 0 < b < 1,

$$\int_1^{n+1} \frac{1}{x^b} dx < \sum_{i=1}^{n} \frac{1}{i^b} < \int_1^{n+1} \frac{1}{(x-1)^b} dx \qquad \text{i.e.,} \qquad \frac{(n+1)^{1-b}-1}{1-b} < \sum_{i=1}^{n} \frac{1}{i^b} < \frac{n^{1-b}}{1-b} \tag{40}$$

when b = 1,

$$\int_1^{n+1} \frac{1}{x} dx < \sum_{i=1}^{n} \frac{1}{i} < \int_1^{n+1} \frac{1}{x-1} dx \qquad \text{i.e.,} \qquad \ln(n+1) < \sum_{i=1}^{n} \frac{1}{i} < \ln(n)+1 \tag{41}$$

when b > 1,

$$\int_1^{n+1} \frac{1}{x^b} dx < \sum_{i=1}^{n} \frac{1}{i^b} < 1 + \int_2^{n+1} \frac{1}{(x-1)^b} dx \qquad \text{i.e.,} \qquad \frac{(n+1)^{1-b}-1}{1-b} < \sum_{i=1}^{n} \frac{1}{i^b} < \frac{n^{1-b}-b}{1-b} \tag{42}$$

The errors of using lower limits to substitute the series of $\sum_{i=1}^{n} \frac{1}{i^b}$ are given:

When 0 < b < 1,

$$\left| \frac{\frac{1}{2}\left[\frac{(n+1)^{1-b}-1}{1-b} - \frac{n^{1-b}}{1-b} \right]}{\frac{1}{2}\left[\frac{(n+1)^{1-b}-1}{1-b} + \frac{n^{1-b}}{1-b} \right]} \right| = \frac{n^{1-b} - (n+1)^{1-b} + 1}{n^{1-b} + (n+1)^{1-b} - 1} \tag{43}$$

In this study, for eight tested materials, the *b* value of 0.71 (upper limit) will produce the largest error. As shown in Table 27, the error of using lower limits to substitute the series of $\sum_{i=1}^{n} \frac{1}{i^b}$ decreases as the load cycle increases. When n = 10,000 cycles, the error was about 3.6 percent, which is acceptable in practice since the pavement life is much longer than this value.

When b = 1,

$$\left|\frac{\frac{1}{2}\left[\ln(n)+1-\ln(n+1)\right]}{\frac{1}{2}\left[\ln(n)+1+\ln(n+1)\right]}\right| = \frac{\ln\left(\frac{n}{n+1}\right)+1}{\ln\left(n^2+n\right)+1} \tag{44}$$

Assuming a material has a *b* value of 1, as shown in Table 27, the error of using lower limits to substitute the series of $\sum_{i=1}^{n}\frac{1}{i^b}$ will increase as the load cycle increases. When n=10,000 cycles, the error was about 5.1 percent, which is acceptable in practice since the pavement life is much longer than this.

When b > 1,

$$\left|\frac{\frac{1}{2}\left[\frac{(n+1)^{1-b}-1}{1-b}-\frac{n^{1-b}-b}{1-b}\right]}{\frac{1}{2}\left[\frac{(n+1)^{1-b}-1}{1-b}+\frac{n^{1-b}-b}{1-b}\right]}\right| = \frac{n^{1-b}-(n+1)^{1-b}+1-b}{n^{1-b}+(n+1)^{1-b}-1-b} \tag{45}$$

Assuming a material has a *b* value larger than 1.5, as shown in Table 27, the error of using lower limits to substitute the series of $\sum_{i=1}^{n}\frac{1}{i^b}$ will be larger than about 20 percent, which is unacceptable for this substitute. However, based on the laboratory tests for various pavement materials in this study, no *b* value was found larger than 1.

Table 27

Errors of using lower limits to substitute the series of $\sum_{i=1}^{n}\frac{1}{i^b}$

Condition	b	Errors of using lower limits to substitute the series of $\sum_{i=1}^{n}\frac{1}{i^b}$			
		n=1,000	n=10,000	n=100,000	n=1,000,000
b<1	0.71	7.2	3.6	1.8	0.9
b=1	1	6.7	5.1	4.2	3.5
b>1	1.0001	6.7	5.2	4.2	3.5
	1.2	11.8	10.6	10.0	9.6
	1.5	20.5	20.2	20.1	20.0
	2	3.4	33.3	33.3	33.3
	3	50.0	50.0	50.0	50.0

From equations (43), (44), and (45), when b ≠ 1, the lower limit has the same form of $\frac{(n+1)^{1-b}-1}{1-b}$, while when b = 1, the form of lower limit is ln(n + 1). Table 28 presents the comparison of different lower limits for $\sum_{i=1}^{n}\frac{1}{i^b}$. As shown in Table 28, when *b* is equal or very close to 1, the different lower limits are very close. This means these different lower limits can be unified as one form of $\frac{(n+1)^{1-b}-1}{1-b}$, and when a material has a *b* value of 1, a number that is very close to 1 (e.g., 0.9999 or 1.0001) can be assigned to calculate the lower limit of $\sum_{i=1}^{n}\frac{1}{i^b}$ by formula $\frac{(n+1)^{1-b}-1}{1-b}$.

Table 28

Comparison of different lower limits for $\sum_{i=1}^{n}\frac{1}{i^b}$

b	Lower limit	n				
		10	100	1,000	10,000	100,000
0.9999	$\frac{(n+1)^{1-b}-1}{1-b}$	2.3982	4.6162	6.9111	9.2147	11.5196
1.0	$\ln(n+1)$	2.3979	4.6151	6.9088	9.2104	11.5129
1.0001	$\frac{(n+1)^{1-b}-1}{1-b}$	2.3976	4.6141	6.9064	9.2062	11.5063

As aforementioned, equation (38) could be further simplified as:

$$\varepsilon^p \approx \frac{\sigma-\sigma_y}{h_c}+\frac{\sigma}{E_L}\frac{a}{1-b}\left[(n+1)^{1-b}-1\right] \tag{46}$$

P-D Index

To characterize or compare material permanent deformation property, P-D parameters *a* and *b* are needed, which makes the comparison inconvenient. In this study, the conception of a P-D index is introduced to characterize or compare material permanent deformation property easily. The P-D index (A) is defined as the area of between curves d_n and d = 1, from n = 1 to 10,000 (Figure 65), which can be calculated from equation (47).

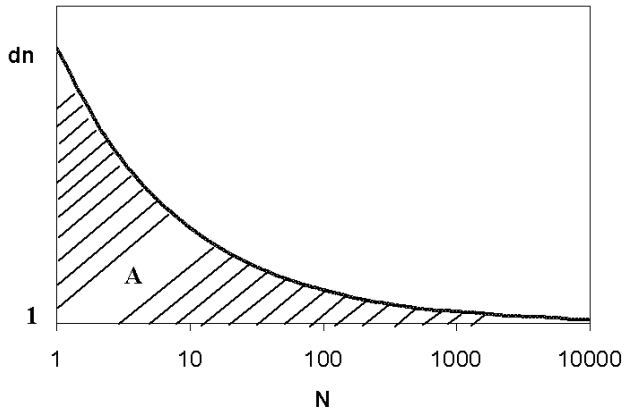

Figure 65
Area between curve d_n and d = 1

$$A=\int_1^{10000}\frac{a}{x^b}dx=\frac{a}{1-b}(10000^{1-b}-1) \tag{47}$$

For the P-D test in this study, the load number *n* is 10,000. Equation (46) can be written as:

$$\varepsilon^p \approx \frac{\sigma-\sigma_y}{h_c}+\frac{\sigma}{E_L}\frac{a}{1-b}\left[(10{,}001)^{1-b}-1\right] \tag{48}$$

From equations (47) and (48):

$$\varepsilon^{p}(10{,}000) \approx \frac{\sigma - \sigma_{y}}{h_{c}} + \varepsilon \cdot A \qquad (49)$$

where, $\varepsilon^{p}(10{,}000)$ = permanent strain after 10,000 cycles; σ = effective stress; σ_y = yield stress; h_c = hardening constant; E_L = loading modulus, a; and b = P-D parameters; A = P-D index; and ε = the elastic strain.

As shown in equation (49), permanent strain after 10,000 cycles approximates to the first cycle plastic strain plus the product of elastic strain and the P-D index (A).

Table 29 presents the P-D index of tested materials. The calculated permanent strains by equation (49) were close to those measured by P-D tests.

Table 29
P-D index of tested materials

Materials	$(\sigma-\sigma_y)/h$ (με)	ε (με)	A	ε *A (με)	$\varepsilon_p(10{,}000)$ calculated by Eq. (49)	Measured Permanent Strain (με)
BCS/Slag	6.1	105.3	0.36	37	44	42
BCS/Fly ash	8.6	156.7	0.94	147	156	154
Limestone	39.6	407.5	7.08	2,884	2,924	2,738
FA50	70.6	486.4	10.56	5,139	5,209	5,079
FA100	71.0	534.0	41.47	22,143	22,214	21,100
Cement Treated soil	6.4	83.3	0.35	29	35	34
Lime treated soil	7.8	179.8	0.41	74	82	80
Subgrade	163.8	758.5	3.54	2,683	2,846	2,865

APPENDIX C

The P-D test data analysis spreadsheet was developed to obtain P-D model parameters. This spreadsheet was developed in the Microsoft Office Excel 2007 by Visual Basic Macros. This document provides main procedures information related to using the spreadsheet. For other detailed concepts, refer to the LTRC Final Report 452. This document does not contain detailed instructions regarding the normal file operations associated with the Windows operating environment.

1. Start Spreadsheet

- Double click the Excel file "P-D Test Template .xlsm," and it is recommended to save this spreadsheet as a new file with another name before processing data.
- In the first worksheet named "Original Data," Click "Options…" after "Security Warning: Some active content has been disabled," select "enable the content," click "OK."

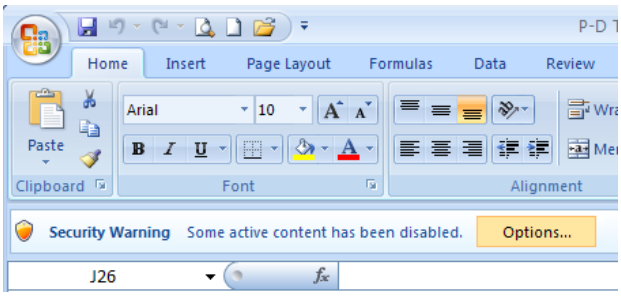

2. Input and Check Raw Data

- Open the P-D test data file by Excel; copy the test head information to spreadsheet.

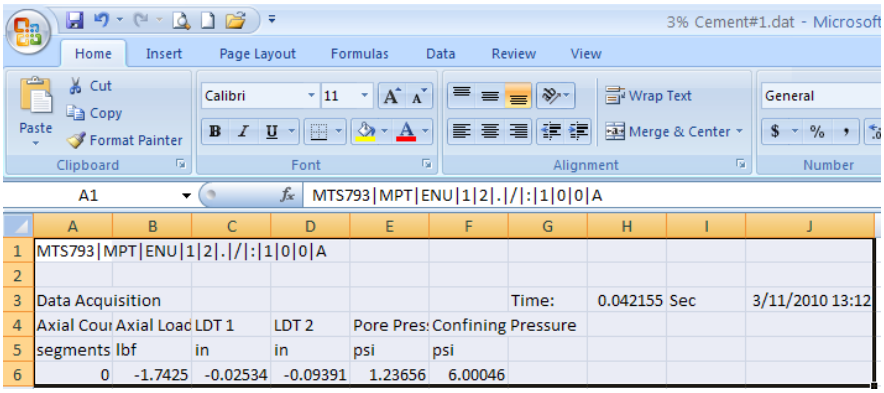

- Copy the raw data of "Time," "Axial Count," "Axial Displacement," "Load," "LVDT1," "LVDT2," and "confining pressure" from test result ".dat" file to the spreadsheet.

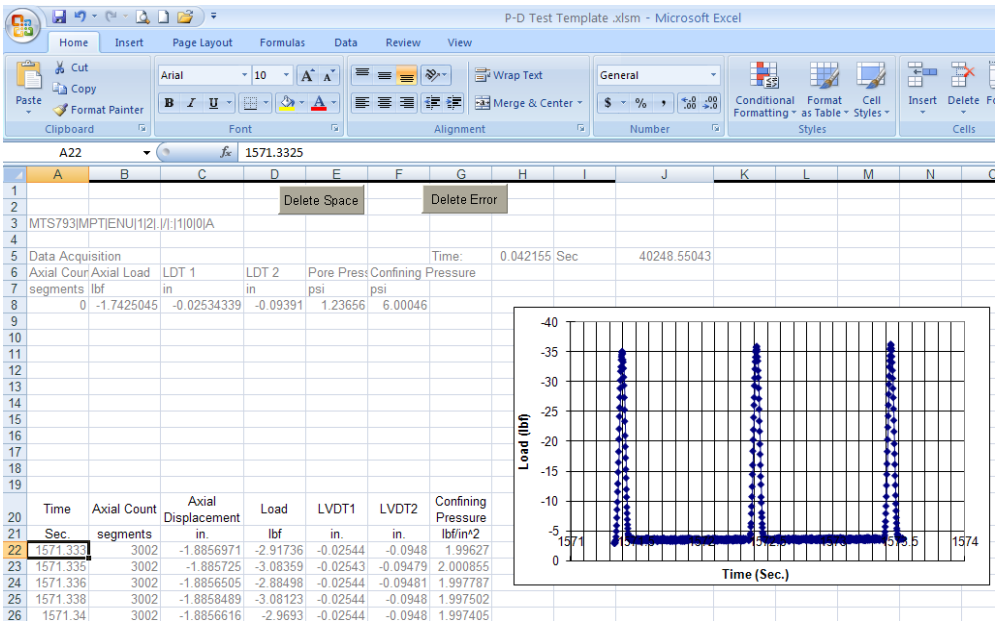

- Click the "Delete Space" button and wait until the function is finished. This step is to delete the head information and blank rows between two recorded cycles.
- Click the "Delete Error" button and wait until the function is finished. This step is to delete the redundant rows between two recorded cycles.
- A curve between loads and time for the first three cycles is created automatically for the user to check whether the loads were applied correctly during the P-D test. Users can change the data range to check loads for other cycles.

3. Preprocess Data

- In the second worksheet named "Preprocess," click the "Calculate" button and wait until the function is finished. In this step, the first row of data of "Time," "Axial Displacement," "LVDT1," and "LVDT2" are considered as the reference points with a value of zero. And the load cycles are calculated based on the "Axial Count" information.

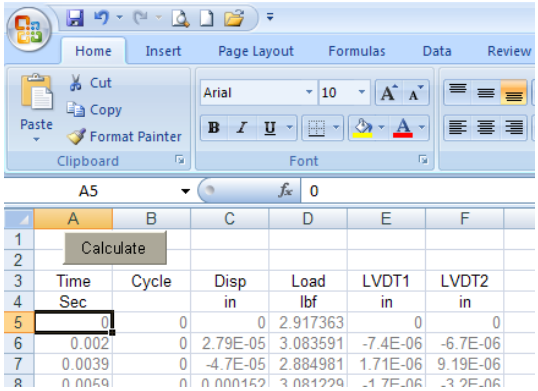

4. Calculate Peak Strains

- In the third worksheet named "Peak," input the sample height (by inches) in the cell marked in red; click the "Peak Deformation" button waiting until finished. In this step, the peak strains are calculated, and a curve between peak strains and cycles is created automatically.

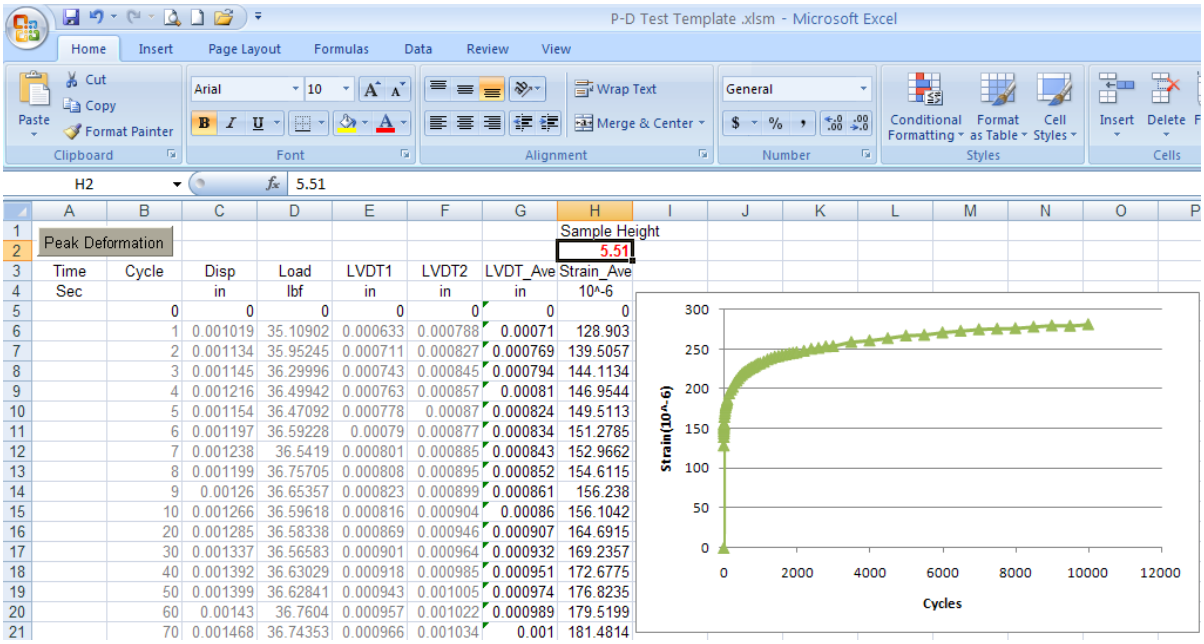

5. Calculate Permanent Strains

- In the fourth worksheet named "PD," click the "Permanent Deformation" button and wait until the function is finished. In this step, the permanent strains are calculated, and a curve between permanent strains and cycles is created automatically.

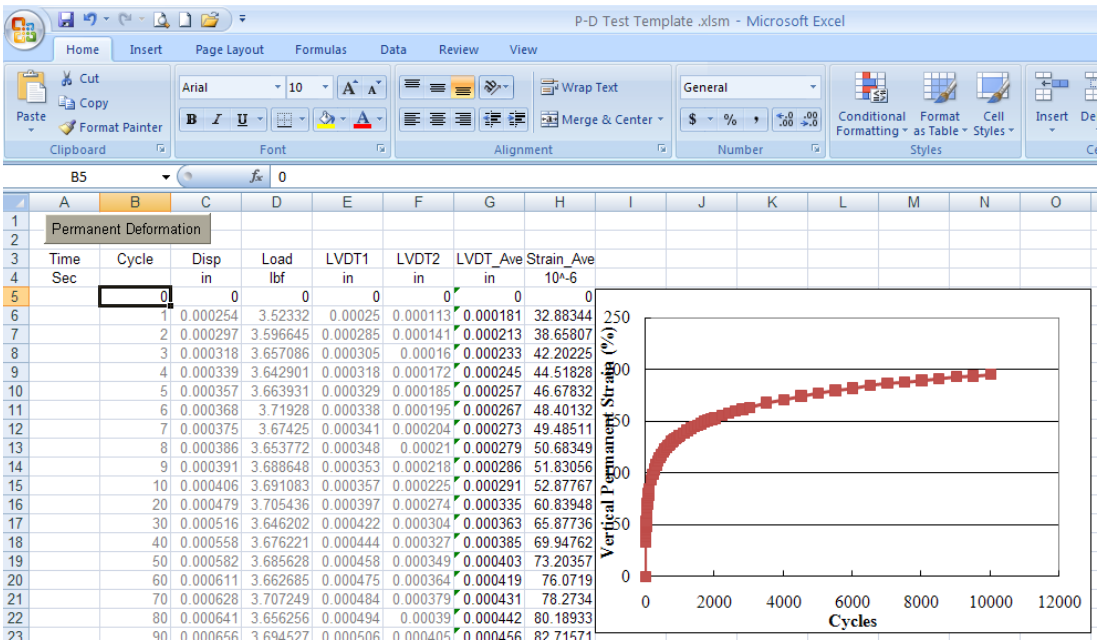

6. Calculate Resilient Modulus

- In the fifth worksheet named "resilient," the resilient modulus for collected cycles and the average value are calculated with units of both "psi" and "MPa." This information is not required for the P-D model, but can be a reference for user.

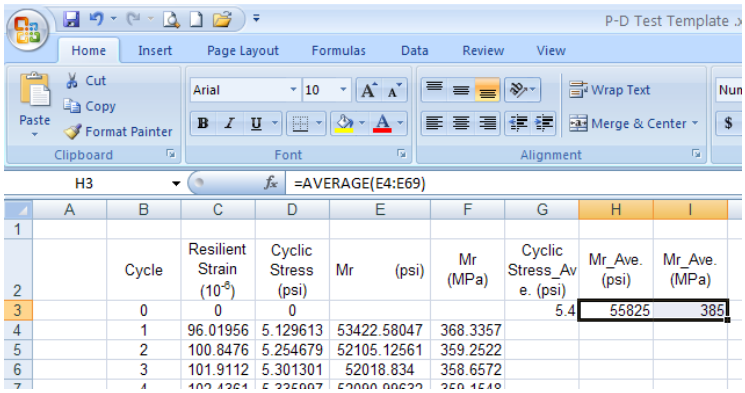

	A	B	C	D	E	F	G	H	I
1									
2		Cycle	Resilient Strain (10^{-6})	Cyclic Stress (psi)	Mr (psi)	Mr (MPa)	Cyclic Stress_Ave. (psi)	Mr_Ave. (psi)	Mr_Ave. (MPa)
3		0	0	0			5.4	55825	385
4		1	96.01956	5.129613	53422.58047	368.3357			
5		2	100.8476	5.254679	52105.12561	359.2522			
6		3	101.9112	5.301301	52018.834	358.6572			

7. Calculate P-D Parameters *a* and *b*

- In the sixth worksheet named "d_n," a curve between Ln (d-1) and Ln (N) and a regression equation as Y=pX+q is created automatically. Input the "p" and "q" values to cells marked in red from the regression equation. The P-D parameters "a" and "b" are calculated automatically.

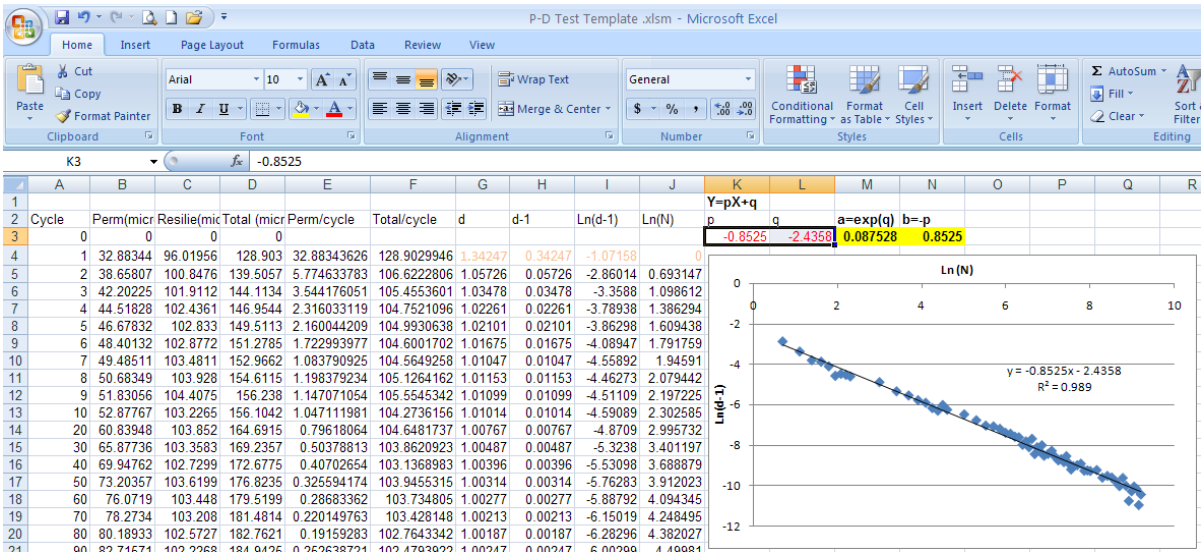

	A	B	C	D	E	F	G	H	I	J	K	L	M	N	O	P	Q	R
1											Y=pX+q							
2	Cycle	Perm(micr	Resilie(mic	Total (micr	Perm/cycle	Total/cycle	d	d-1	Ln(d-1)	Ln(N)	p	q	a=exp(q)	b=-p				
3	0	0	0	0							-0.8525	-2.4358	0.087528	0.8525				
4	1	32.88344	96.01956	128.903	32.88343626	128.9029946	1.34247	0.34247	-1.07158	0								
5	2	38.65807	100.8476	139.5057	5.774633783	106.6222806	1.05726	0.05726	-2.86014	0.693147								
6	3	42.20225	101.9112	144.1134	3.544176051	105.4553601	1.03478	0.03478	-3.3588	1.098612								
7	4	44.51828	102.4361	146.9544	2.316033119	104.7521096	1.02261	0.02261	-3.78938	1.386294								
8	5	46.67832	102.833	149.5113	2.160044209	104.9930638	1.02101	0.02101	-3.86298	1.609438								
9	6	48.40132	102.8772	151.2785	1.722993977	104.6001702	1.01675	0.01675	-4.08947	1.791759								
10	7	49.48511	103.4811	152.9662	1.083790925	104.5649258	1.01047	0.01047	-4.55892	1.94591								
11	8	50.68349	103.928	154.6115	1.198379234	105.1264162	1.01153	0.01153	-4.46273	2.079442								
12	9	51.83056	104.4075	156.238	1.147071054	105.5545342	1.01099	0.01099	-4.51109	2.197225								
13	10	52.87767	103.2265	156.1042	1.047111981	104.2736156	1.01014	0.01014	-4.59089	2.302585								
14	20	60.83948	103.852	164.6915	0.79618064	104.6481737	1.00767	0.00767	-4.8709	2.995732								
15	30	65.87736	103.3583	169.2357	0.50378813	103.8620923	1.00487	0.00487	-5.3238	3.401197								
16	40	69.94762	102.7299	172.6775	0.40702654	103.1368983	1.00396	0.00396	-5.53098	3.688879								
17	50	73.20357	103.6199	176.8235	0.325594174	103.9455315	1.00314	0.00314	-5.76283	3.912023								
18	60	76.0719	103.448	179.5199	0.28683362	103.734805	1.00277	0.00277	-5.88792	4.094345								
19	70	78.2734	103.208	181.4814	0.220149763	103.428148	1.00213	0.00213	-6.15019	4.248495								
20	80	80.18933	102.5727	182.7621	0.19159283	102.7643342	1.00187	0.00187	-6.28296	4.382027								

8. Calculate Loading Modulus (E_L)

- In the seventh worksheet named "E," the loading modulus (E_L) for collected cycles and the average value are calculated automatically.

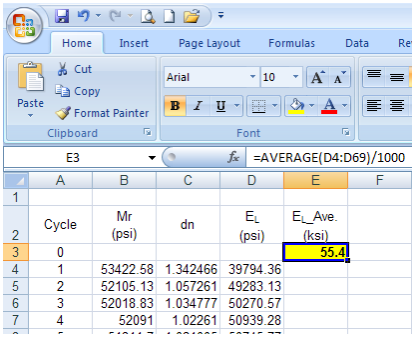

	A	B	C	D	E	F
1						
2	Cycle	Mr (psi)	dn	E_L (psi)	E_L_Ave. (ksi)	
3	0				55.4	
4	1	53422.58	1.342466	39794.36		
5	2	52105.13	1.057261	49283.13		
6	3	52018.83	1.034777	50270.57		
7	4	52091	1.02261	50939.28		

9. Calculate Yield Stress (σ_y) and Harden Constant (h_c)

- In the eighth worksheet named "first cycle," input the sample diameter (by inch). A curve between stress and strain for the first cycle is created automatically. Select the point where the slope begins to change smaller as the yield point. Input the stress and strain values of the yield point to cells marked in red from figure or columns "G" and "H." The harden constant (h_c) is calculated automatically.

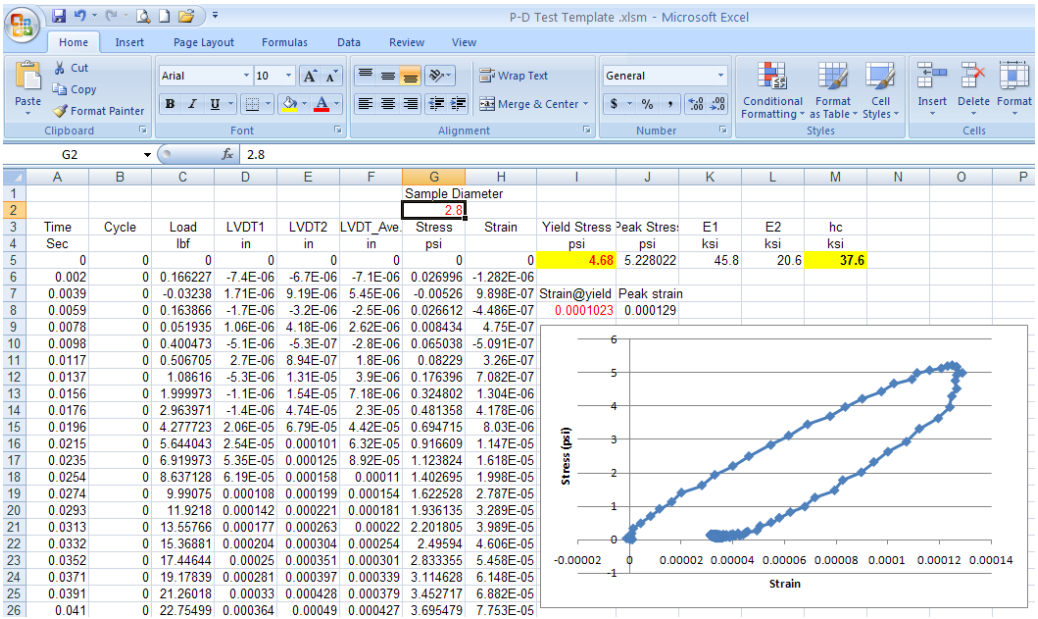

10. Export and Validate Parameters

- In the last worksheet named "Parameter & Validation," parameters needed for P-D model are exported. To validate the obtained parameters, two curves between permanent strains and cycles from P-D test and prediction based on obtained parameters are created automatically.

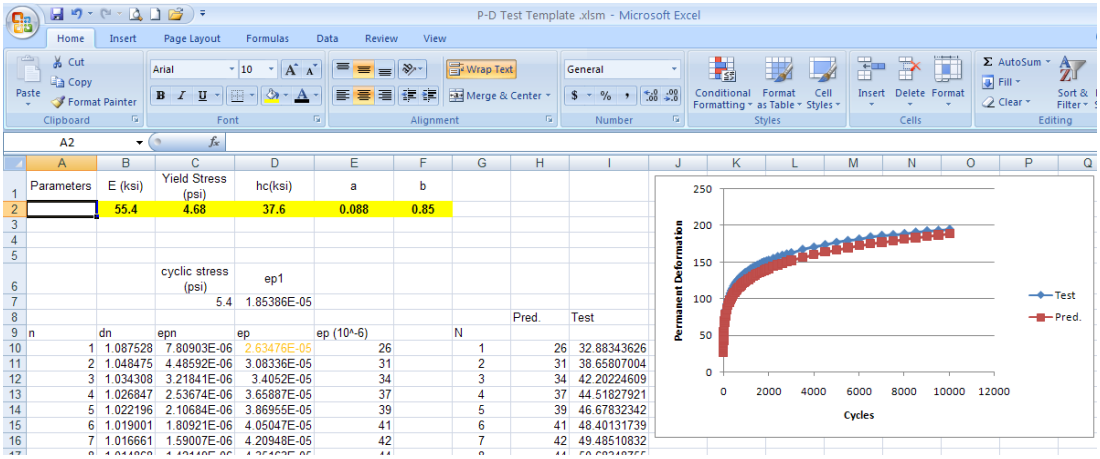

APPENDIX D

Table 30 presents the soil properties of untreated soil. It was classified as CL soil based on USCS and A-6 soil based on the AASHTO Soil Classification System. Figure 66 presents the particle size distribution of untreated soil.

Table 30
Physical properties of untreated soil

Soil Type	Silt (%)	Clay (%)	LL (%)	PL (%)	PI (%)	W_{opt} (%)	Maximum Dry Density, pcf	Specific Gravity	Classification USCS/AASHTO
Lt. Sandy Clay	23.7	31.0	32.5	15.7	16.8	15.7	111.4	2.65	CL / A-6

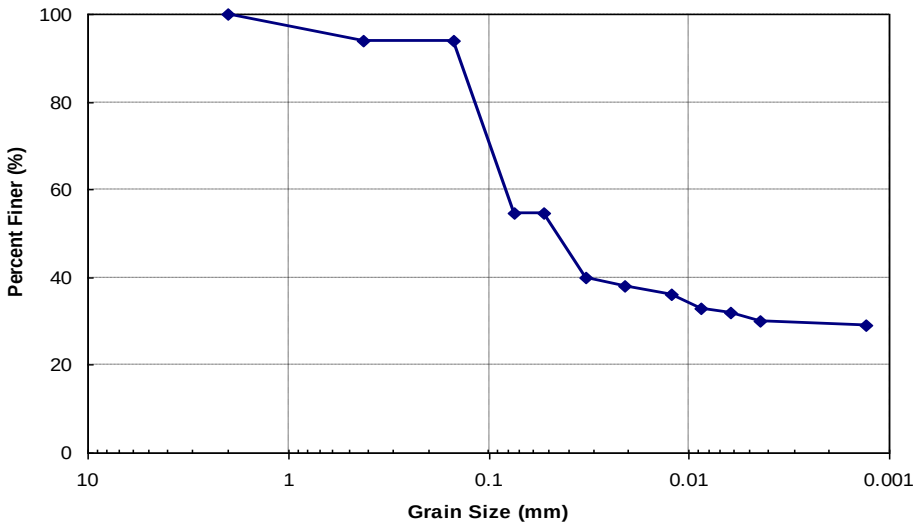

Figure 66
Particle size distribution of the untreated soil (1 in. = 25.4 mm)

Figure 67 presents the compaction curves of untreated, lime/fly ash treated, and cement treated soils. Table 31 presents the optimum moisture and maximum dry density of untreated and treated soils. The additions of lime/fly ash and cement increased the optimum moisture contents and decreased the dry weight density.

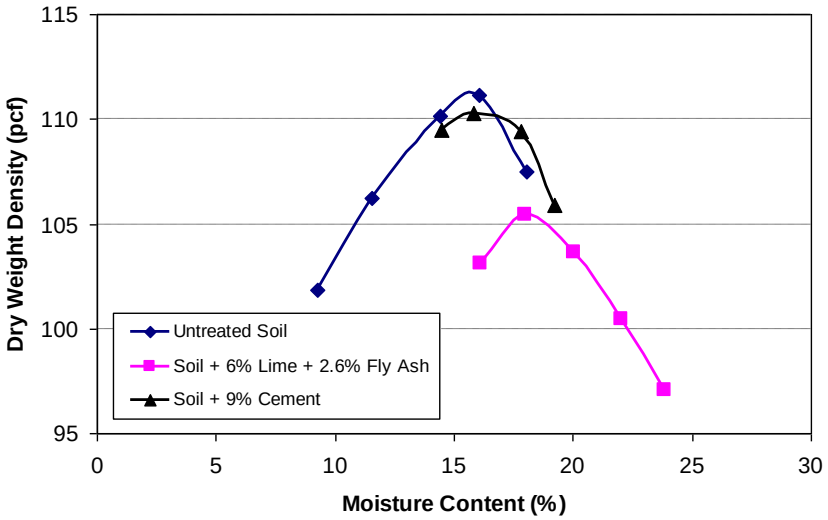

Figure 67
Compaction curves of untreated and treated soils

Table 31
Optimum moisture and maximum dry density of untreated and treated soils

Material	Optimum Moisture Content (%)	Maximum Dry Density (pcf)
Untreated Soil	15.7	111.4
Soil + 6% Lime + 2.6% Fly Ash	18.0	105.5
Soil + 9% Cement	15.8	110.3

Three samples were prepared for the UCS test for each untreated and treated soils. For treated soils, the molded samples were sealed in plastic bags immersed in a water bath at 104^{o}F (40^{o}C) for 7 days. After the 7-day curing, the samples were taken out from plastic bags. The lime/fly ash treated soil samples were wrapped with wet absorptive fabric and placed on a porous stone in a shallow pan for 24 hours prior to testing at room temperature for the capillary soak. The cement treated soil samples were immersed in water at room temperature for 4 hours prior to testing. Table 32 presents the UCS test results for untreated and treated soils. It can be found that the additions of lime/fly ash and cement increased the UCS strength. To achieve 150-psi design strength for subbase layer, the content of 2.6 percent lime with 6 percent fly ash (by weight) was selected for lime/fly ash treated soil, while the cement content was about 3 percent (by weight) by the interpolation method.

Table 32
UCS test results for untreated and treated soils

Materials	UCS after 7 day curing with 40°C (psi)					
	#1	#2	#3	Average	Stdev.	Cov.(%)
Untreated soil	33.1	23.9	24.1	27.0	5.3	19.4
Soil + 2.6% Lime +6% Fly Ash	167.8	148.0	135.4	150.4	16.3	10.9
Soil + 4 % Lime + 1.7% Fly Ash	159.1	166.9	141.8	155.9	12.9	8.3
Soil + 6% Lime + 2.6% Fly Ash	126.2	139.8	155.6	140.5	14.7	10.5
Soil + 8% Lime + 3.4% Fly Ash	132.2	119.7	145.0	132.3	12.7	9.6
Soil + 2% Cement	68.1	85.9	-	77.0	12.5	16.3
Soil + 4% Cement	253.5	229.9	271.4	251.6	20.8	8.3
Soil + 6% Cement	373.1	385.9	370.8	376.6	8.1	2.2
Soil + 9% Cement	584.1	599.9	537.1	573.7	32.7	5.7
Soil + 12% Cement	585.7	575.5	627.5	596.2	27.6	4.6

Soil samples with 2.6 percent lime/6 percent fly ash, 3 percent cement, and 4 percent cement were selected to conduct the P-D test. The samples had a diameter of 2.8 in. and a height of 5.6 in. The same curing method was applied as the UCS samples. The confining pressure of 2 psi and a cyclic stress of 5.4 psi were applied in the P-D test for 10,000 cycles. Figure 68 presents the P-D test results for 2.6 percent lime/6 per fly ash, 3 percent cement, and 4 percent cement treated soils. The permanent strain of 2.6 percent lime/6 percent fly ash treated soil after 10,000 cycles was between those of 3 percent cement and 4 percent cement treated soils.

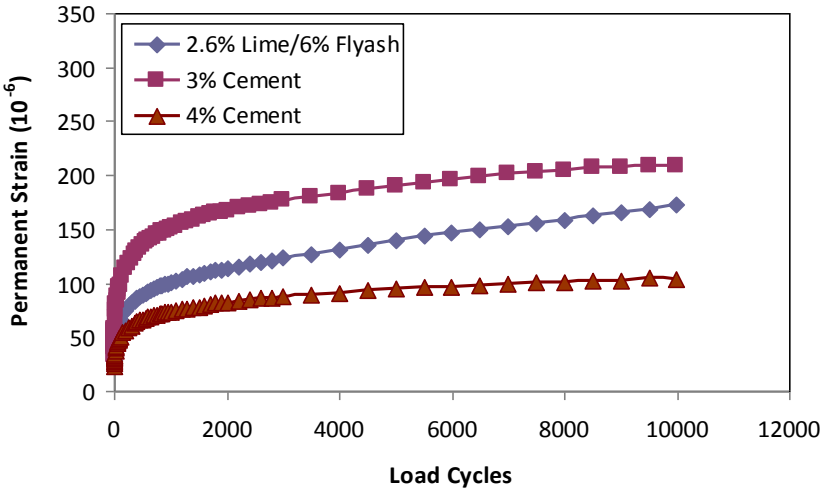

Figure 68
Permanent deformation test results for lime/fly ash and cement treated soils